12289-TR1

EXCAVATION SEISMOLOGY
First Semiannual Technical Report

Honeywell Inc.
Systems and Research Center
Research Department
2345 Walnut Street
St. Paul, Minnesota 55113

DOCUMENT CONTROL DATA - R & D

(Security classification of title, body of abstract and indexing annotation must be entered when the overall report is classified)

1 ORIGINATING ACTIVITY (Corporate author)	2a. REPORT SECURITY CLASSIFICATION
Honeywell Inc. Systems and Research Center, Research Dept. St. Paul, Minnesota 55113	Unclassified
	2b. GROUP NA

3 REPORT TITLE

EXCAVATION SEISMOLOGY

4 DESCRIPTIVE NOTES (Type of report and inclusive dates)

First Semiannual Technical Report   19 February 1971 - 18 August 1971

5 AUTHOR(S) (First name, middle initial, last name)

Duane E. Soland, Harold M. Mooney, Sudarshan Singh

6 REPORT DATE	7a. TOTAL NO. OF PAGES	7b. NO. OF REFS
September 1971	136	29

8a CONTRACT OR GRANT NO. H0210025	9a. ORIGINATOR'S REPORT NUMBER(S)
b. PROJECT NO. ARPA Order No. 1579, Amend. 2	12289-TR1
c Program Code No. 1F10	9b. OTHER REPORT NO(S) (Any other numbers that may be assigned this report)
d.	

10 DISTRIBUTION STATEMENT

11 SUPPLEMENTARY NOTES	12. SPONSORING MILITARY ACTIVITY
	Advanced Research Projects Agency Department of Defense Washington, D.C.

13 ABSTRACT

The objective of the program is to develop seismic techniques and equipment which can be used in a hard-rock rapid-excavation system to provide indication of potentially hazardous or changing geologic conditions ahead of the working face. The seismic reflection method is considered the most suitable one for the application. The principal technical problem is identification of reflections superimposed on other source-produced coherent interference. Signal processing techniques such as cross-correlation and velocity filtering or beamforming using an array of receiving sensors are being investigated for enhancement of reflections. The initial part of the program has emphasized the development of a seismic source/receiver combination which produces a simple, repeatable transmitted seismic pulse. A field recording system has been assembled and seismic signals recorded and digitized for reflections from free surfaces on granite blocks using a single receiver at various locations to simulate an array of receivers. The digitized signals will subsequently be processed by digital computer to simulate and assess signal processing techniques.

DD FORM **1473** NOV 65   REPLACES DD FORM 1473, 1 JAN 64, WHICH IS OBSOLETE FOR ARMY USE.

KEY WORDS	LINK A		LINK B		LINK C	
	ROLE	WT	ROLE	WT	ROLE	WT
Rapid excavation system						
Seismic waves						
Seismic reflection method						
Seismic array processing						
Cross-correlation						
Matched filtering						
Deconvolution						
Piezoelectric transducer						
Seismic-source radiation characteristics						
Signal averaging						
Field experiments						
Instrumentation						
Seismic models						
Travel-time curves						
Reflection coefficients						
Transmission measurements						

EXCAVATION SEISMOLOGY
First Semiannual Technical Report

Duane E. Soland, Project Engineer (612) 331-5085
Dr. Harold M. Mooney, Subcontract Principal Investigator (612) 373-3137
Sudarshan Singh

Honeywell Inc.
Systems and Research Center
Research Department
2345 Walnut Street
St. Paul, Minnesota 55113

TECHNICAL REPORT SUMMARY

This is the first semiannual technical report of the Excavation Seismology study, sponsored by the Advanced Research Projects Agency under the Military Geophysics Program.

The objective of the excavation seismology program is to develop seismic/acoustic techniques and equipment for use in underground hard-rock excavation. The principal recognized need is to provide early warning of hazardous or geologically changing conditions ahead of the excavation working face or in the roof of the opening. Such conditions include fractures or faults, presence of water, and changes in rock type.

The seismic reflection method is the most suitable technique for this purpose. The major technical problem associated with the reflection method is recognition of the reflection waveform. The reflected signal is never a first arrival and consequently is always superimposed on other signals which have also been produced by the seismic source transmitter. These source-produced interferences consist of other modes of seismic wave propagation, primarily surface waves if the transmitter and receiver are located at the rock surface or the analogous tube waves if they are used in boreholes.

Signal processing techniques which are being investigated to reduce source-produced and other coherent interference include the following:

- Receiver array processing

- Cross-correlation

- Signal averaging

Array processing utilizes the difference in apparent velocity or direction of arrival of the interference to distinguish it from reflections. Cross-correlation is useful in providing unambiguous time-of-arrival measurements and discriminating against interference on the basis of waveform differences. Signal averaging is effective against non-source-produced interference.

Because of the complexity of seismic wave propagation, the evaluation of these techniques for rapid excavation emphasizes controlled field experiments, supplemented by theoretical analysis and seismic model studies where appropriate. Signals recorded in the field are subsequently digitized for computer simulations of the signal processing techniques to provide a realistic evaluation of expected system performance before hardware development is undertaken. Field instrumentation consisting of a seismic source, receiver, and timing, display and recording equipment has been assembled during the first six months of the program covered by this report.

The seismic source consists of a piezoelectric transducer and a pulse generator. The transducer is a cylindrical stack of lead zirconate-lead titanate elements which vibrates in a fundamental longitudinal mode at a resonant frequency of 20 KHz. The choice of frequency is a compromise resulting from poor radiation efficiency at lower frequencies and higher propagation losses from attenuation at higher frequencies. A single hole is provided through the center of the transducer for bolting to the rock surface. The radiation characteristics of this type of transducer are presented in section 2.2.

The receiver is a commercially available piezoelectric accelerometer which has a high resonant frequency (80 KHz) to provide minimum distortion of the received seismic waveform.

The combination of source and receiver is capable of transmission distances of at least 10 meters in crystalline rocks. The addition propagation losses for 100 meters propagation pathlength, including frequency-dependent attenuation and geometrical spreading, are estimated to be 56 db. Signal averaging can provide a gain of over 40 db with averaging times of a few minutes at source repetition rates of about 25 pulses per second. Additional gain can be achieved by higher source-driving voltages. Therefore, with the present approach, we expect to achieve maximum penetration depths of about 50 meters.

Initial field investigations were directed toward achieving a simple transmitted seismic pulse and recording array data for later analysis and simulations. The ideal pulse is of short duration for accurate time-delay measurements and is repeatable with changes in source and receiver location and orientation. The use of a simple impulse driving signal produced a damped sinusoid of several cycles duration because of the acoustic impedance mismatch between the source transducer and the rock surface. The duration and narrowband character of the seismic pulse made it unsuitable for resolving closely spaced reflecting interfaces and obtaining accurate propagation-time measurements. A double-pulse technique was developed in which the second pulse in effect cancels the ringing tail of the first pulse. This technique was successful in producing a simple, short-duration seismic pulse.

Experiments were conducted on large granite quarry blocks which allowed measurement of the transmitted seismic signal as well as reflections and multiple reflections from the free surfaces. The receiver was moved for each record to simulate an array of receivers, a procedure which is valid because of the excellent repeatability of the transmitted signal. Some of the resulting records are presented in section 3.2, and they demonstrate the improvement obtained with the double-pulse method as well as the repeatability of the seismic waveform with changes in receiver location. This repeatability is a must for the proposed array and cross-correlation processing.

Cross-correlation with a master transmitted waveform was reviewed, and the effects of distortion such as might result from source, receiver or propagation through the rock were analyzed. A number of representative cases were computed and are presented and discussed in section 4. 2.

Theoretical data on the effect of angle of incidence on reflection coefficients is presented in section 2. 4 for two cases of particular significance, namely reflection from an open fracture and reflection from a water-filled fracture. It is concluded that the length of the receiver array must subtend an angle necessary to keep the incidence angle less than about 20 degrees to use the PP (compressional) wave reflection.

Experimental data on reflection coefficient versus angle of incidence at a free surface are included in an appendix. The data was taken on a two-dimensional seismic model with the geometry arranged to eliminate the effects of the radiation patterns of source and receiver. The data substantially verifies theoretical predictions, but the large amount of scatter in the measurements indicates the potential difficulty in quantitative use of reflection amplitudes.

The seismic model reflection investigation demonstrated the effective use of of a slit to block unwanted modes of propagation, in that case body shear waves. Additional model studies were initiated to investigate the blocking effect of a slit around the source transducer to reduce surface waves, as well as sinking of the source at depth to achieve the same results. The recorded preliminary data is presented in section 3. 5. Analysis of the data is not yet complete, but significant improvement is not apparent from visual inspection of the records.

CONTENTS

ILLUSTRATIONS

SECTION 1

INTRODUCTION

The objective of the Excavation Seismology program is to develop equipment with which to "see" ahead of a tunnel or excavation in hard rock using sound waves. The equipment should be able to provide geological information about conditions within the rock: location of faults, fractures, or joints, changes in rock types, extent of fracture zones, formation boundaries and the delineation of ore bodies.

Penetration depth into the rock should, at a minimum, be several tens of feet. However, methods of hard-rock excavation are currently under development with the goal of achieving excavation rates of several hundred feet per day. The seismic equipment should ultimately be capable of matching this depth in order to provide timely warning of the existence of changing or hazardous geological conditions.

The technical problem can be subdivided as follows:

- Devise a technique which in principle is capable of achieving the desired results.

- Develop prototype equipment which will validate the technique under controlled conditions, even though it may require scientific personnel, elaborate equipment or the use of computers.

- Adapt the equipment for use under production conditions underground by semiskilled personnel. The goals of the current program are directed toward the solution of the first two problems.

The reflection seismic method is the most obvious choice of techniques. It can conveniently be used from a tunnel or mine face, it can provide adequate resolution between reflecting discontinuities at different depths of penetration, and it lends itself to the use of an array of receivers. On the other hand, the reflection signal is never a first arrival and therefore is always superimposed on other signals which makes it hard to identify on the seismic waveform.

The refraction seismic technique is less suitable for the program goals. The principal problem is in the requirement for a substantial increase in velocity at the refracting interface. This excludes the possibility of detecting joints and fractures, shear zones, and faults and formation boundaries with lower-velocity rocks on the far side of the discontinuity.

1

The potential for identifying the character of the reflecting interface from measurements of the reflection coefficient and its variation with incidence angle also provide motivation to investigate the use of the reflection technique in underground openings.

Previous investigators (Zietz and Pakiser, 1957; Evison, 1957) have obtained reflections at depths of penetration comparable to those of interest here, using very heavy, high-power electromechanical transducers as the seismic source. More recently, Cannady and Leo (1966) obtained substantial depths of penetration with relatively small, low-power piezoelectric source transducers using high-power (several-kilovolt) drive pulses. This approach resulted in stable, repetitive seismic signals but provided substantially little control over the seismic waveform. They described the application of this equipment to sonic transmission measurements but apparently did not attempt to obtain or identify reflections.

The present research program seeks to extend this work by employing array signal processing techniques to achieve sufficient, controllable depths of penetration in hard rock with low-power seismic sources and to enhance signals of interest for easier detection and identification. To accomplish these goals, it is necessary to:

- Bring the transmitted seismic waveform under control

- Determine the characteristics of the interfering "noise"

- Devise techniques to minimize the interference

- Implement these techniques in practical hardware

This technical report covers the initial six months effort on the program, which has been concerned primarily with the first two tasks listed above.

SECTION 2

THEORY AND ANALYSIS

The seismic reflection problem can be represented by the linear model shown in Figure 1. The seismic source, which is assumed to be a transducer producing a force perpendicular to the face of the rock, transmits energy to the rock mainly in the form of:

- Compressional, or P waves

- Shear, or S waves

- Surface waves

Each of these propagate away from the source, may be reflected by discontinuities, and subsequently sensed by the receiver transducer.

The outputs of the receiver transducers may be processed as indicated in Figure 2. With reference to both Figures 1 and 2, the system design problem consists of the specification of:

- Source and receiver transducers

- Source waveform

- Receiving array configuration

- Signal processing algorithms

- Display

The signal processing, which has the sole purpose of enhancing the desired reflection signal relative to the interfering noise, will consist of two steps as shown in Figure 2.

The principal function of the temporal processor is to reduce the effects of noise which is random or uncorrelated with the signal. The function of the beam-forming or spatial processing step is to reduce the effects of noise which may be coherent and correlated with the signal but differ in spatial characteristics as observed across the array of n receivers.

3
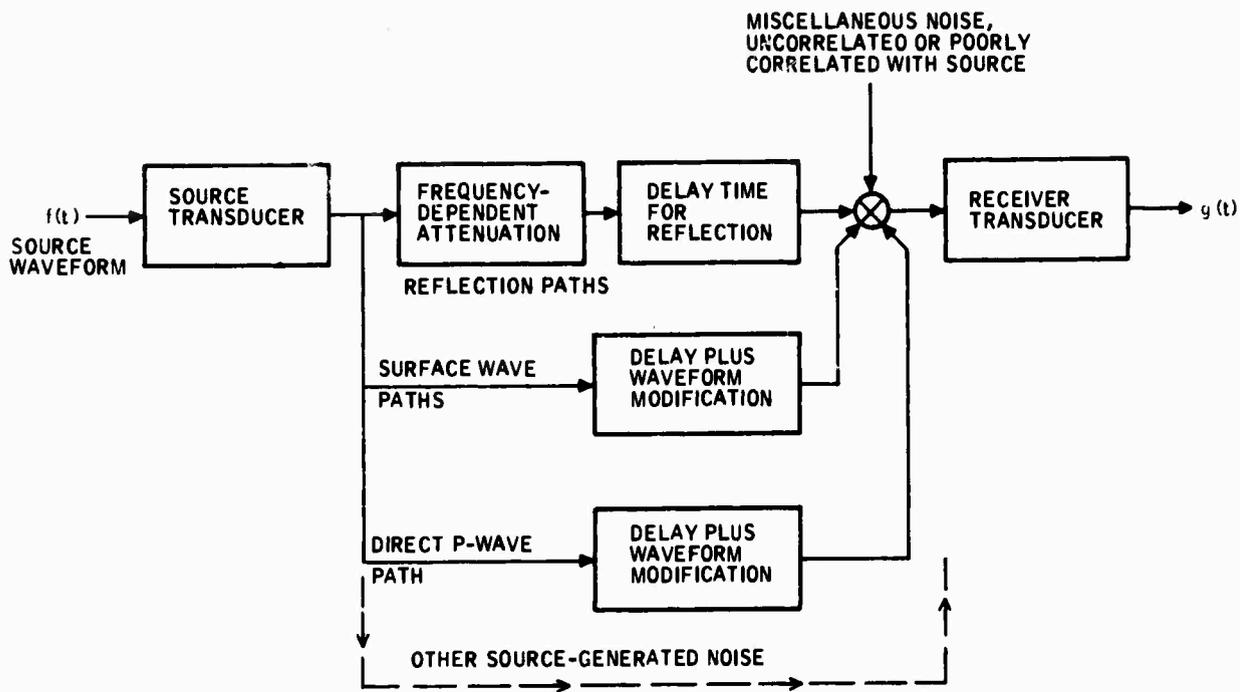
Figure 1.   Linear Model for Excavation
Seismology Program

n RECEIVERS   k PREFORMED BEAMS
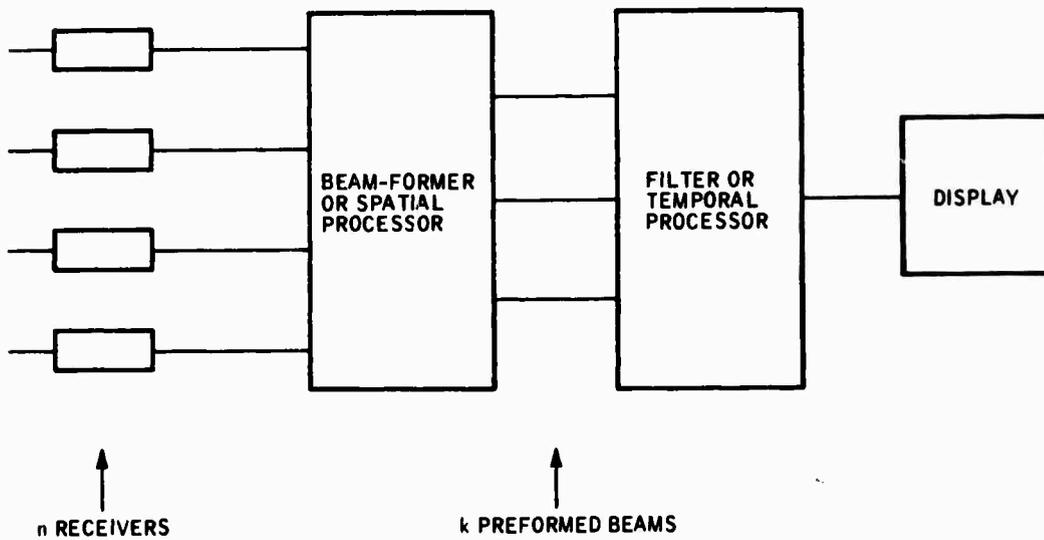
Figure 2.   Generalized Signal Processor for
Excavation Seismology

4

2.1 CHARACTERISTICS OF ANTICIPATED SEISMIC NOISE

The term, "seismic noise", is used to designated all seismic disturbances other than the desired signal. If the desired signal is a reflection, then the noise includes not only the ambient background from wind and machinery but also all other wave types and wave paths originating with the source.

The problem of maintaining a satisfactorily high signal-to-noise ratio (S/N) is of critical importance for the Excavation Seismology program. The problem becomes particularly severe when the desired signal is a reflection because travel-time considerations show that this must always appear superposed on a noise background created by earlier-arriving waves.

An attempt to improve the S/N must include some specification of the nature of the noise. One approach is to assume that the noise is white; that is, that the noise is a continuous random signal whose power spectrum is flat up to the highest frequency of interest in the investigation. This assumption provides a good starting point for evaluation of various data-processing techniques. It will be more realistic for non-source-generated noise than for source-generated noise. The former type often exists in earthquake seismic data analysis. It may represent an appreciable contribution for the excavation seismology program, particularly at greater depths of penetration where receiver noise must be overcome, but source-generated noise will probably have greater significance for the identification of reflections.

Source-generated noise is particularly difficult to overcome because it shares several characteristics with the desired signal. These include a strong correlation with the source waveform and a strong similarity in spectral content. On the other hand, the characteristics of source-generated noise can be predicted and measured to some extent. This can provide guidance in reducing the noise problem.

The discussion which follows provides a brief listing of anticipated noise sources for the excavation seismology program. Only passing mention is made of such matters as the waveform distortion produced by the transducers the radiation pattern of the transducers, and waveform differences for the various seismic wave types. These are considered elsewhere. Our concern in this subsection is simply to list the noise sources and to comment on their probable importance to the excavation seismology program.

Some of the noise sources to be mentioned can be illustrated as shown in Figure 3.

2.1.1 Source-Generated Noise

Source-generated noise can be considered in the following categories:

5
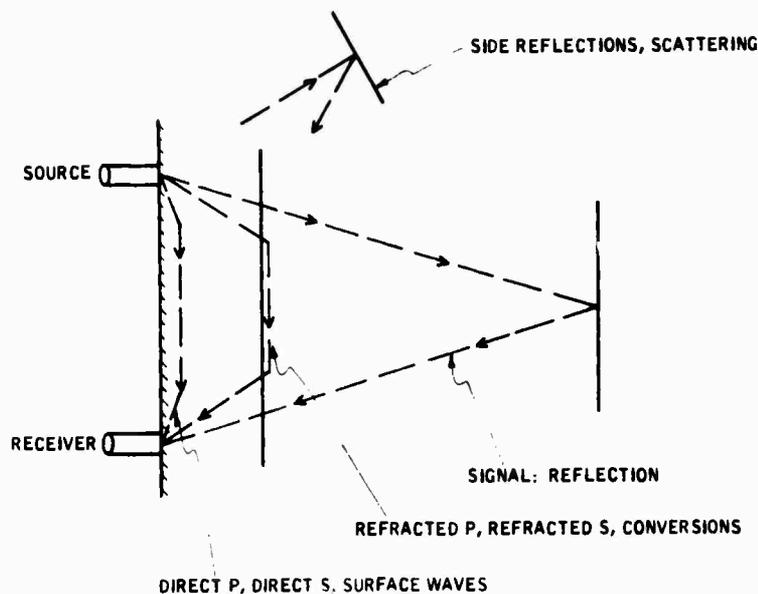
Figure 3. Noise Sources

- More Serious -

  (1) Direct P - The direct compressional wave will be the first arrival but may be quite small due to the radiation pattern of the source. The waveform should be very similar to the reflection signal.

  (2) Surface Rayleigh - The Rayleigh wave promises to be the most serious noise problem of all due to its large amplitude and its late arrival time. The wave will _not_ be the reverberant dispersed wave train familiar to earthquake and exploration seismologists but rather a large pulse with a distinctly different waveform* from the direct and reflected signals.

- Less Serious -

  (1) Direct S - The S wave may be a troublesome noise source because the source may have a strong horizontal lobe in the radiation pattern. It will arrive very close to the Rayleigh wave, however, and the waveform will probably differ somewhat from those of the direct and reflected signals.

  (2) Refracted P, refracted S, and converted waves - The existence of waves in this category depends on the presence of a nearby velocity discontinuity, with higher velocity on the further side. We do not expect the situation to occur except occasionally, so this source of noise should have little importance.

*Different, to the extent that the waveform is determined from seismic considerations rather than the impulse response of the source transducer.

(3) Side reflections and scattered waves - Seismic energy can be reflected back from boundaries above, below, or to the sides. The reflections may be either coherent wavefronts or, for small reflectors, incoherent and somewhat random disturbances. In all cases, they can contribute to the noise problem.

2.1.2 Non-Source-Generated Noise

Seismic vibrations at some level are always present in the earth. At the surface, the largest contributors are wind and cultural sources such as traffic and machinery. Within a mine or tunnel, we would expect the effect of winds at the surface to be negligible. Machinery can presumably be turned off during the seismic work.

An additional factor which minimizes the importance of non-source-generated noise is the high frequencies at which the seismic study will be conducted. Most seismic noise of natural origin lies in the spectral region below 100 Hz, dying off rapidly above. The proposed system will use frequencies well above this range.

2.2 SEISMIC RADIATION INTO A ROCK SURFACE

The seismic wave pattern produced by a longitudinal transducer on a rock surface is more complicated than might at first appear, for two reasons:

- The presence of the free surface produces surface waves plus a diffracted S wave (Figure 4).

- The directionality of the source (vibrations normal to the rock surface) produces a radiation pattern which differs from that of an isotropic pressure source. Miller and Pursey (1954) calculated the components of displacement for each wave type.

At large distances such that $R >> a$, where a is the radius of the source, and also wavelengths $L >> a$ (see Figure 5), the amplitudes of the compressional and shear wave are calculated as shown in the following paragraphs.

2.2.1 Compressional Wave

Particle displacement is entirely radial, given by:

7
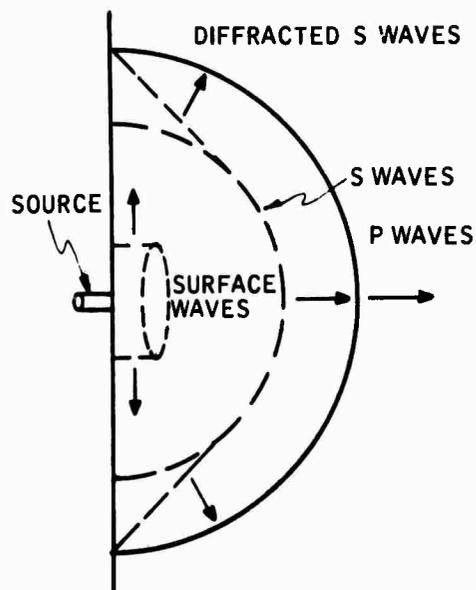
Figure 4. Seismic-Wave Pattern Produced by a Force Transducer on a Rock Surface
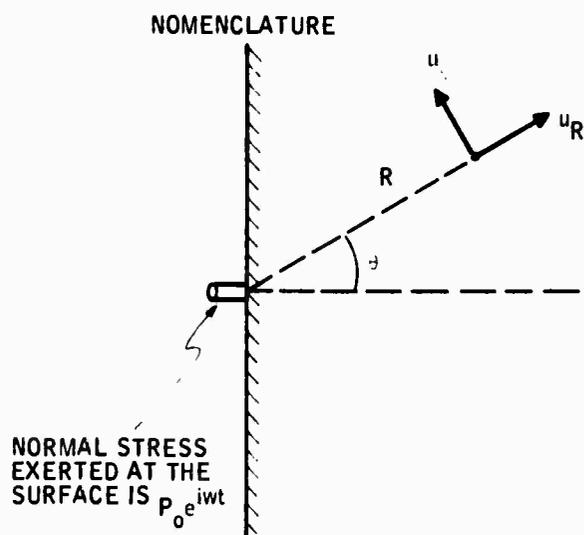
Figure 5. Problem Geometry

8

$$U_R = \frac{a^2 P_o}{2\mu} \frac{1}{R} \theta_1 (\theta) \epsilon^{i(Wt - k_1 R)}$$

$$= \frac{F_s}{2\pi\mu} \frac{\theta_1(\theta)}{R} \epsilon^{i(Wt - k_1 R)}$$

(1)

where

W = frequency of the vibrating source

μ = rigidity modulus of the rock

k_1 = $W/V_P = 2\pi/L_P$

L_P = wavelength of P wave

V_p = velocity of P wave

F_s = $\pi a^2 P_o$ = force generated by the seismic source

$$\theta_1(\theta) = \frac{\cos\theta}{F_o(\sin\theta)} \left[\frac{V_P^2}{V_S^2} - 2\sin^2\theta \right]$$

(2)

$$F_o(\nu) = \left(2\nu^2 - \frac{V_P^2}{V_S^2} \right)^2 - 4\nu^2 \sqrt{\nu^2 - 1} \sqrt{\nu^2 - \frac{V_P^2}{V_S^2}}$$

(3)

For normal incidence ($\theta = 0$), the displacement amplitude of the compressional wave reduces to

$$U_R = \frac{F_s}{2\pi\rho V_p^2} \frac{1}{R} \epsilon^{-i(Wt - k_1 R)}$$

(4)

9

2.2.2 Shear Wave

Particle displacement is entirely tangential, given by

$$U_\theta = -i \frac{F_s}{2\pi\mu} \left(\frac{V_P}{V_s} \right)^3 \frac{1}{R} \, \theta_2(\theta) \, \epsilon^{\, i(Wt - k_2 R)} \tag{5}$$

where

$$k_2 = W/V_s = 2\pi/L_S$$
$$L_S = \text{wavelength of S wave}$$
$$V_s = \text{velocity of S wave}$$

$$\theta_2(\theta) = \frac{\sin 2\theta}{F_0\left(\dfrac{V_P}{V_s} \sin \theta \right)} \left[\frac{V_P^2}{V_s^2} \sin^2 \theta - 1 \right]^{1/2} \tag{6}$$

For our purposes, the disc radius a will be substantially less than P or S wavelength. If this were not the case, then U_R and U_θ as given above should be multiplied respectively by

$$\frac{2J_1(k_1 a \sin \theta)}{k_1 a \sin \theta} \quad \text{or} \quad \frac{2J_1(k_2 a \sin \theta)}{k_2 a \sin \theta}$$

both of which go to 1 in the limiting case. The general expressions may be found in Lord (1966).

2.2.3 Power Distribution Among Wave Types

Miller and Pursey (1955) show that for $\sigma = 1/4$, the total power radiated by the source is

$$W = 4.836 \, W_o \quad \text{with} \quad W_o = \frac{\pi f^2 F_s^2}{\rho V_p^3} \tag{7}$$

The power into individual waves is proportional to the same physical parameters, in the ratio of

$$\text{compressional } W = 0.333\ W_o, \text{ or } 6.89\%$$
$$\text{shear} \qquad W = 1.246\ W_o, \text{ or } 25.77\%$$
$$\text{surface} \qquad W = 3.257\ W_o, \text{ or } 67.35\%$$

2.2.4 Discussion

The radiation patterns for compressional and shear waves, as functions of polar angle θ, are contained in $\theta_1 (\theta)$ and $\theta_2 (\theta)$ which are shown in Figure 6. Only the compressional P wave is transmitted in the forward direction, which will be of principal concern in underground excavation. Shear wave reflections may be expected to predominate at larger angles, where they will be separable from P waves on the basis of apparent velocity across the receiver array.

The power radiated increases with the square of the force produced by the transducer, as might be expected, but also increases as the square of the frequency. Most of the power is radiated as surface-wave noise.

The directivity pattern will be the same whether the transducer is used for the source or the receiver. Experimental data obtained by Anzai (1959) which confirms the theoretical analysis are reproduced in Figure 7.

2.3 MINIMIZING INTERFERENCE FROM SURFACE WAVES

The preceding discussion, verified by experimental data taken in Cold Spring granite quarry suggest that a serious problem for excavation seismology will be interference from surface waves. The following methods for minimizing this interference appeared worthy of consideration (experimental tests of some of these methods were made, and the results are discussed in Section 3):

- Shortening pulse length produced by the source transducer - The experimental observations suggest that the length of the surface wave train arises principally from ringing of the source transducer rather than from propagation effects. If so, an obvious means for shortening the surface wave train is to shorten the source pulse length. An approach which was investigated is the use of a double pulse of special waveform as described by Brown (1956). The method would greatly attenuate the tail end of the source waveform, but it would do so at the cost of increasing the complexity of the early part of the source waveform. The double pulse approach will automatically overcome the dynamic range problem. The problem arises because the surface wave signal has much greater amplitude than the

11

COMPRESSIONAL WAVES

SOURCE DIRECTION

-90°   90°

θ = 0°

SHEAR WAVES

-90°   90°

35°   35°

θ = 0°
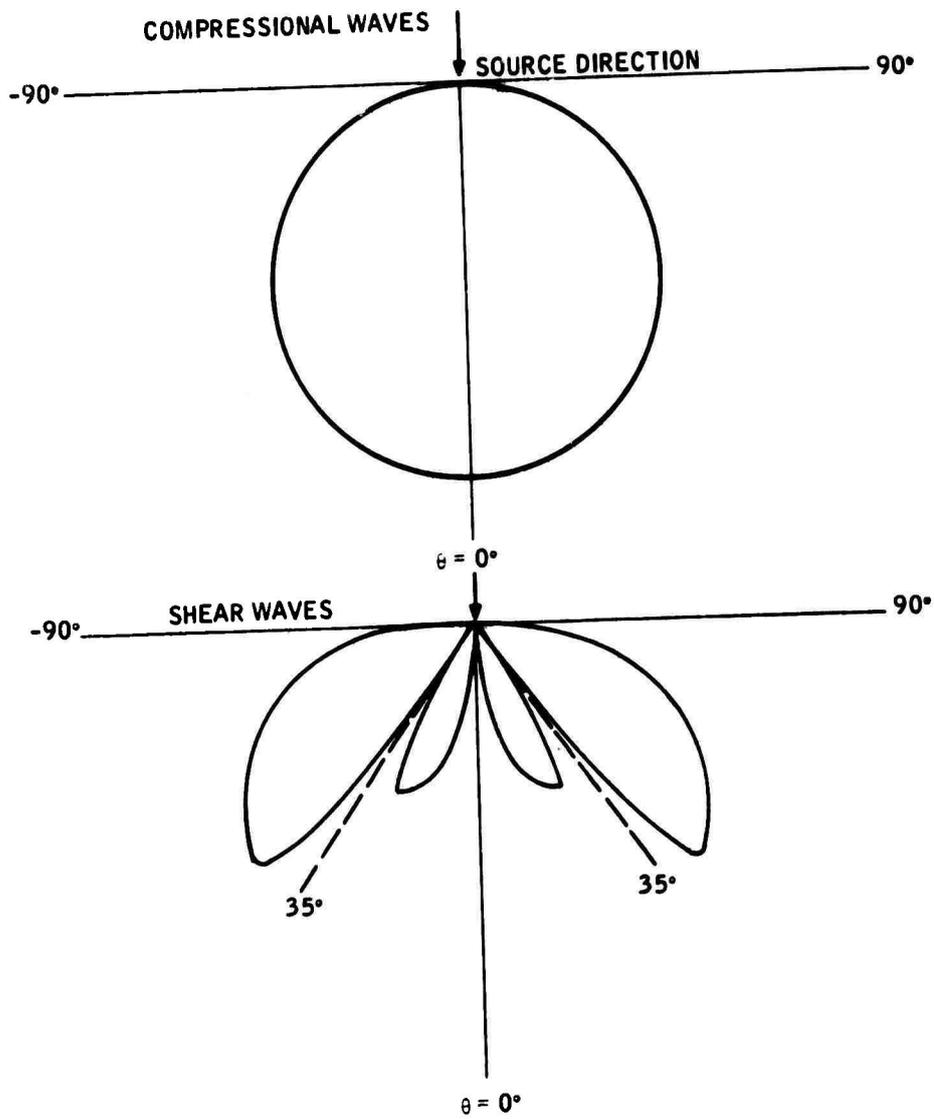
Figure 6. Theoretical Radiation Patterns from a Small
Transducer (computations for a special case
of ρ = 0.25)

12

RELATIVE RADIAL
DISPLACEMENT OF P WAVE

RELATIVE TANGENTIAL
DISPLACEMENT OF S WAVE
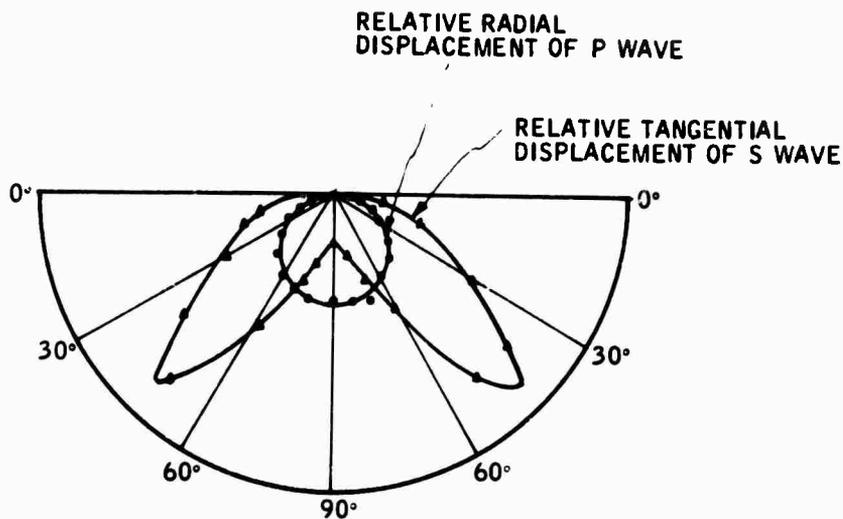
Figure 7. Directivity Pattern of Barium-Titanate
Transducer in Three-Dimensional Model
(after Anzai, 1959)

reflected signal. Any linear analysis technique requires that both
signals be recorded without distortion; this may impose severe
demands upon the instrumentation. If we are able to compress the
source signal in time, then we can simply "throw away" the surface
wave signal by permitting the instrumentation to saturate during
its arrival. No reflected signal will be identifiable during this time
interval of course, but later signals should be free from the surface-
wave interference, except for possible reflected surface waves of
lower amplitude, and would be recorded without distortion.

• Array processing - A principal goal of array processing is to reduce
signals with low apparent velocity across the receiver spread. The
surface wave has this characteristic.

• Block surface waves by a cut - In principle, the amplitude of surface
waves can be greatly reduced by interposing a saw cut between source
and receiver. The required depth of cut would be determined
experimentally, but it depends strongly on the dominant wavelength
of the signals. The excavation seismology problem would require
a circular cut all the way around the source transducer. This
approach was investigated experimentally on a two-dimensional
seismic model. The results and conclusions are presented in
section 3.7.

13

- Reducing surface wave generation by putting the source at depth - As a field procedure, this approach would be simpler than blocking the surface waves by a cut. It should not be particularly difficult to implement, particularly since some preparatory smoothing of the rock surface would normally be required in any case. Sinking the receivers would be an alternative or an additional possibility. Experimental data on the seismic model to test this approach were taken and are also discussed in Section 3.7.

- Placing absorbent material along path of surface wave - In principle, one could place absorbent material along the rock surface which would block the surface waves. This was tried with modeling clay along the surface of the two-dimensional seismic model, and it succeeded in cutting the amplitude in half. However, the clay had to be placed along the sides of the model for an inch or two as well as along the surface to achieve this.

2.4 THEORETICAL RESULTS ON SEISMIC REFLECTION COEFFICIENT VERSUS INCIDENCE ANGLE

An important factor in this investigation is the intensity of the seismic wave reflected from the target joints, fractures, faults, offsets, etc. For a simple plane reflecting surface and an array of detectors, three terms contribute to the reflection intensity factor which are dependent on the angle of the ray path:

- The reflection coefficient at the reflecting boundary

- The free-surface effect at the receiver (that is, the fact that the amplitude and direction of the surface motion differ from that of the arriving seismic ray)

- The radiation pattern of source and receiver

In this subsection we review the theoretical results for seismic reflection coefficients and consider their implications for the program. In addition, we present in the appendix some experimental data obtained with a laboratory seismic model which not only confirm the theoretical results but also verify their relevance to the excavation seismology program.

One of the significant factors to emerge from the theoretical analysis is the existence of zeros in the reflection coefficient. This conclusion is confirmed by the experimental results. The presence of a zero means that, at a particular angle of incidence, no energy is reflected as a particular wave type. For the case of a P wave reflected at a free surface, in a medium with Poisson ratio = 0.25, zeros occur at two incidence angles: 63 and 75 degrees.

14

The practical significance of this result lies in the possibility of identifying the character of the joint or fracture from which the reflection takes place. If the reflecting horizon is an actual air-filled crevice, then the free-surface reflection coefficients are appropriate; conversely, if the coefficients can be determined experimentally, the horizon may be identifiable as a free surface. If the opening is water-filled, on the other hand, a different reflection behaviour and zero location would be anticipated. Still another type of reflecting horizon might have no opening at all, with still a third type of behaviour.

In practice, we would not require complete zeros in the reflection coefficient in order to carry out the analysis. The presence of amplitude minima and maxima (after making due allowance for the other two contributing factors noted above) would provide the necsssary data.

As a preliminary comment, it should be pointed out that three types of representation for the reflection coefficient are in common use:

- Ratio of the displacement amplitudes (Zoeppritz formulation)

- Ratio of the displacement potential amplitudes (Knott formulation)

- Ratio of the energy densities, or the square root of the energy densities (Gutenberg formulation)

Any one of the three would be satisfactory for purposes of the present discussion, but we will select the third because it permits utilization of the conservation of energy theorem as a check on the results. The quantities are all inter-related and may be computed from each other by the following expressions (Gutenberg, 1944):

$$F = p^2 \frac{D_2}{D_1} \frac{\text{ctn } \theta_2}{\text{ctn } \theta_1} = D^2 \frac{D_2}{D_1} \frac{\sin 2\theta_2}{\sin 2\theta_1} \tag{8}$$

where F is the energy ratio, D is the displacement amplitude ratio, P is the displacement potential amplitude ratio, D_1 and D_2 are the densities in the incident and departure medium, and θ_1 and θ_2 are the incident angles in the two media. This expression covers reflection and refraction, as well as P waves, S waves, and conversion from P to S or S to P waves.

The quantity used in this discussion is $F^{1/2}$, i.e., (reflected energy/ incident energy)$^{1/2}$. From the above formulation, we note that $D_1 = D_2$ for a wave reflected back into the incident medium. Thus the quantity $F^{1/2}$ is closely equal to or identical with the displacement amplitude ratio P:

$$F^{1/2} = P \qquad \text{for P-to-P reflection}$$
$$\qquad\qquad \text{for S-to-S reflection}$$

$$F^{1/2} = P \, \frac{\text{ctn } \theta_s}{\text{ctn } \theta_p} \qquad \text{for P-to-S reflection}$$

$$F^{1/2} = P \, \frac{\text{ctn } \theta_p}{\text{ctn } \theta_s} \qquad \text{for S-to-P reflection}$$

Theoretical results are presented for two cases which have particular significance -- reflection from an open fracture and reflection from a water-filled fracture. Additional cases for a faulted offset in solid contact, with different rocks on the two sides, can be easily calculated as needed.

Figures 8 and 9 show reflection coefficients from a free surface, such as an open fracture (these are taken from Ewing, et al, 1956, as reproduced from Gutenberg, 1944). Different curves show the influence of Poisson ratio variations; for the rock types expected in the excavation seismology program, a value of $\sigma = 0.25$ appears reasonable. Figure 8 shows results for an incident P wave and Figure 9 for an incident S wave.

It may be seen that at normal incidence and for incidence angles up to about 10 degrees, incident P waves produce reflected P waves and incident S waves produce reflected S waves. From 30 degrees onward, an incident P wave produces dominantly reflected S, and in fact the conversion is total at angles of 63 and 75 degrees. (Within these angles, the small P reflection has a phase reversal.) We conclude that the length of the receiver array must subtend an angle such as to keep the incidence angle less than 20 degrees or so if we wish to use reflected PP. This conclusion is reinforced if we take the radiation pattern of the piezoelectric transducer into consideration, since the maximum lobe for P energy coincides with normal incidence onto a parallel reflecting interface.

Figure 9 for an incident SV wave should also be considered in the context of the radiation pattern for the transducer, which, as shown in Figure 6, has a maximum lobe at an angle of approximately 45 degrees and a zero at an angle of 0 degrees. We conclude that the reflected wave will be undetectable for an incidence angle up to 10 degrees (due to the source radiation pattern), dominantly P reflection from 10 to 35 degrees, and totally S reflection beyond 35 degrees.

Figures 10 and 11 show corresponding results where the fracture zone is filled with fluid rather than with air. The principal conclusion to be drawn is that the results are qualitatively similar, although the numerical details differ in some respects. We draw the further conclusion that the analysis for reflection at a free surface will display the most important features of the characteristics of the reflection coefficients (source: Ergin, 1952).
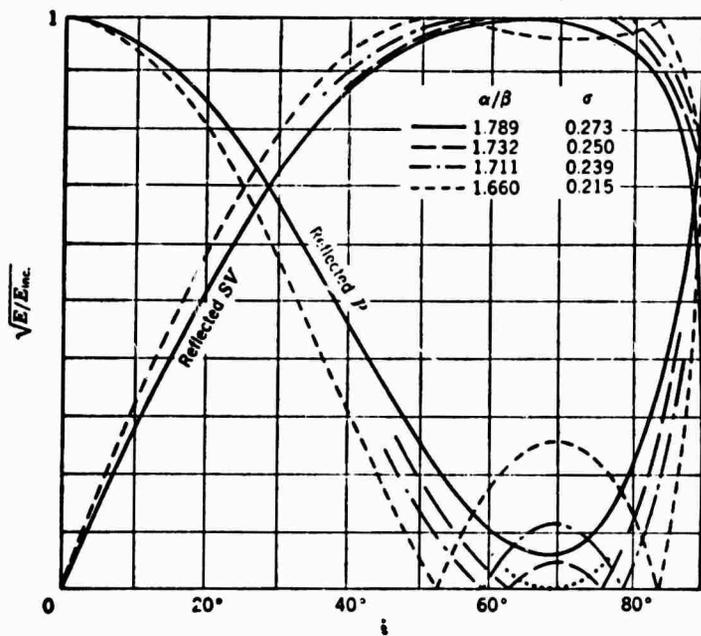
16

Figure 8. Square Root of Ratio of Reflected to Incident
Energy for P-Wave Incident at Free Surface
for Various Values of Poisson's Constant
(after Gutenberg, 1944)
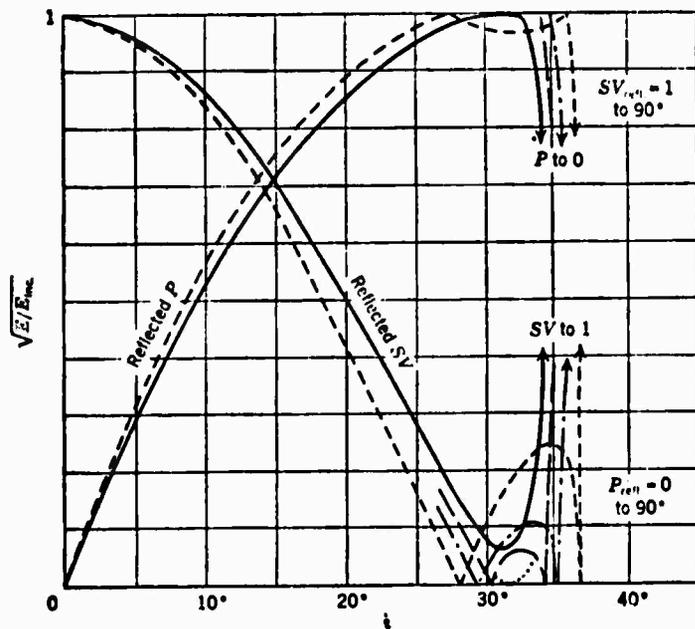
Figure 9. Square Root of Ratio of Reflected to Incident
Energy for SV-Wave Incident at Free Surface
(after Gutenberg, 1944)

17
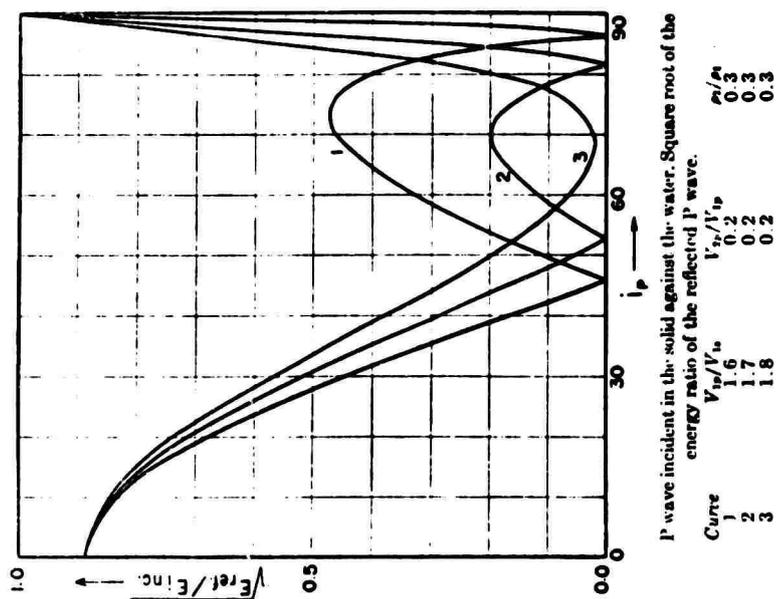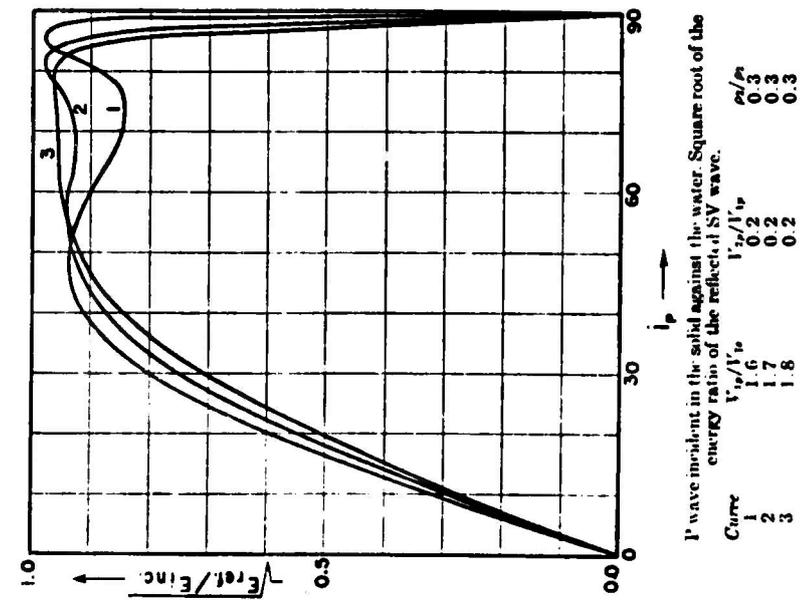
Figure 10.   Incident P-Wave

18
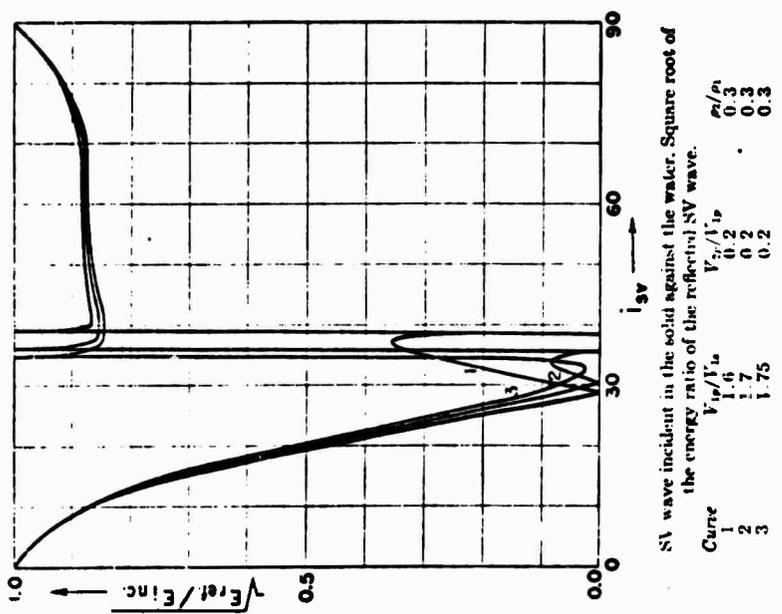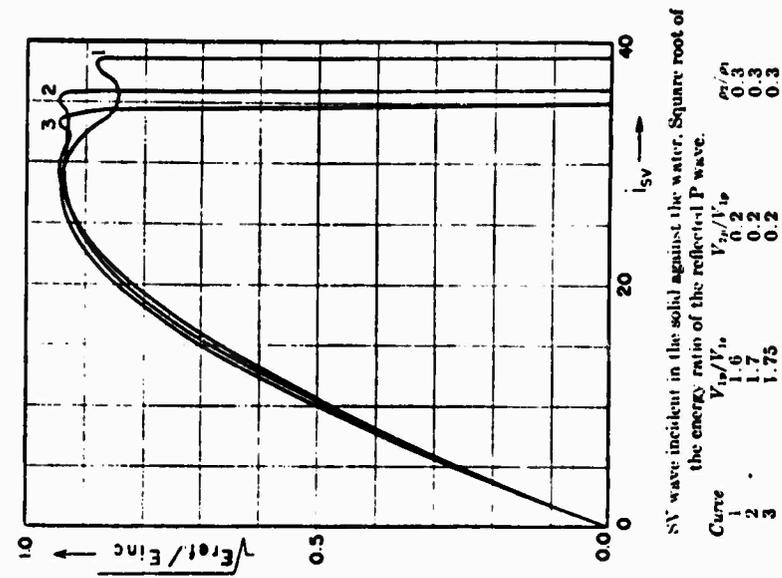
Figure 11. Incident SV-Wave

19

Some laboratory results from seismic model studies are included in the appendix. These results confirm the theoretical conclusions and verify their relevance to the excavation seismology program.

2.5 SEISMIC WAVE ATTENUATION

The principal causes of attenuation of sound wave in rocks, with a corresponding decrease in signal-to-noise ratio, are:

- Geometrical spreading

- Inelastic, frequency-dependent attenuation

- Reflection at interfaces

The first two of these depend on the distance the wave propagates to the reflecting interface. We wish to estimate the amount of signal loss for the depths of penetration and rock types of interest in hard-rock excavations. These estimates will, in turn, provide estimates of the required signal processing gain to provide useful signal-to-noise ratios at maximum depths of penetration. Conversely, if the signal processing gain is fixed, the expected maximum depth of penetration can be estimated.

Inelastic attenuation increases with wave frequency in rocks of all types. It would then appear that low frequencies would give better signal-to-noise than higher frequencies, and therefore greater depths of penetration. However, as discussed in section 2.2.3, the power transmitted into the rock from a small seismic source increases with the square of the frequency, thereby tending to offset the increase in attenuation with frequency.

2.5.1 Geometrical Spreading

An elastic-body P or S wave, propagating outward from a point source (and ignoring the nonuniformity of amplitude across the spherical wavefront from the directional radiation pattern of the source), suffers a loss in amplitude of a factor of two, or 6 db for every doubling of distance traveled. This follows from the result that at sufficiently great distances from the source, the displacement amplitude of the wave varies as $1/R$ where R is the distance to the source [Section 2.2, Equation (1) and (5)]. The energy in an elastic wave is constant, and since the energy is distributed over an ever increasing sphere of area $4\pi R^2$, the geometrical spreading energy loss varies as $1/R^2$, or a factor of four for each doubling of distance.

20

2.5.2 Frequency-Dependent Attenuation

Geometrical spreading attenuation is independent of rock type, but inelastic attenuation depends both on rock type and on frequency content of the seismic wave. The most suitable parameter to characterize inelastic attenuation in rocks is $1/Q$, the specific attenuation factor, which is a reduction to dimensionless form of the more usual measures of attenuation. Q has been found experimentally by many investigators to be independent of frequency for a wide range of rock types. Typical values of $1/Q$ for various hard rocks are shown in Table 1.

Table 1. Internal Friction in Rocks, $1/Q$*

Rock Type	$1/Q$ (Longitudinal Vibrations)
Limestone, Pennsylvania	760×10^{-5}
Quartzlitic sandstone	770
Gneiss, Pelham, Massachusetts	1800
Granite, Quincy	500 - 1000
Norite, Sudbury	340
Diabase, Vinal Haven	170
Gabbro, French Creek	590

*At ordinary pressure and temperature -- selected from "Handbook of Physical Constants", p 92, (Birch, 1953)

The amplitude of a propagating harmonic wave, including both geometrical spreading loss and inelastic attenuation can be written as

$$A = A_o \frac{e^{-\alpha R}}{R} \tag{9}$$

The coefficient of attenuation α is related to $1/Q$ by

$$\alpha = \frac{\pi f}{VQ}$$

where f is the frequency and V is the appropriate phase velocity for the rock and the wave type.

Attenuation curves are shown in Figures 12 and 13 for two values of $1/Q$ which are representative of the range of values contained in Table 1. The ordinate is attenuation in db, referenced to the amplitude A_o of an elastic wave ($\alpha = 0$) at a distance of one meter. The abscissa is frequency. Distance (twice depth of penetration of reflected waves) is the parameter.

21
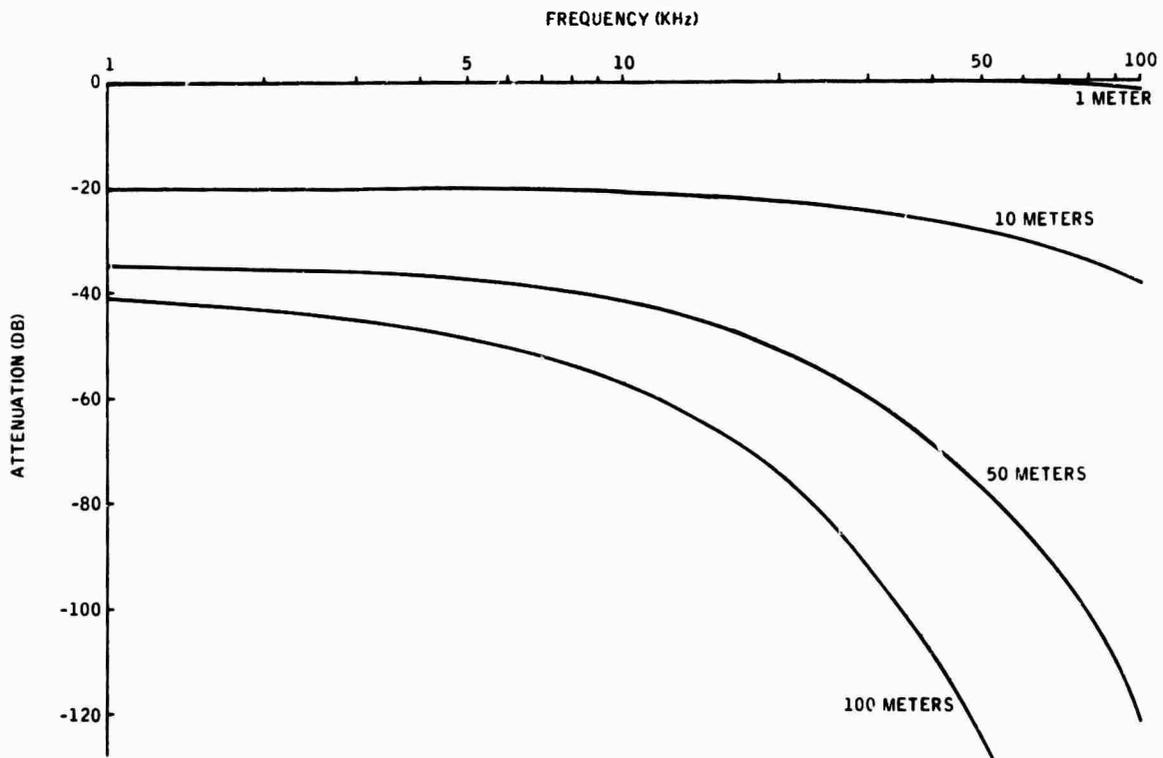
Figure 12. Propagation Loss Referenced to Elastic-Wave Amplitude at 1 meter -- Rock Q = 300
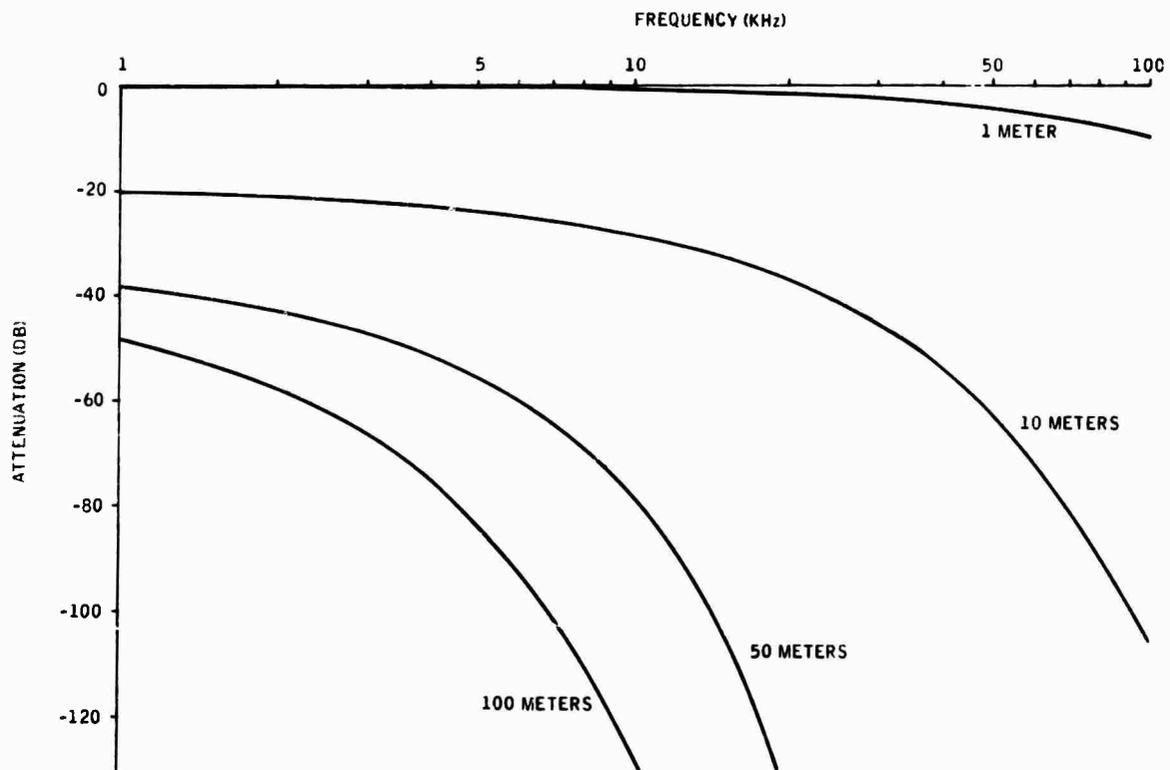
Figure 13. Propagation Loss Referenced to Elastic-Wave Amplitude at 1 meter -- Rock Q = 60

22

2.5.3 Discussion

The advantage of lower frequencies to achieve substantial penetration depths is apparent, particularly in lower-Q rocks such as gneisses as Figure 13 illustrates. On the other hand, Figure 12, which is representative of higher-Q rocks such as limestone or diorite, shows only a modest loss with frequency up to about 10 KHz. For example, a signal processing gain of 36 db with a transducer operating at 10 KHz would provide the same signal-to-noise ratio for a reflector at a depth of 50 meters (R = 100 meters) as the same reflector at a depth of five meters. However, Figure 13 shows that the same situation requires a signal processing gain of 119 db in the lower-Q rocks. Reducing the transmitted frequency to 5KHz reduces the processing gain required to 59 db, which is more easily attained.

The disadvantages of lower frequencies include longer wavelengths with a correspondingly larger source transducer, larger array dimensions, and lowered resolution.

23

SECTION 3

EXPERIMENTAL PROGRAM

3.1 OBJECTIVES

The primary objective of the experimental part of the excavation seismology program is to provide a realistic evaluation of seismic techniques and system components before hardware development is undertaken. This experimental approach seems particularly appropriate because the complexity of seismic/acoustic wave generation, propagation, and detection introduces considerable uncertainty into results based principally on theoretical analysis.

Emphasis during the first six months has been on the field program, supplemented by model studies in the laboratory to provide an initial data base for computer simulations of signal processing techniques and to investigate specific problems under well-controlled conditions.

The initial goals of the field program are:

- To achieve repeatable observed waveforms

- To build up a suite of waveforms for later analysis

The waveform which we observe at the receiver depends on:

- Source waveform from the signal generator

- Transducer response at the receiver and at the transmitter, including effects of coupling to the rock surface

- Propagation effects within the rock volume, including attenuation, reflections, refractions

The first of these is easily controllable, and the third constitutes the desired result. Success of the program depends critically on achieving control over the second factor, namely the effect of the transducers on the seismic waveform. Ideally, the transducers would be broadband devices which would transmit the waveform without distortion. In practice, the transducers do distort the waveform, so that we adopt the lesser but irreducible goal of achieving repeatable and, hopefully, low distortion of the waveform arising from the transducers and their coupling to the rock.

Preceding page blank

To illustrate, consider our proposed analysis methods based on array processing. The seismic waveforms from one receiver position to the next are to be added together (with appropriate time delays) to enhance signals which are in phase. If one receiver distorts the signal in a different manner than the next, the summation may be useless.

The next most important goal of the field program is to build up a data base of waveforms for later processing and analysis. To be of value, these waveforms must be taken only after the first goal, that of achieving repeatable waveforms, has been realized so that transducer effects will be the same on all of the waveforms.

Other goals of the experimental program, stated only in general terms, include the following:

- Compare methods of transducer coupling

- Develop optimum transducers

- Identify noise problems and learn noise characteristics

- Investigate methods of eliminating surface waves

- Evaluate various source waveforms

- Build up experience in hard-rock environment

These goals, however, are subordinate to the initial two.

3.2 DESCRIPTION OF FIELD EXPERIMENTS

The field experiments to date have included two types of measurements:

- Transmission through uniform rock

- Reflection from a free surface

All these experiments have been carried out on St. Cloud grey granite at the Cold Spring Granite Company quarry near St. Cloud, Minnesota.

3.2.1 Transmission Measurements

For the transmission measurements, we selected a large volume of rock of uniform composition positioned so that the transmitter could be placed on one side and the receiver on the other. The thickness of the rock chosen (6 feet) was such that the direct compressional P wave could be observed on

26

the receiver side with a minimum of interference from side reflections, shear waves, and surface waves. The transmitted seismic waveform was then measured and changes observed as appropriate parameters were varied, including receiver location, transducer coupling, source waveform and bandpass filter settings.

The receiver positions for the transmission measurements included a central one directly opposite the source transducer. Subsequent positions were along perpendicular straight lines through the "center" position at 3- to 6-inch intervals to a distance of about 4 feet.

3.2.2 Reflection Measurements

Reflections from a free surface were measured at receiver positions on the same surface of the rock as the source transducer. As in the transmission measurements, the receiver positions were along perpendicular straight lines through the center (in this case, the source transducer) at 3-inch intervals. Seismic signals were recorded on perpendicular lines to simulate both line and crossed arrays, or "spreads".

In contrast to the transmission geometry, this experimental setup would not be expected to provide good measurements of the direct P wave because of the dominant surface wave and diminished amplitude of the P wave radiation pattern of the transducer (Figure 6).

Experimental measurements of reflection from a free surface were chosen for the initial part of the study because:

- They provided the greatest possibility for early success in detecting, identifying and enhancing reflection waveforms

- The free surface is possibly a good representation of a rock fault or fracture.

3.3 FIELD EXPERIMENTAL RESULTS

3.3.1 Impulse Source

The first goal of the field work was to obtain the best possible waveform under the simplest conditions possible. A simple impulse would be the ideal transmitted waveform. Consequently, an impulse was initially used as the source waveform. The source and receiving transducers were aligned on opposite faces of a homogeneous granite mass. The received signal is shown in the top trace of Figure 14 (a).
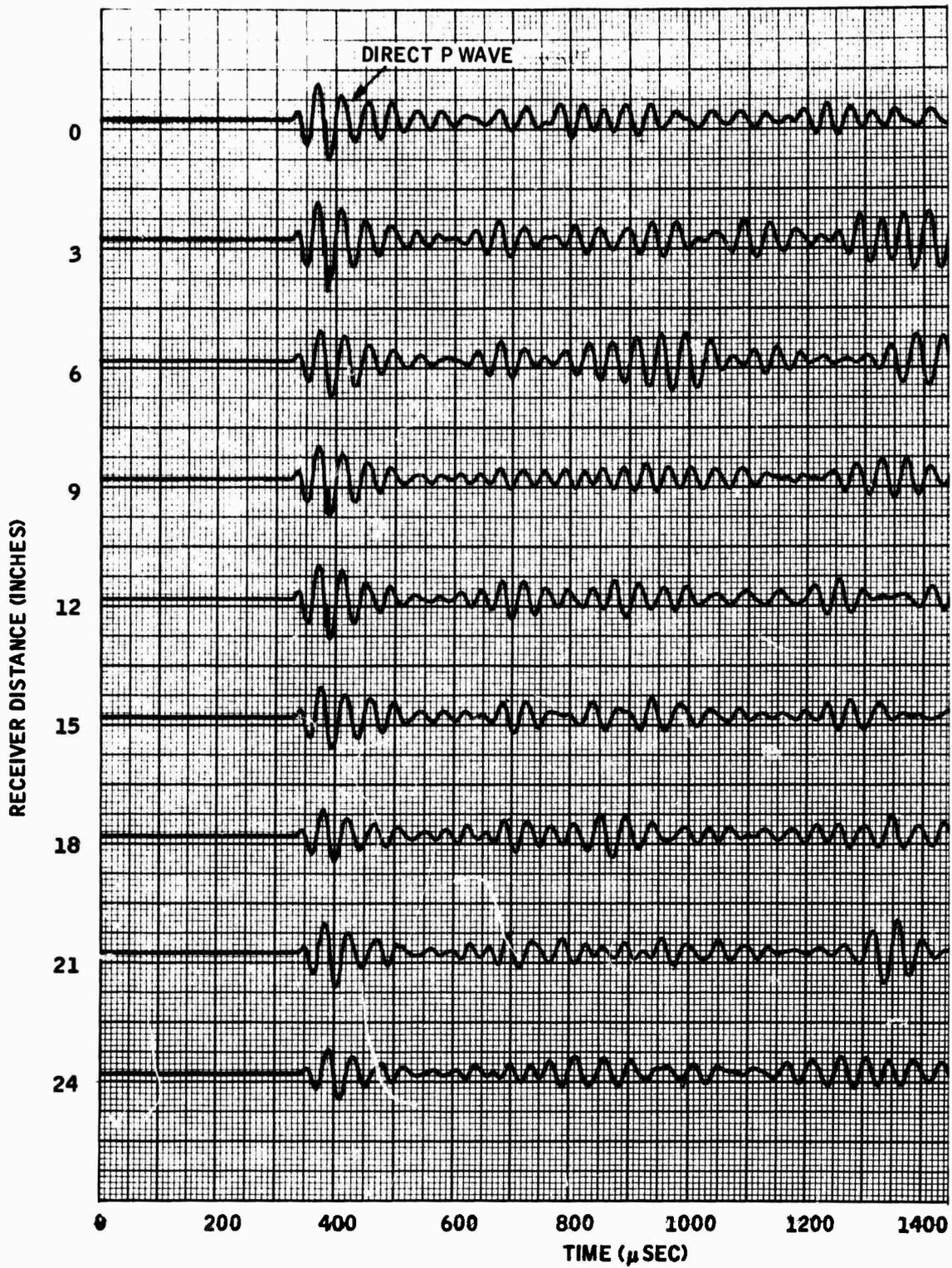
27

Figure 14(a).   Seismic Transmission Through a 6-foot Granite Block
Using an Impulse Source Waveform (receiver positions
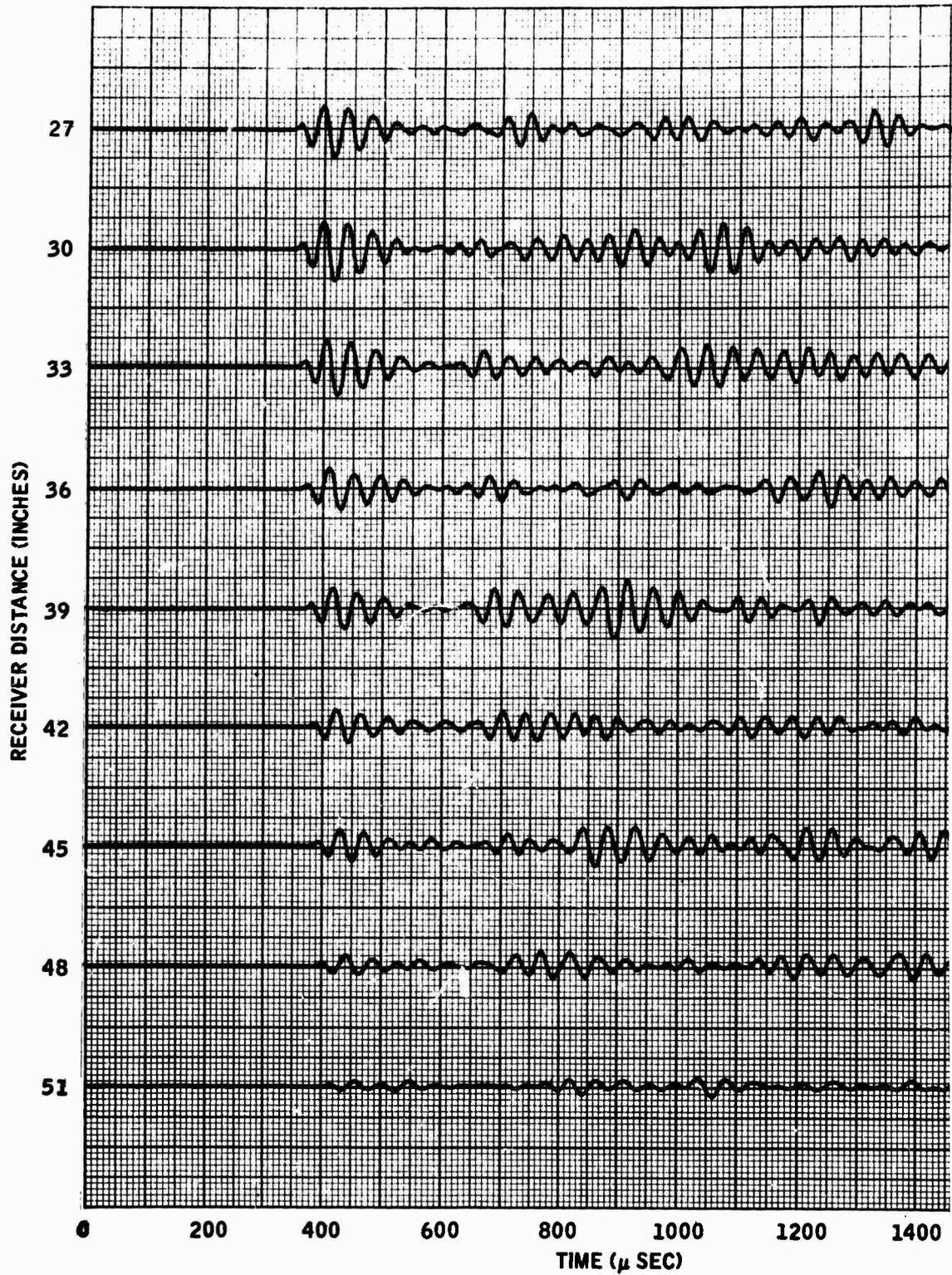out to 24 inches from epicenter)

28

Figure 14(b). Seismic Transmission Through a 6-foot Granite Block
Using an Impulse Source Waveform (receiver positions
beyond 24 inches; reduction in signal beyond 45 inches
apparently results from crack through that station)

29

The earliest arrival is the direct compressional, or P wave, pulse as modified by the transmitting and receiving transducers and the intervening rock medium. The received waveform resembles a narrowband damped sinusoid which grades into following arrivals. It is apparent from the frequency of the damped sinusoid (~20 KHz) that the distortion results from "ringing" of the source transducer at its fundamental resonant frequency. Efforts were made to reduce the ringing by improving the coupling between the transducer and the rock load, but no substantial improvement resulted.

The remainder of the traces in Figure 14 were recorded at 3-inch intervals along a straight line as described previously. The seismic source was kept fixed. The receiver accelerometer was moved to each successive position between records. The accelerometer was held in place while each record was made, with a thin layer of petroleum jelly used for coupling to the rock. Comparisons of the P wave arrivals on the records of Figure 14 demonstrated a high degree of coherence and repeatability of the seismic source waveform despite its ringing character.

A similar set of waveforms from an impulse excitation were recorded at receiver positions on the same rock surface as the source transducer (Figure 15). The predominant early arrival is the Rayleigh surface wave, consisting of several cycles of ringing at the fundamental resonant frequency of the source transducer superimposed on a higher-frequency oscillation which probably results from another transducer mode resonance. This higher-frequency oscillation is attenuated rapidly in propagation through the rock and has essentially disappeared at a source-receiver separation of about 36 inches (it was also not in evidence on the transmitted P wave, Figure 14).

The reflected PP wave is clearly visible at about 800 microseconds, particularly at receiver distances greater than 6 inches. Again, the narrowband ringing character of the wave detracts from the ability to distinguish it from other possible arrivals.

The time of arrival (peaks and valleys) for those waves which could be identified are plotted in Figure 16 versus receiver distance for the data of Figure 15. The readily identifiable waves are the small-amplitude P wave, the predominant surface wave and the PP reflection.

3.3.2 Source Waveform Optimization

Various other types of source waveforms, including step function and single-cycle sine waves, were investigated experimentally in an attempt to more nearly approach the ideal seismic impulse. The source waveform which best meets this requirement consists of a combination of two pulses as developed by Brown (1956) for seismic model investigations.

30

Figure 15(a). Reflection Seismogram Using Impulse Source Waveform
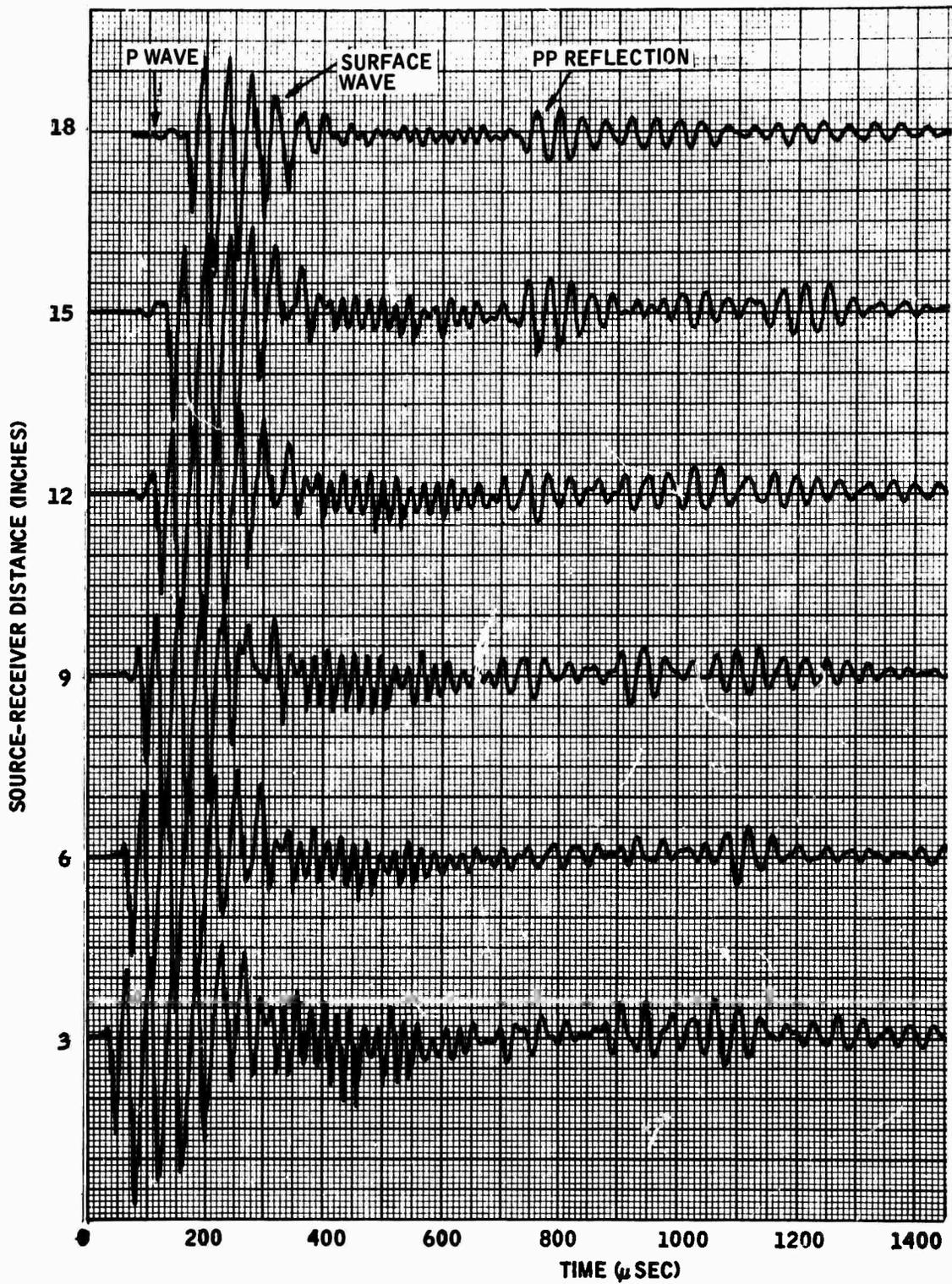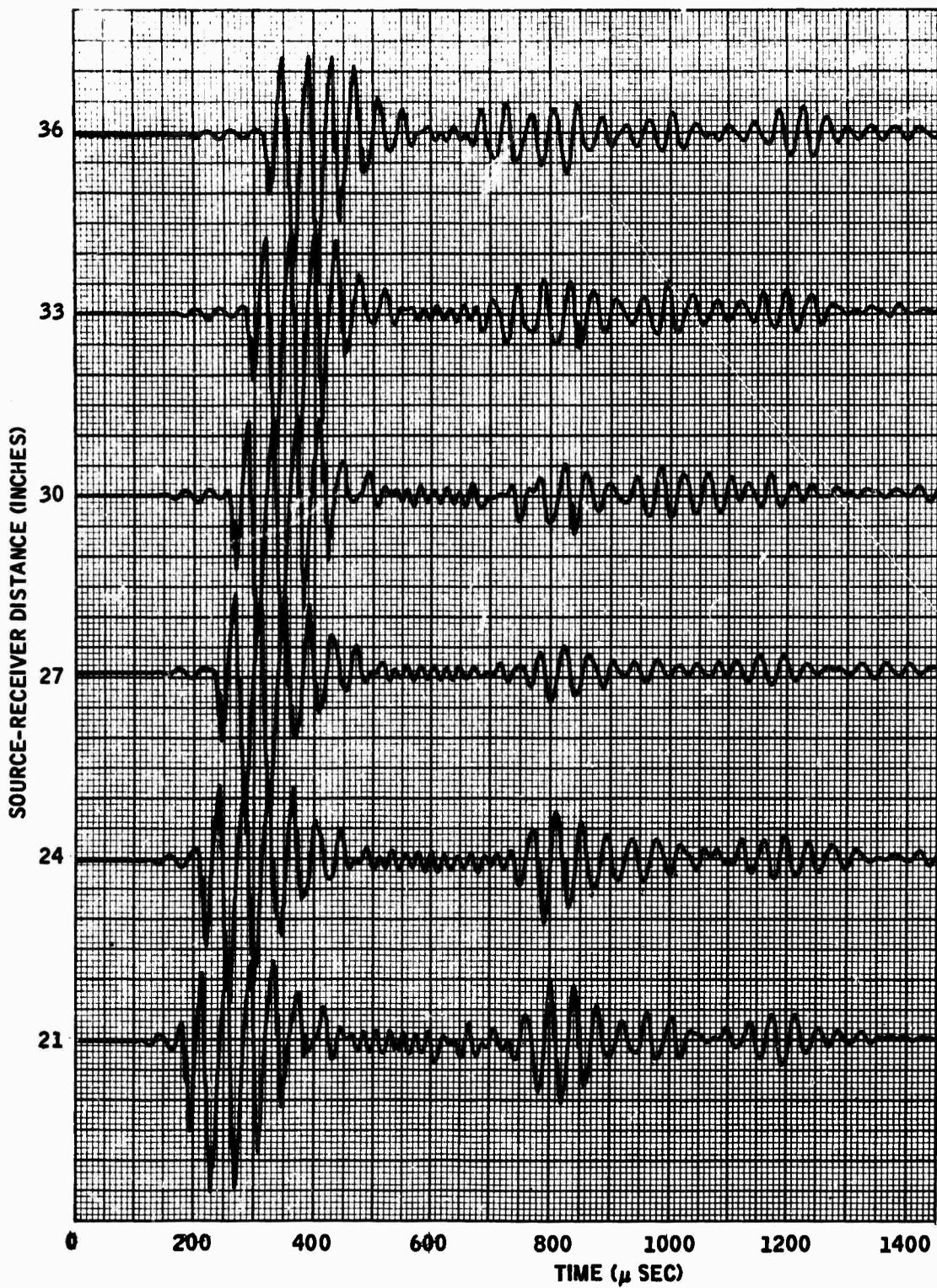(receivers in-line with source to 18 inches)

31

Figure 15(b). Reflection Seismogram Using Impulse Source Waveform
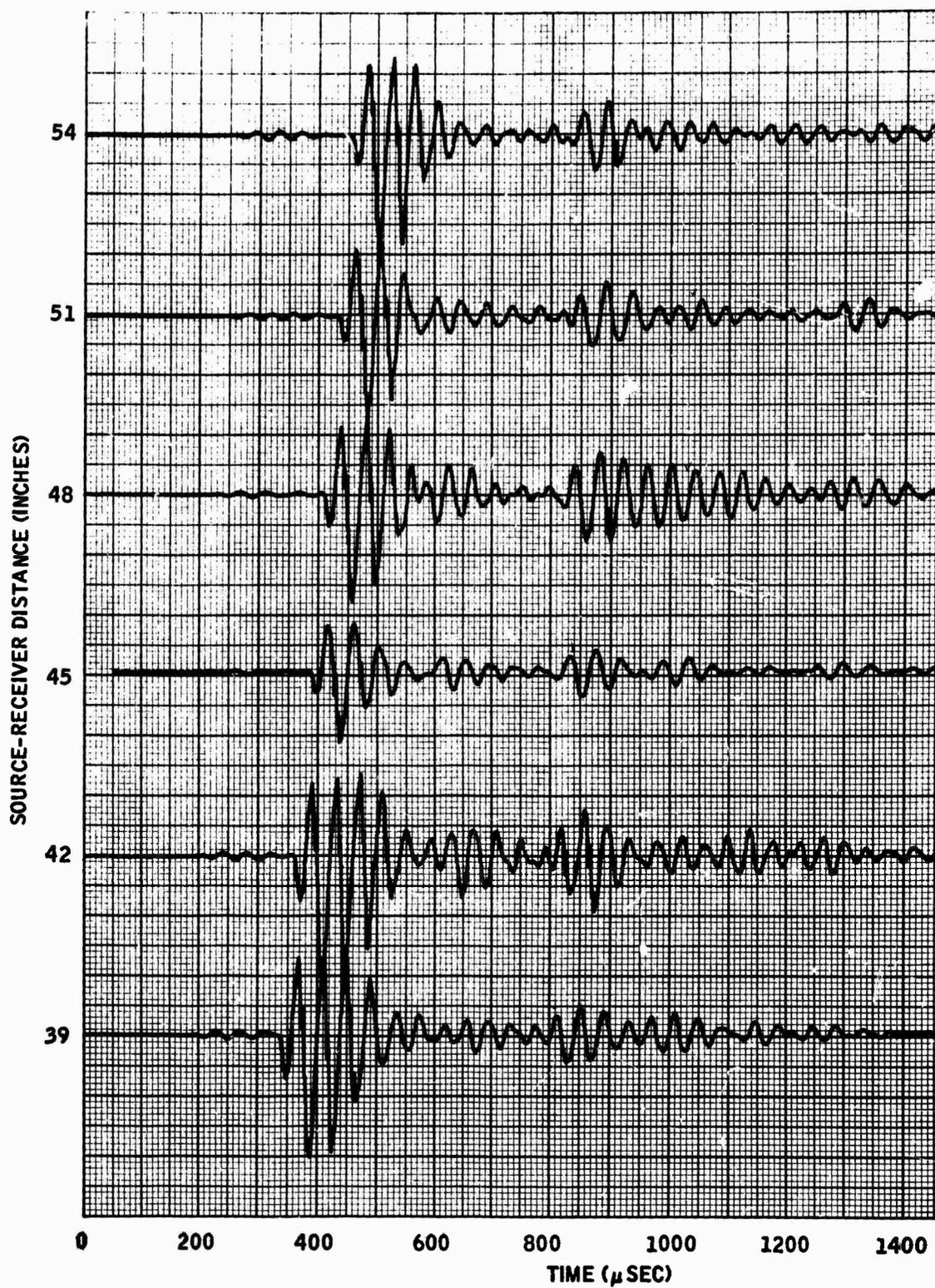(receivers in-line with source from 21 to 36 inches)

32

Figure 15(c). Reflection Seismogram Using Impulse Source Waveform
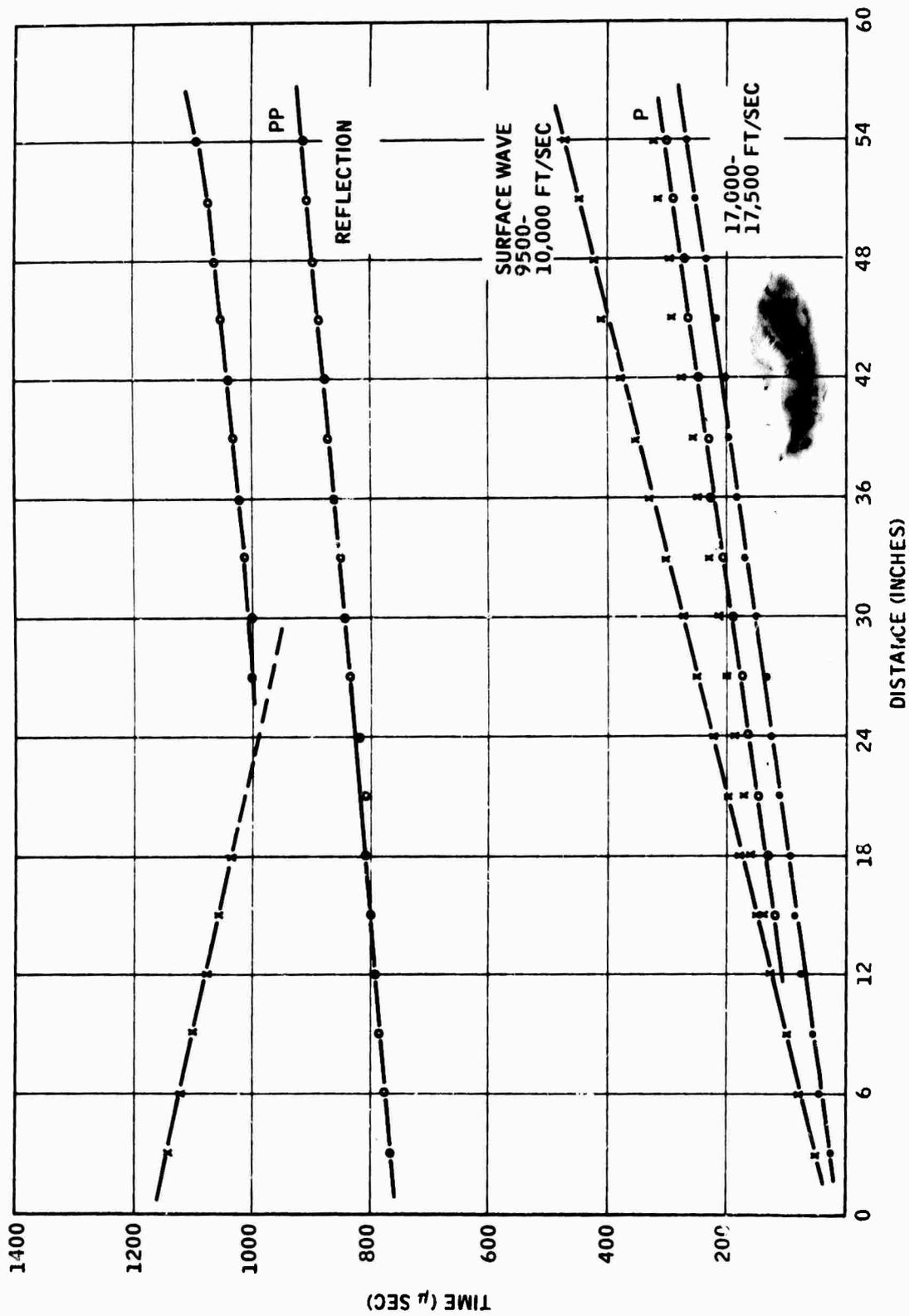(receivers in-line with source from 39 to 54 inches)

33

Figure 16. Travel-Time Curves for the Data of Figure 15

34

In his dissertation, Brown derived the form of the electric field required to produce known simple transient stresses on the surface of a solid medium using a longitudinal piezoelectric transducer. The required excitation consists of the sum of two pulses, with different durations and amplitudes (Figure 17). The duration of the second pulse must be equal to the time it takes a signal to travel twice the length of the transducer. The fundamental resonance frequency of the transducer is determined physically by the same two-way propagation time, so that the required time T is the same as the period of the fundamental transducer resonance.

The amplitude required for the second pulse, relative to the first, depends in theory on the characteristic acoustic impedances of the transducer material and the rock. Since these will not be known with the necessary degree of accuracy, it is necessary to experimentally adjust the amplitude of the second step to achieve the desired result.

In Figure 18, the two-level drive pulse voltage is shown as it appears across the transducer. The small oscillations occurring after the first level change are voltage fluctuations produced by the mechanical "ringing" of the transducer at its fundamental resonant frequency due to the piezoelectric effect. The following procedure was successfully used to optimize the parameters of the two-level drive pulse to reduce the ringing to a minimum and thereby produce a simple transmitted seismic pulse:

- The duration, T, of the second pulse was set equal to the period of the ringing as observed on an oscilloscope.

- The amplitude V_2 of the second pulse was adjusted to minimize the ringing as observed on the oscilloscope. The oscillations reverse in polarity at the minimum, so the adjustment is quite simple.

- The duration of the first pulse was set equal to or greater than the greatest time of interest on the received seismic signal.

The upper trace is the received seismic signal when the source function below was used to drive the transducer on a small granite block in the laboratory. The absence of ringing is apparent on the P wave. The large later arrivals consist primarily of surface waves.

3.3.3 Field Experiments Using a Two-Level Pulse

Seismic transmission and reflection profiles were recorded using the two-level waveform as the source excitation voltage. The source transducer and receiver locations were the same as described previously for an

PULSE GENERATOR 1

ADD

PULSE GENERATOR 2

(TRIGGERED FROM SAME SIGNAL)

(a)

V_1

V_2

(V$_2$ AND T CAN BE ADJUSTED TO PRODUCE SHORTEST IMPULSE RESPONSE)

(b)
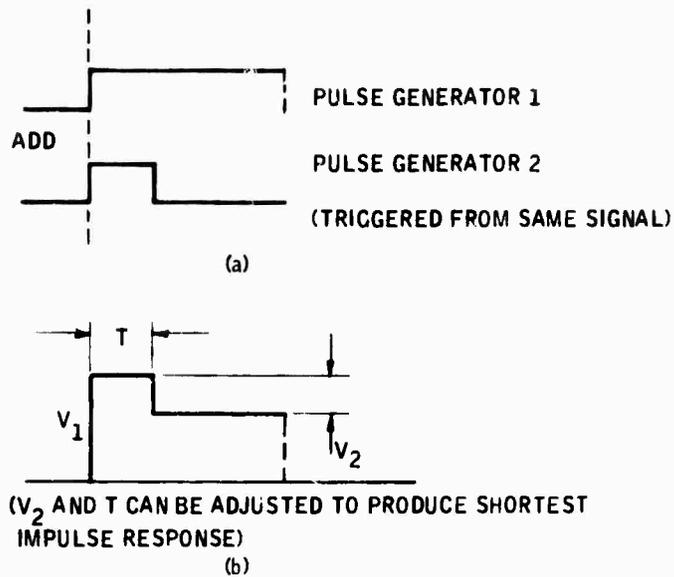
Figure 17.   Two-Level Waveform Producing a Simple Seismic Pulse

TIME OF INITIAL STEP

SECONDARY PIEZOELECTRIC EFFECT (OSCILLATIONS)

SIMPLE P-WAVE

BOTH STEPS TURNED OFF

RECEIVED SIGNAL

INPUT WAVEFORM

TIME OF SECOND STEP
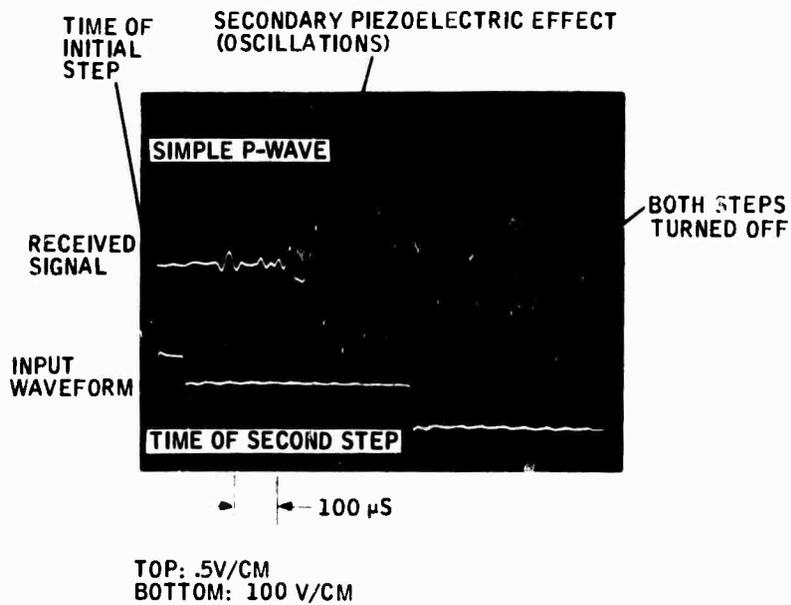
100 µS

TOP: .5V/CM
BOTTOM: 100 V/CM

Figure 18.   Effect of Two-Level Drive Pulse

36

impulse source voltage. The parameters of the drive voltage were optimized according to the procedure prescribed above and were not readjusted during the recording of the data.

Figure 19 contains the seismic transmission measurements using the two-level source waveform, with the receiver locations the same as for the previous measurements for the impulse source function (Figure 14). Comparison of these two sets of data, particularly the first-arriving P wave, shows that the ringing has been significantly reduced with the two-level drive pulse, resulting in a more suitable waveform for seismic methods.

The reflection measurements, corresponding to Figure 15 for the impulse, are contained in Figure 20. Comparison of these two figures illustrates the shortening of the surface-wave duration, the reduction of the high-frequency ringing in the transducer, and the ease with which more seismic events can detected. For example, the reflected surface wave from the edge of the rock is readily observed. Figure 21 is a travel-time plot for this data, which can be compared with Figure 16.

3.4 FIELD INSTRUMENTATION

A block diagram of the basic elements of the field instrumentation is presented in Figure 22. The seismic source repetitively transmits an acoustic signal into the rock volume. Timing and control circuits provide a trigger for the seismic source and establish the repetition rate. The timing and control circuits also provide synchronization and gating pulses to the display and recording elements. The received signal, after amplification and filtering, is displayed in real time on an oscilloscope and recorded both on analog magnetic tape and chart recorders for subsequent analysis and processing.

3.4.1 Seismic Source

The seismic source consists of signal generator, amplifier, and piezo-electric transducer. The signal generator consists of two commercial pulse generators, Wavetek Model 134 VCG and Data Pulse Model 110A, whose outputs are summed to provide the double-pulse waveform required to minimize transducer ringing. Also, the Wavetek generator is used by itself to provide tone bursts, impulses, and other functions for comparative source waveform investigations.

The waveform from the signal generator is amplified by a McIntosh 60-watt power amplifier which provides up to 200 volts across the transducer with an output impedance of 600 ohms. The frequency response is substantially flat up to 100 KHz.

37
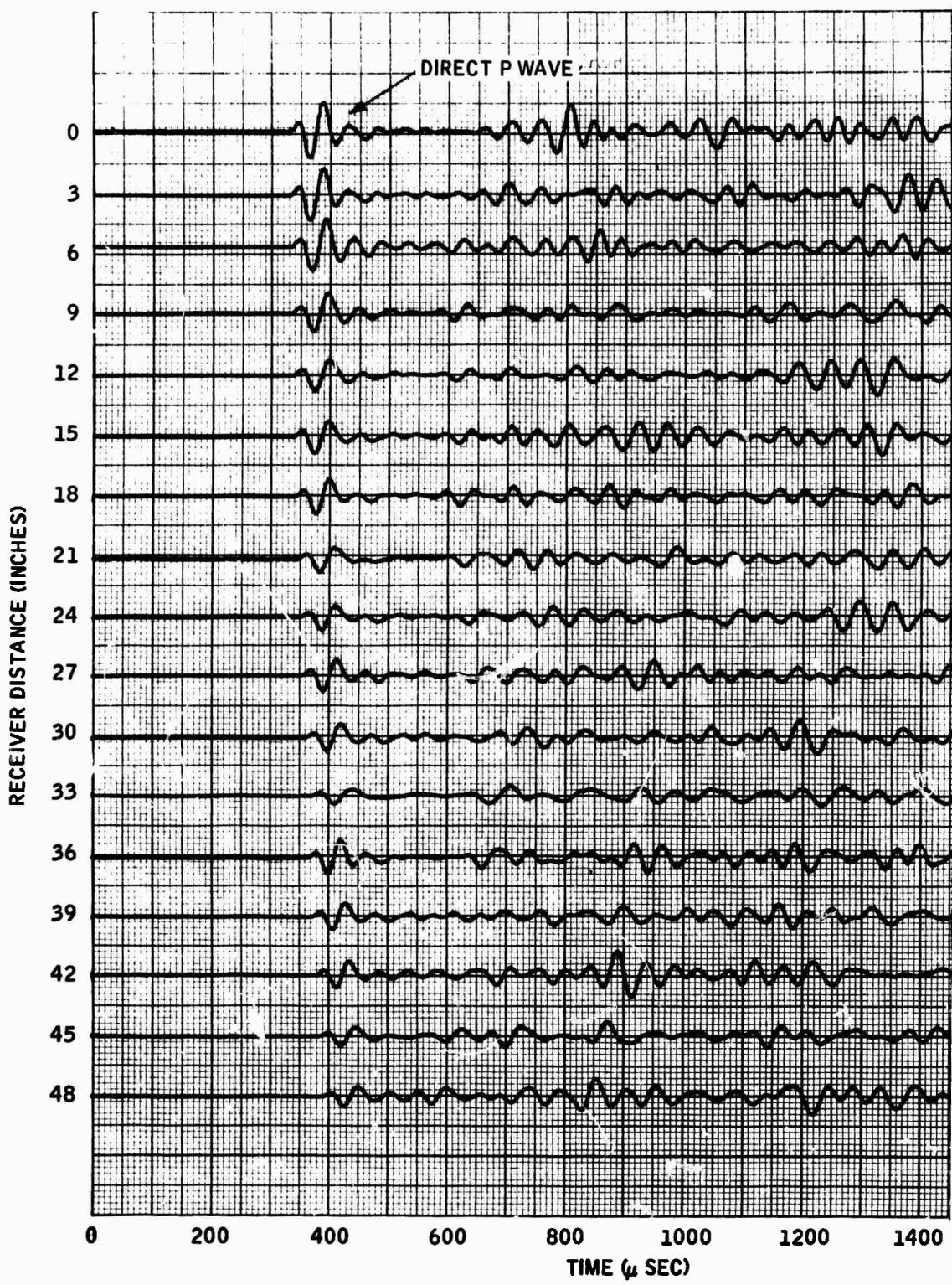
Figure 19. Seismic Transmission Through a 6-foot Granite Block Using a Two-Level Pulse Source Waveform
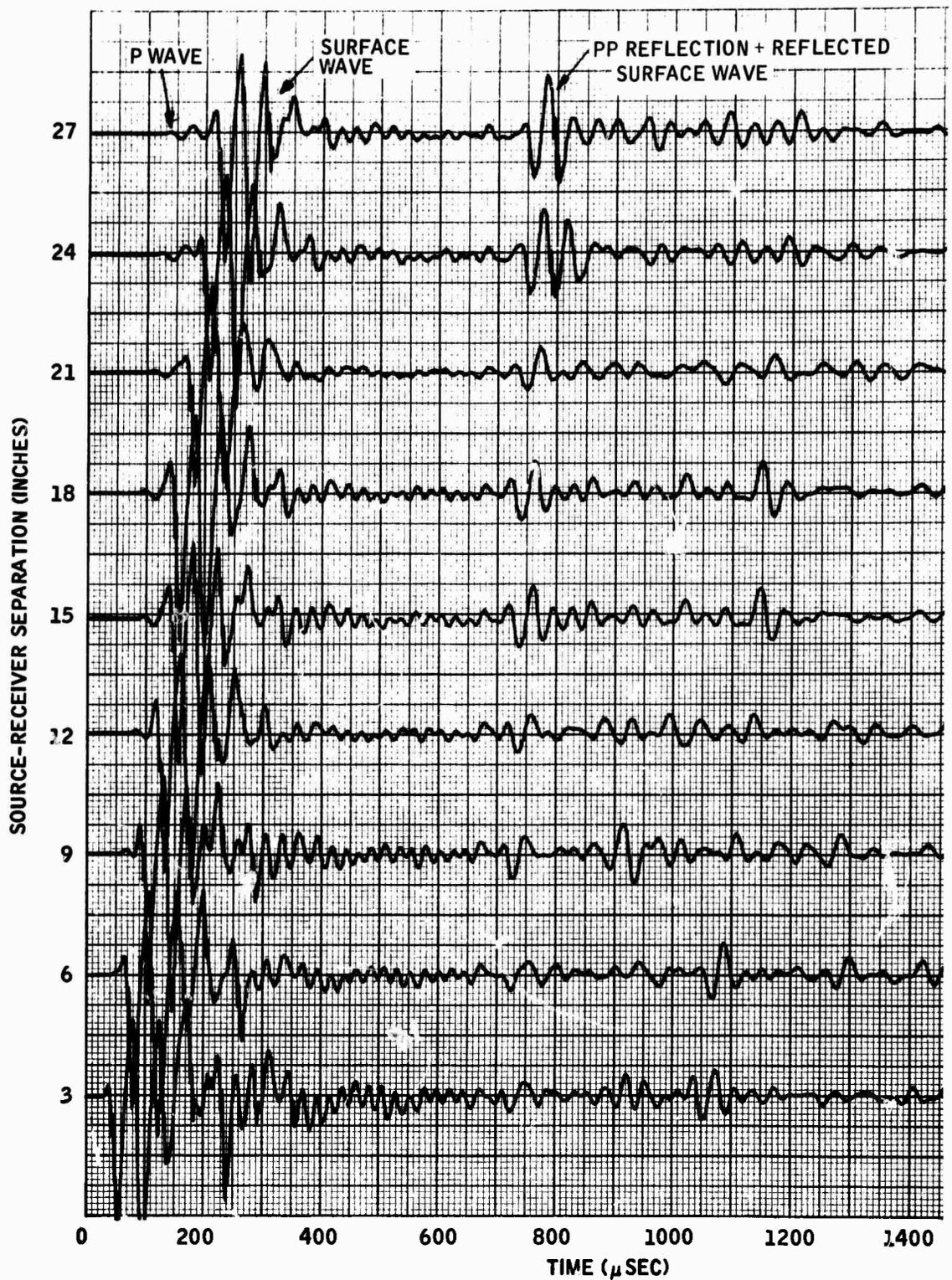
Figure 20(a). Reflection Seismogram Using Two-Level Pulse Source
Waveform, Producing a Simple Seismic Signal
(receiver in-line with source to 27 inches)

39
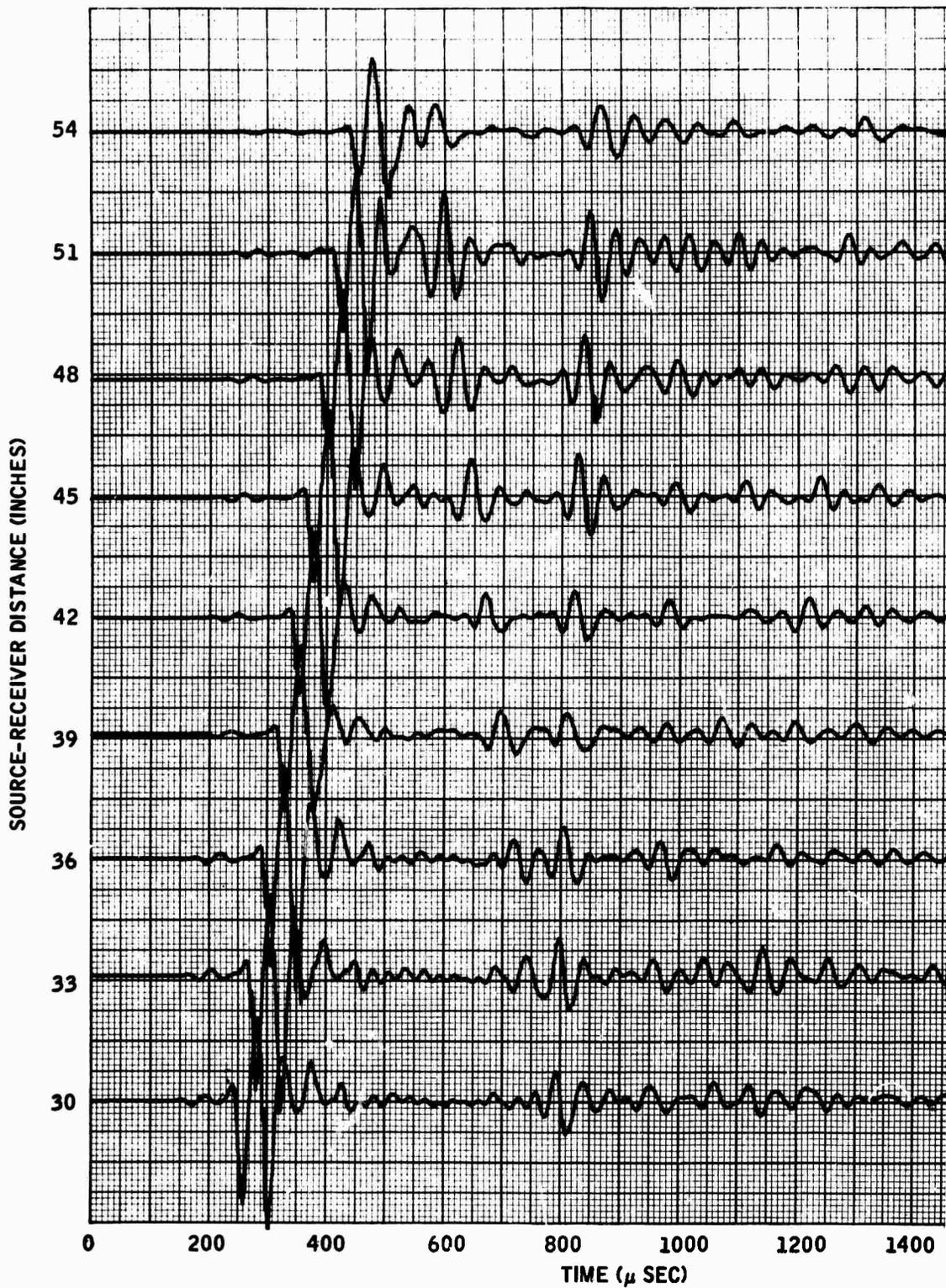
Figure 20(b). Reflection Seismogram Using Two-Level Pulse Source
Waveform, Producing a Simple Seismic Signal
(receivers in-line with source from 30 to 54 inches)

40
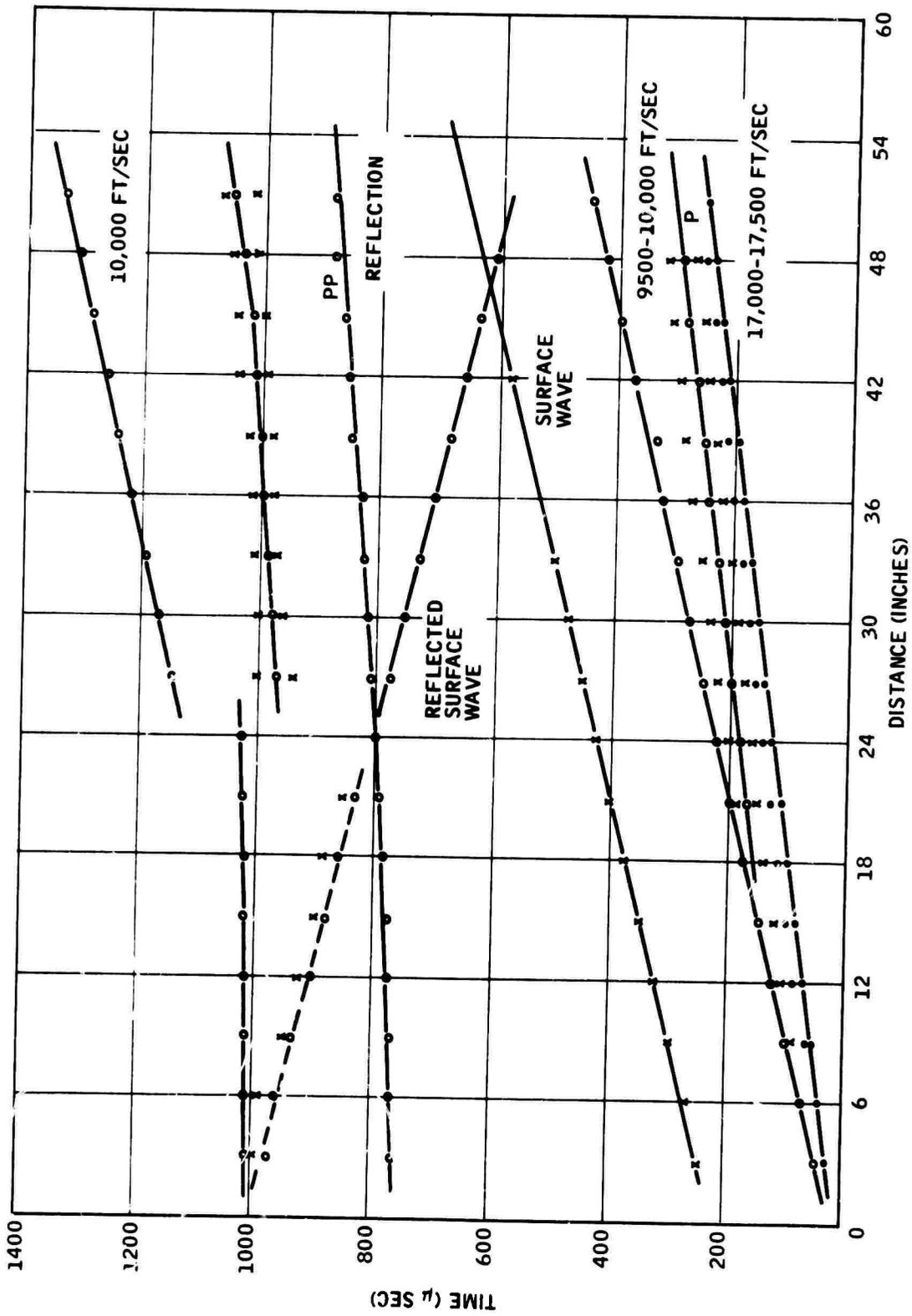
Figure 21. Travel-Time Curves for Data of Figure 20

41
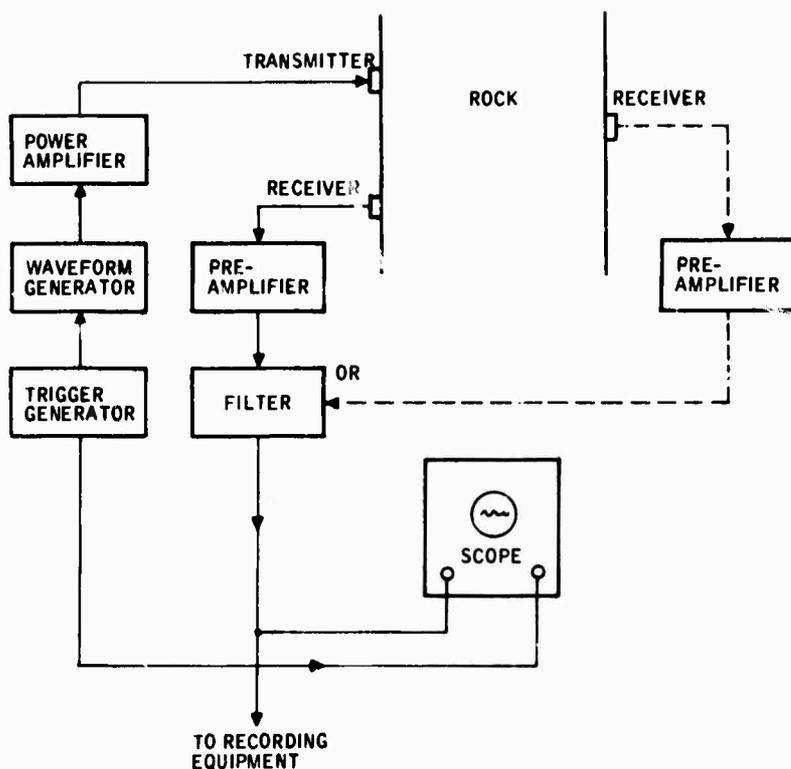
Figure 22. Basic Elements of Field Instrumentation

The piezoelectric transducers used were fabricated by Honeywell for this program. These are longitudinal transducers, which provide a piston-like motion at the transducer-rock interface. Eight active elements are stacked as shown in Figure 23. The elements are electrically in parallel with a resulting static capacitance of 0.013 microfarad. The material used is Honeywell K-type, similar in properties to PZT-4, and it provides a K_{33} coupling coefficient for the stack of 0.65.

Several other transducers with fewer active elements were constructed, all of them half-wavelength cylinders designed to be resonant at 20 KHz. The piezoelectric K-type ceramic was used for the active piezoelectric elements, either with brass backing or directly air-backed Aluminum, bonded to the front surface of the ceramic, provided the coupling to the rock. A thin layer of petroleum jelly between the transducer and the rock excludes air in the interface and maximizes power transfer.

42

NOTE:
ARROWS INDICATE POLARIZATION (ELEMENTS IN
STACK ARE ELECTRICALLY PARALLEL, MECHANICALLY
IN SERIES). LENGTH = 2.5 INCHES, DIAMETER =
1.4 INCHES, CENTER MOUNTING HOLE DIAMETER =
0.4 INCH.
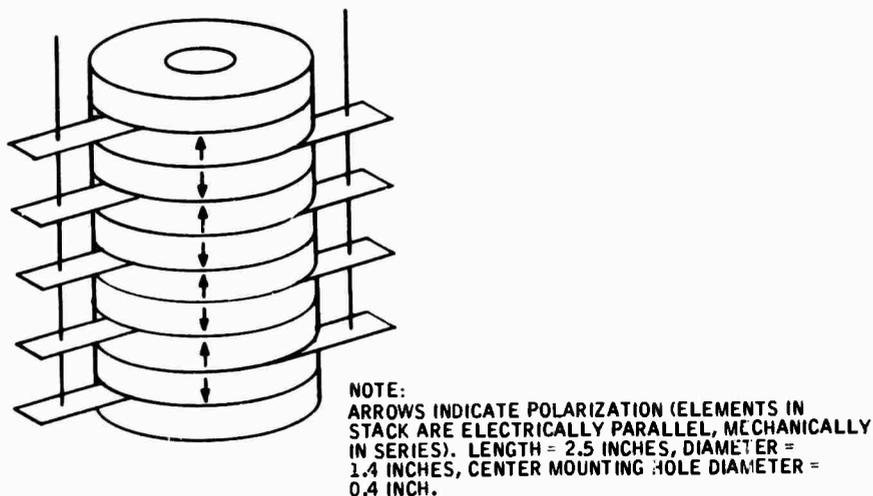
Figure 23.   Piezoelectric Transducer Used for Field
Experiments

A single hole was provided along the axis of the transducer to allow the
transducer to be bolted to the rock. While this method of mounting appears
to be satisfactory, it was found to be more convenient in the early stages
of the field work to hold the transducer firmly pressed against the rock with
a laboratory jack.

3.4.2 Receiver

The receiver includes an Endevco Model 2225 accelerometer which has
a high resonant frequency (80 KHz) for minimum distortion in the received
waveform. The nominal sensitivity of the transducer is 0.65 mv/g. Trans-
ducer capacitance is 800 pF.

The accelerometer output is amplified by a battery-powered voltage
preamplifier made by Radiation Electronics, Inc. (Model TA-5) which
provides switch-selected voltage gains of 20, 40 and 60 db. The input
resistance and capacitance of the connecting cable and amplifier are 370K
ohms and   38 pF, respectively. The amplified signal is filtered by a
Krohn-Hite Model 3100 bandpass filter. The low-frequency cutoff was set
at 100 Hz to reduce 60-Hz interference, the high-frequency cutoff varied
from 30 KHz to 60 KHz; the actual settings were not at all critical.

The accelerometer was mounted on the rock surface at each successive
receiver position and the received waveforms recorded. Various methods
of mounting were tried, including cementing with model plaster, petroleum
jelly, and Permatex nonhardening gasket cement. The most suitable
approach was simply to hold the transducer in position with a thin coupling
layer of petroleum jelly.

43

3.4.3 Recording and Display

The received signal is displayed on an oscilloscope (HP Model 180A) with the sweep triggered externally by the same initiating pulse used to trigger the source signal generator. The received signal is also sampled. The sample-and-hold circuit is triggered by a pulse from the timing and control circuitry. The sampling trigger pulse is delayed with respect to the pulse which triggers the seismic source. Each time the source is triggered, the sampling pulse time delay is incremented, thereby slowly sweeping the sample time through the received seismic waveform. The delay is initially set to zero manually by a pushbutton switch.

The output of the sample-and-hold circuit is identical to the seismic waveform displayed on the oscilloscope, but with a greatly expanded time base. The longer time base permits the permanent recording of the waveform on a Honeywell Model 550 X-Y recorder and on an FM channel of the Ampex FR-1300 magnetic tape recorder for later analysis and array processing experiments. Also recorded on magnetic tape are a pulse from the pushbutton initiating the slow sweep and a time-coded reference which is used for indexing and later identification of the recorded signal. The recorded initiating pulse provides a means of re-establishing precise time and synchronization relations for such subsequent processing as analog-to-digital conversion.

A two-channel Brush, Model 220 strip chart recorder is used to monitor the tape-recorded signals as they are recorded. The time-coded reference is recorded on the strip chart, using the event marker pen. Any recorded waveform can then be relocated on the magnetic tape using the common time code. Descriptive annotations such as receiver location are written directly on the strip chart, and other pertinent information is recorded in a log book.

3.4.4 Timing and Control

The timing and control equipment includes an Eldorado Model 1710 time code generator, two Beckmann Model 6014 preset accumulators, and a pushbutton switch. The time code generator provides a precise 1-MHz oscillator signal as well as the time-coded signals for use as described above. The Beckmann accumulators count the 1-MHz pulses to a preset value. When the preset value is reached, the counters automatically reset, provide an output pulse, and begin counting again. Thus, if the number preset on one counter is N, the counter sends out a pulse every N microseconds. This pulse provides the trigger for the seismic source and the oscilloscope sweep. The second counter is set to $N + n$ and sends out a pulse every $N + n$ microseconds. This pulse is used to trigger the sample-and-hold circuit.

44

Typical values used are N = 50,000 and n = 2. Initially, the two counters are reset simultaneously with the manual pushbutton. After 50,000 micro-seconds and every 50,000 microseconds thereafter, that counter sends out a master trigger pulse, resulting in source repetition rate of 20 per second. The second counter sends out pulses at 50,002 microseconds, 100,004 micro-seconds, etc., which consequently follow the master trigger pulse at intervals of 2 microseconds, 4 microseconds, etc. Thus, each sample occurs 2 microseconds later on the received seismic waveform than the previous sample. Since one sample, representing an increment of 2 microseconds of real time, is recorded every 50,000 microseconds, the time base is expanded by a factor of 50,000/2, or 25,000. Frequencies are compressed by the same ratio, so that the nominally 20,000-Hz seismic signals become 0.8 Hz for recording purposes.

The push button is used to simultaneously reset the two counters to zero and to initiate the internal sweep of the X-Y recorder.

Figure 24 is a block diagram of the system used for field recording, including seismic source, receiver, display and recording, and timing and control elements.

3.5 SEISMIC MODEL STUDIES SUMMARY

The laboratory model represents the use of a receiver and/or source array to achieve simple and easily controlled experimental conditions.

The methods of two-dimensional seismology employed are similar to those described by Oliver, et al (1954). A waveform generator is used to trigger the pulse generated and initiate the oscilloscope sweep simultaneously. The pulse is applied to a piezeoelectric transducer (PZ-PT) which is in contact with the model. The resulting vibrations are detected by a similar transducer receiver and displayed on the oscilloscope. The oscilloscope trace is recorded photographically.

From travel-time curves, the P-wave velocity was found to be 2350 m/sec and the surface-wave velocity 1175 m/sec. For the small model (5 x 1 feet) the outstanding events on the seismogram are PP, surface waves, PPPP, and reflected surface waves from the sides of the model. For large model (4 x 3 feet) the reflected wave could be recognized up to a certain separation between the source and receiver, after which the surface waves cause interference and reflection is no longer recognized.

To block the interfering surface waves, a cut was made on one of the models. The cut succeeded in eliminating certain interfering waves, but
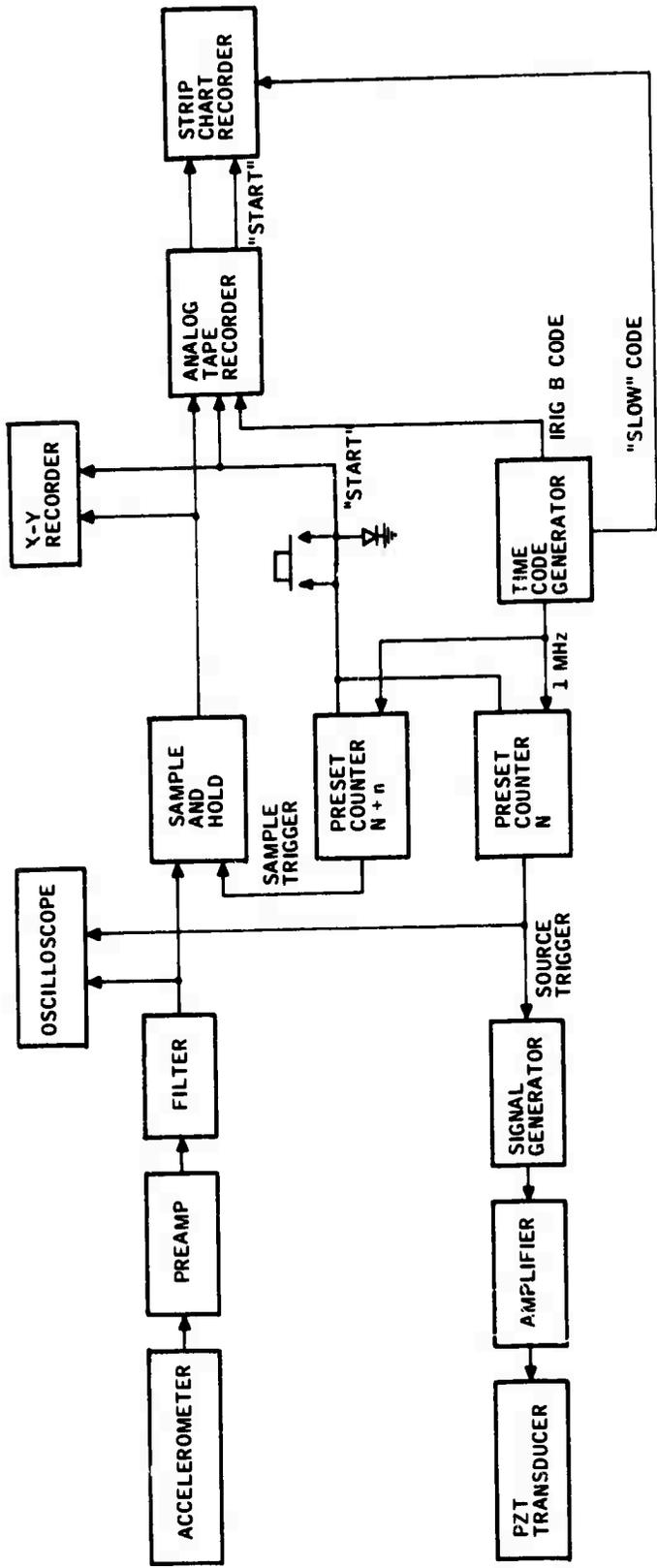
45

Figure 24. Field Recording System

it introduced a diffracted wave which complicated the seismogram to a great extent. Another experiment to block surface waves was the sinking of the source in the model. Theoretical calculations for these seismograms are under way in an effort to understand the nature of the arrivals.

3.6 MODEL DESCRIPTION

The general arrangement of the equipment used in the two-dimensional model studies is shown schematically in Figure 25. The arrangement is very similar to that used by Oliver et al (1954).

The high-voltage pulse drives the piezoelectric transducer where conversion of electrical to mechanical energy takes place. At the transducer the energy in the form of mechanical pulse is transmitted to the model and travels through to the receiver as a sonic pulse. There the mechanical energy is converted back to an electric pulse, amplified by preamplifiers and displayed on an oscilloscope as an upward (or downward) deflection of the sweep which is triggered by the transmitted pulse. This completes the operating cycle. When the operating cycle is repeated regularly, the display on the oscilloscope screen will appear as continuous. The pulses being uniformly the same, the display of pulse arrivals are steady and can easily be photographed.

3.6.1 Types of Models

The first two-dimensional model was a thin sheet of plexiglass (5 x 1 feet). Measurements made by positioning the transmitter and receiver on the same edge of the model, as shown in Figure 25, result in studying the reflection from the opposite edge of the model.

Since the model is only 1 foot wide, the time for the reflected wave PP is very small and seems to appear very near the first arrival.

A second model, also a plexiglass sheet (4 x 3 feet) was then used. The results for reflection were satisfactory with this model, but it was observed that, after the separation between transmitter and receiver became large, the surface waves dominated the waveform, and the reflected signal became difficult to recognize.

3.6.2 Electronic Components

A Tektronix type 162 waveform generator was used to trigger the pulse generator and initiate the oscilloscope sweep simultaneously. This unit could also be triggered manually. A Tektronix type 160A power supply was used to furnish power for the waveform generator and pulse generator.
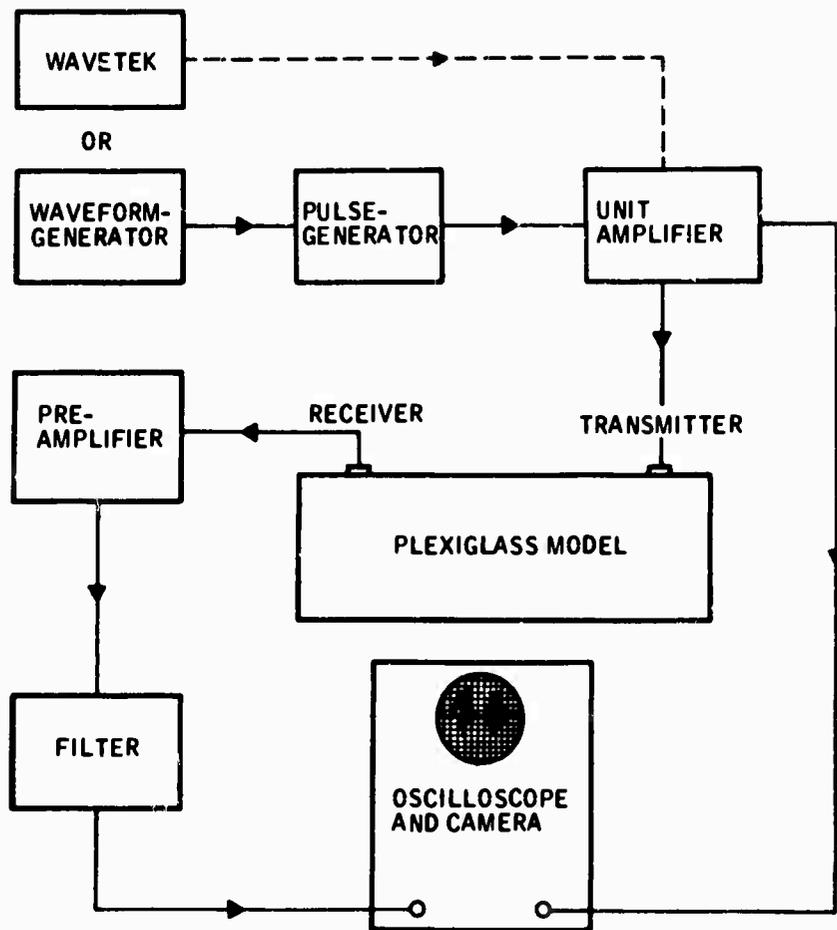
47

Figure 25. Seismic Model Instrumentation

It is also possible to get pulses using a Wavetek model 134 sweep generator. The mode dial may be set at toneburst to produce a single pulse or a number of pulses whose rate, frequency and length can be controlled.

For most of the experiments an impulse was used as the input signal to the transmitter. Before the signal is passed to the transmitter it is amplified by the unit amplifier General Electric type 1206B. The gain is controlled with a variable voltage knob.

A Tektronix type 502A dual-beam oscilloscope is used for the display. To photograph the records, a Wollensak camera with Polaroid back is used. Film is high-speed (3000) Polaroid type 47, exposure time is 1 second and the lens opening is f16. The camera back is movable, thus permitting several exposures on the same print.

As the receiver is moved away from the transmitter, it becomes necessary to amplify the signal. For this purpose a Burr-Brown model 100AC decade amplifier is used. This is a transistorized unit with a gain of 100 and frequency response up to 800 KHz.

A filter system is necessary to eliminate external electromagnetic and acoustic noise that is picked up and amplified. Different sources of electromagnetic and acoustic noises are flourescent lamps, switches, normal 60-cycle hum, movement in the laboratory, machinery in the building, etc.

For this purpose a commercial Krohn-Hite 3500 variable bandpass filter is used. For a signal amplification of 100 it is found that setting the low cutoff dial at 3 KHz effectively eliminates ordinary electromagnetic and acoustic noise.

3.6.3 Ceramic Transducers

For the transmitter and receiver, ceramic transducers with high mechanical Q, lead zirconate-lead titanate (PZ-PT) ceramics materials are used. These were obtained from the Honeywell Ceramic Department and are K-type materials in various shapes and sizes. Those used in the experiment are cylindrical with a length of 0.7 cm and a diameter of 0.8 cm. This size transducer is used for the transmitter only. For the receiver, a smaller size gives better results. The receiver transducer is also cylindrical in shape but measures 0.35 x 0.5 cm.

3.6.4 Mechanical Arrangements

Devices to hold the transducers were constructed as shown in Figure 26. The holders provide both mechanical mounting for the transducers against the model and also a means for applying an electrical signal across the transducers.
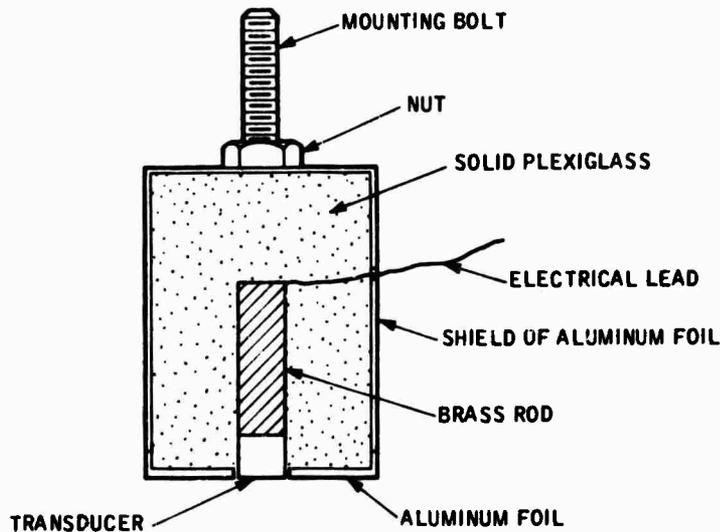
49

Figure 26. Transducer Holder

For the transmitter assembly, a brass rod 1/2 inch long and the same diameter as that of transducer is used for backing. In this case the rod also serves the purpose of electrical connection. For the receiver assembly, a 1/2 inch aluminum rod with same diameter as that of the small receiver transducer is used. It was noticed that use of brass or aluminum as backing material does not change the waveform significantly.

Brackets to support both the model and the transducer holders were constructed first to hold the small model (5 x 1 feet) only, but later as larger models (4 x 3 feet) were used, the transducer holders were held against the model by using chemical test tube stands. As the transducer position is changed on the model, it is necessary to make sure that the transducers are forced against the model in the same manner for successive positions. For this purpose the present mechanical arrangement is not adequate and needs further modifications, especially for detailed amplitude studies.

3.7 EXPERIMENTS WITH SINGLE-LAYER MODEL

3.7.1 Small Model

The small model consists of a 5 x 1 foot plexiglass sheet. The transmitter is placed 22 cm from one side of the model, and the receiver is moved successively on the model at 10 cm spacing.

The seismograms of Figure 27 are photographic recordings of the oscilloscope waveform for successive receiver positions. Throughout the experiment the position of the transmitter was kept fixed. Thus the only variable is the receiver position.

50

Several arrivals can easily be identified on the seismogram of Figure 27. The most obvious arrivals are plotted on a travel-time curve in Figure 28. All of the plotted points are calculated from peaks and troughs rather than first motion. Some theoretically calculated arrivals are also plotted as dotted lines. For detailed and accurate identification of the arrivals, more theoretical arrivals have to be calculated. The slight variations in the observed and the theoretical travel-times is because the observed arrivals represent peaks and troughs rather than first motion.

From the slopes of the lines in the travel-time curve, the P-wave velocity is found to be 2350 m/sec and the surface wave velocity 1175 m/sec. It was not possible to identify the direct S-wave on the seismogram. Previous studies also indicate this difficulty in identifying the direct S-wave.

The outstanding events on the seismograms are identified as PP, PPPP, surface waves, and reflected surface waves from the sides of the model.

The amplitudes of the first arrivals are very small as compared to the later surface-wave arrivals. Any attempt to increase the voltage of the source signal to get higher gain results in the distortion of the waveform. At this point it is worth mentioning that the pressure on the receiver against the model controls the amplitude to a great extent. With the present experimental setup it is difficult to determine accurately if the pressure is the same at all positions of the receiver.

3.7.2 Large Model

One of the reasons for selecting a large model was to overcome the difficulty in recognizing reflections. The large model is a 4 x 3 foot plexiglass sheet. With the transmitter position fixed as in the previous case, the receiver is moved, with 1-cm spacing, up to a separation of 12 cm, with 4-cm spacing, up to 28 cm and with 10-cm spacing, up to 78 cm.

Figure 29 shows waveforms for successive positions of the receiver. The travel-time curve for this seismogram is plotted in Figure 30.

Since the size of the model is now three times larger in width than the previous model, the reflection time is longer and appears after the surface waves on the seismograms. This is clearly seen from the traveltime curve and also from the seismograms in Figure 29.

It is seen that this is true so long as the separation between the receiver and transmitter is relatively small so that the surface waves arrive earlier than the reflected signal. But as the distance between the receiver and transmitter increases, surface waves take more time to reach the receiver, and, because of its greater amplitude, the reflected signal becomes difficult to recognize as it gets mixed up with the surface waves.
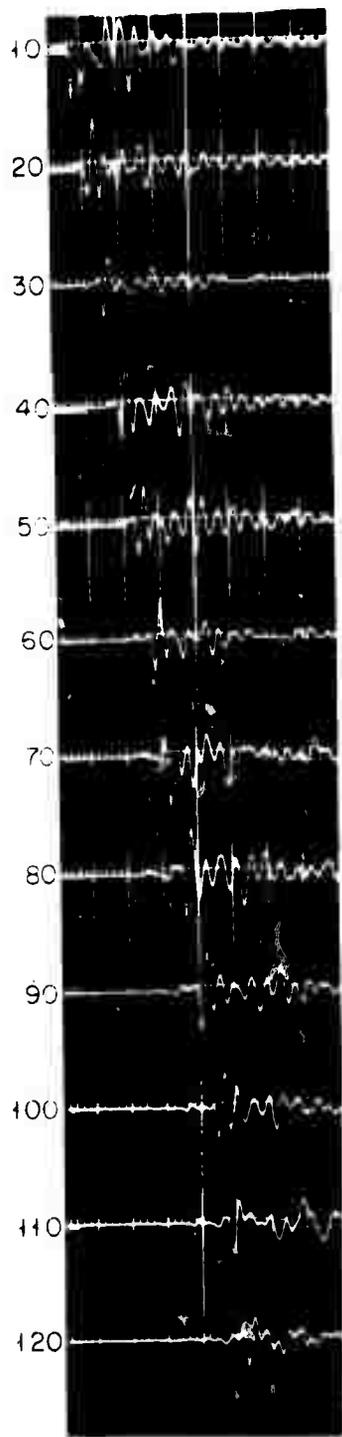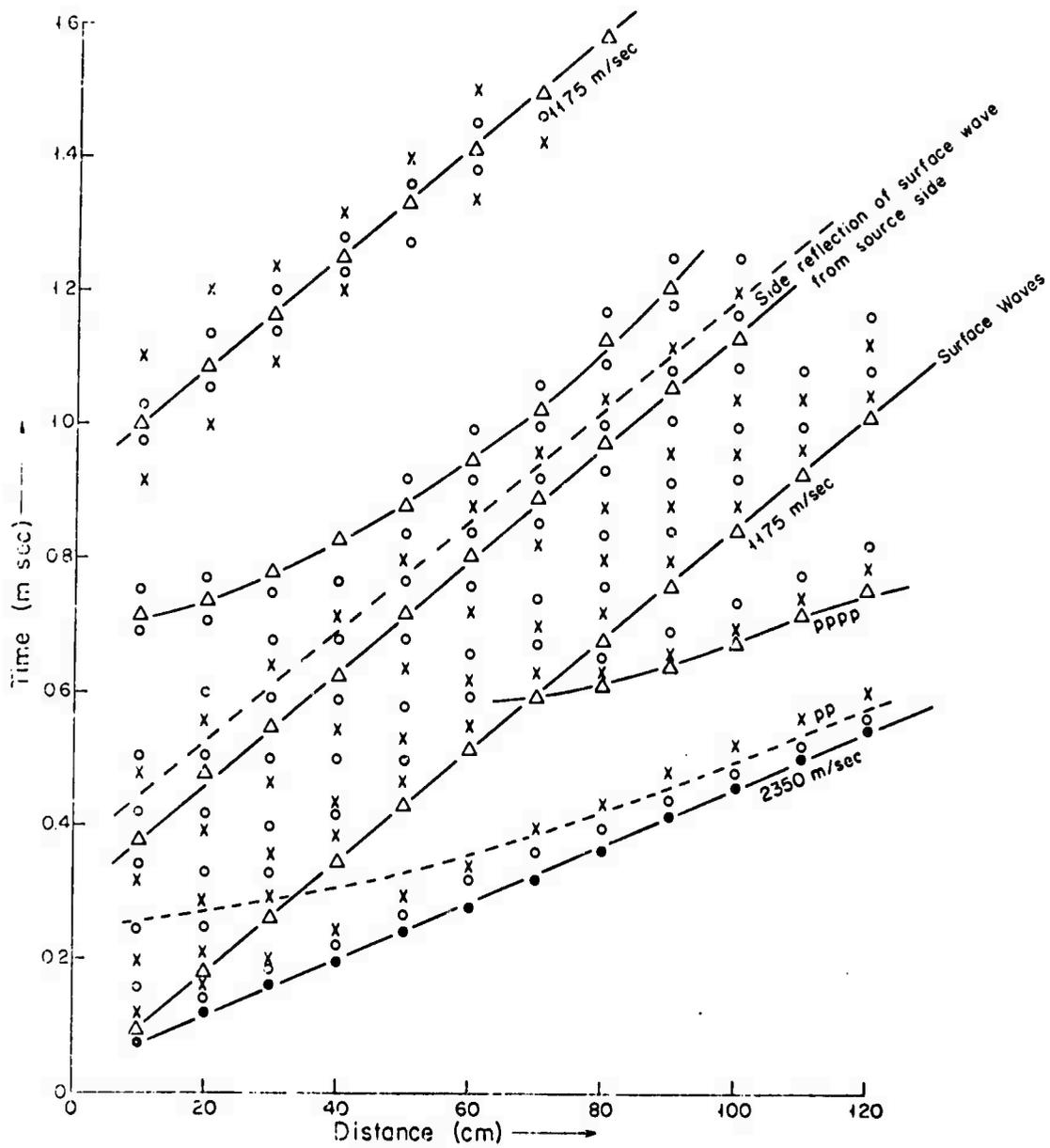
51

Figure 27.   Seismograms for Small Model

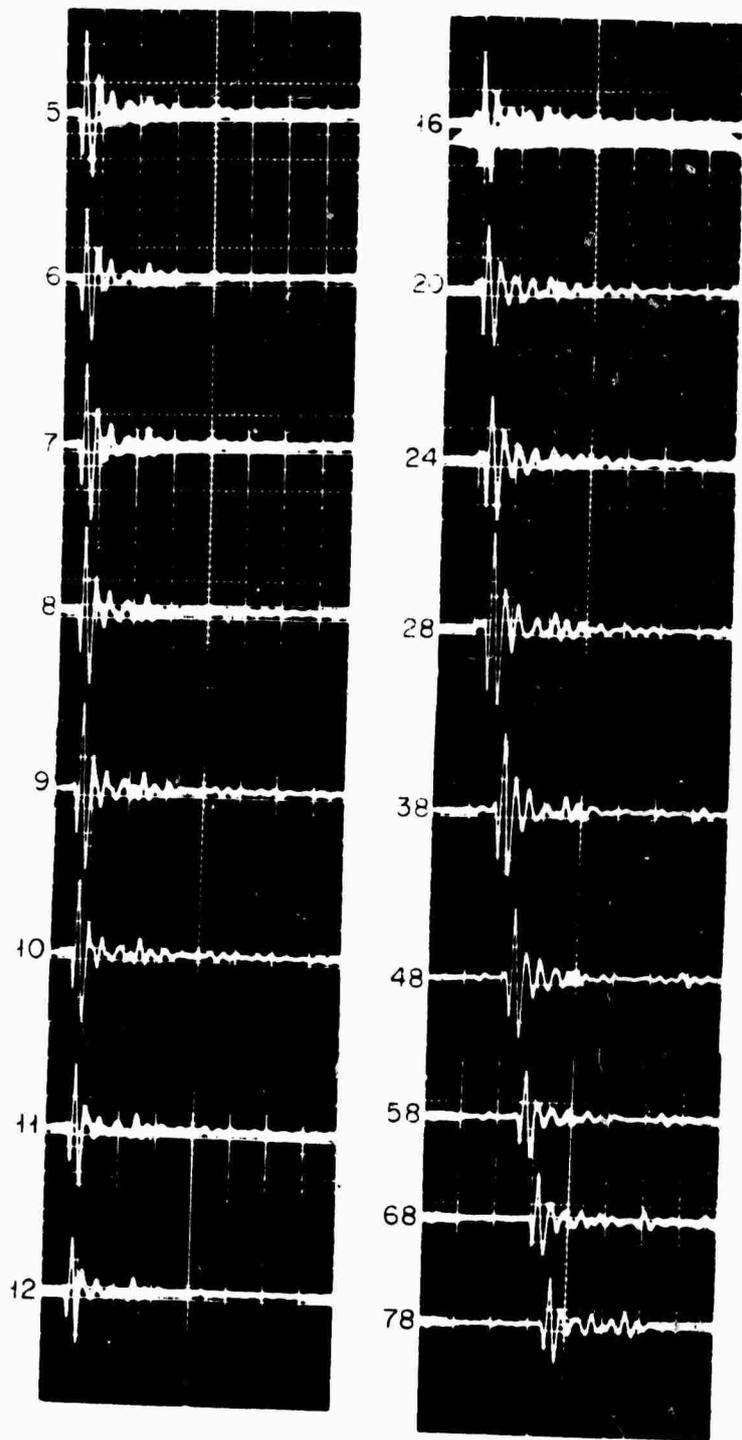Figure 28. Travel-Time Curves for Small Model
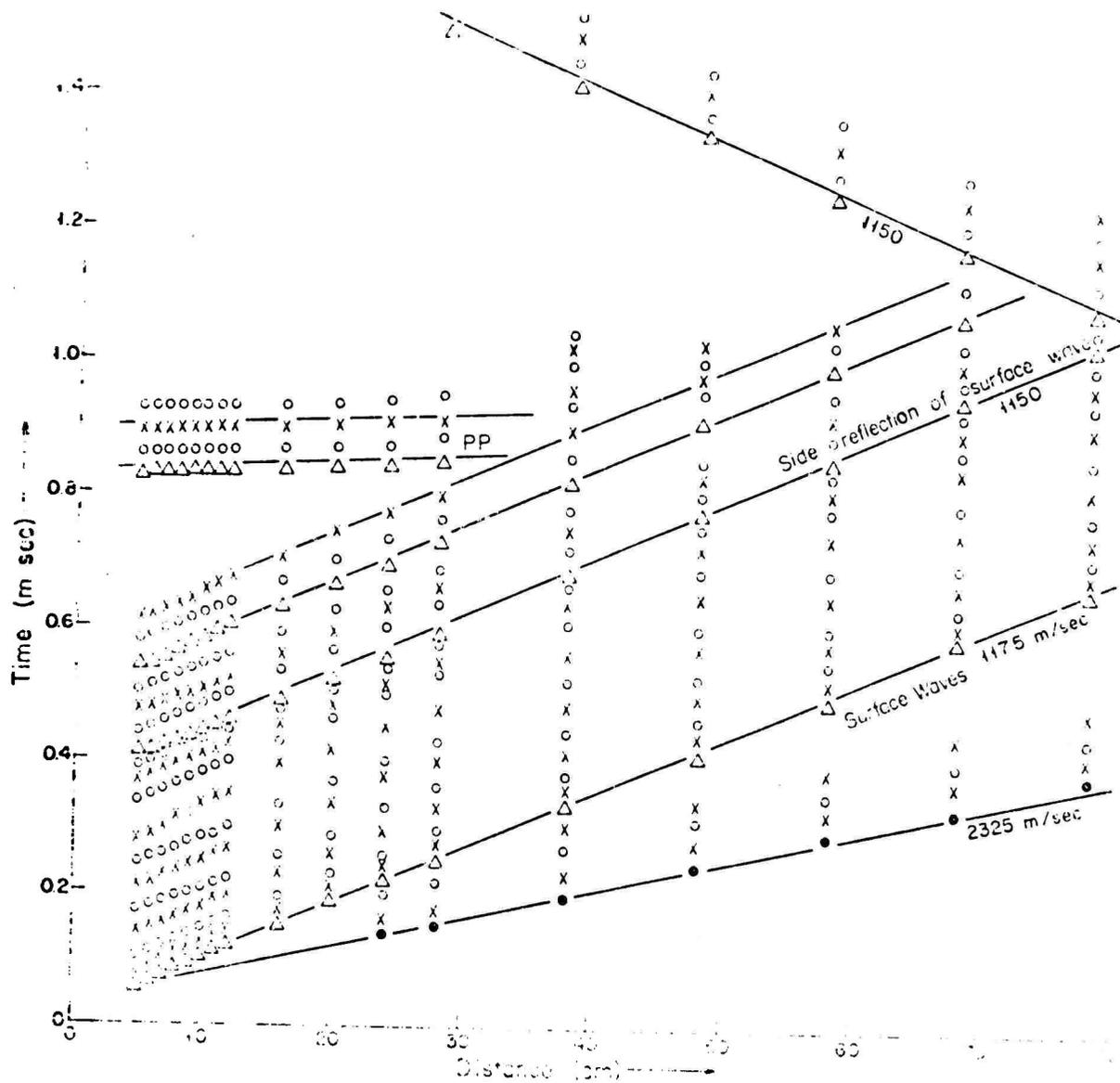
Figure 29. Seismograms for Large Model

Figure 30.   Travel-Time Curves for Large Model

Methods of blocking surface waves by a cut and by source sinking were carried out on the seismic model using a 5 x 1-foot plexiglass sheet.

3.7.3 Blocking Surface Waves by a Cut

The amplitude of surface waves can be greatly reduced by making a saw cut between the source and the receiver.

The depth of the cut is determined experimentally and will vary for models of different shapes and sizes. If the cut is too shallow, some or all the interfering waves are not eliminated, whereas, a deep cut can cause interference with the desired reflection.

Because of the cut, a diffracted wave is also introduced. The ray path associated with a diffracted wave is shown in Figure 31.
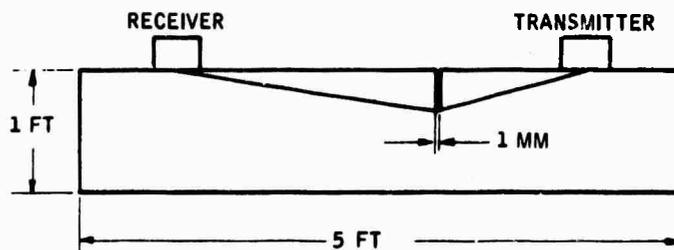
Figure 31.   Ray Path Associated with a
Diffracted Wave

We can also expect to detect other diffracted waves such as SP, PS, etc; thus the seismogram will be slightly complicated by the presence of a cut. Loren (1961) suggests that clamping at the bottom of the cut effectively reduces the amplitude of the diffracted wave.

Figures 32 through 35 show the results of blocking surface waves by a cut. The depths of the cut were 1/2 inch, 1 inch, 2 inches and 3 inches. The distance between the source and the cut was first fixed at 10 cm, and the same set of readings was then taken for a separation of 30 cm between the source and the cut. The 30-cm separation was used to provide a sufficient path for surface waves to develop before being affected by the cut.

56
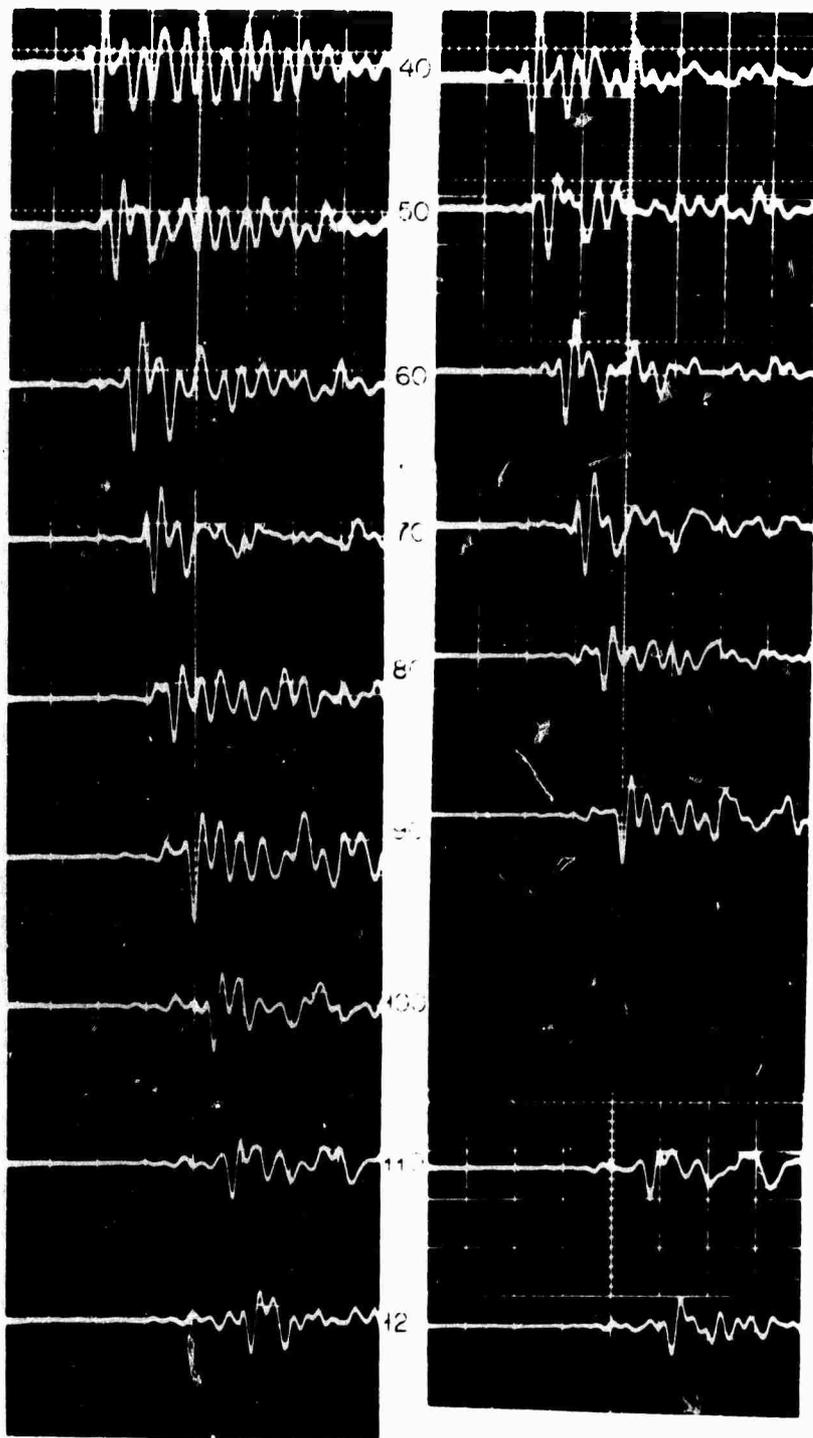
Figure 32. Seismograms for a 1/2-inch Cut 10 cm
from Source (left) and 30 cm from
Source (right)

Figure 33. Seismograms for 1-inch Cut 10 cm from
Source (left) and 30 cm from Source (right)
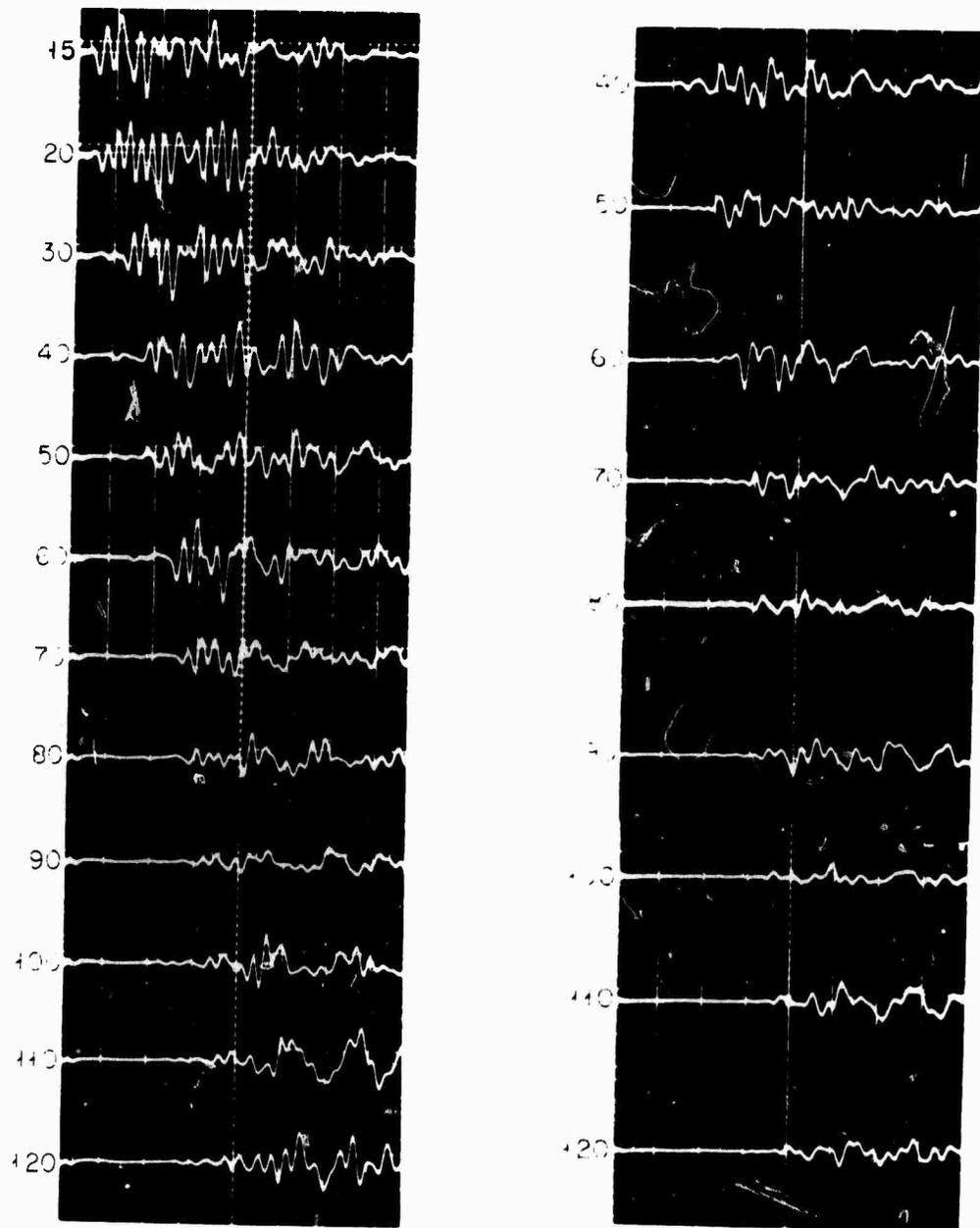
Figure 34.   Seismograms for 2-inch Cut 10 cm from
Source (left) and 30 cm from Source (right)
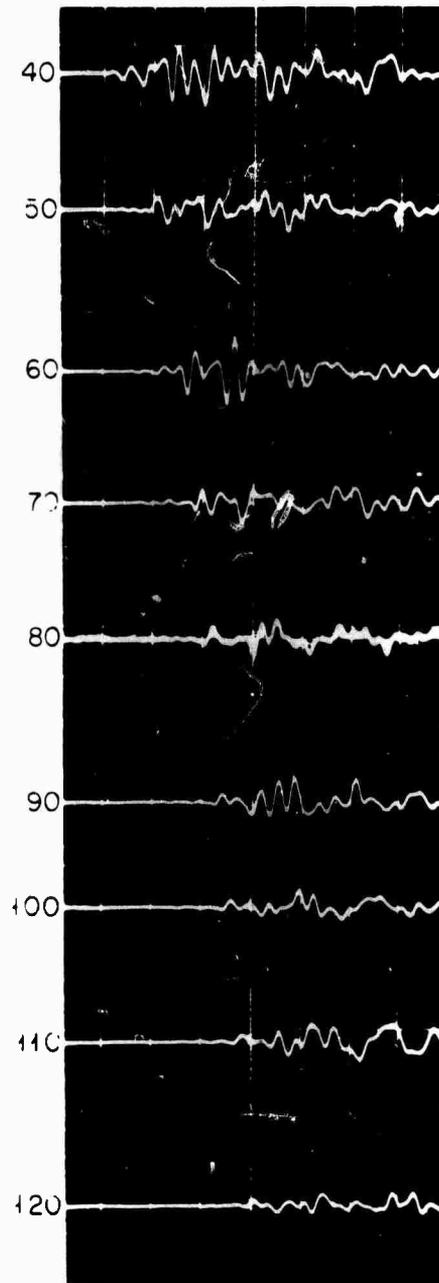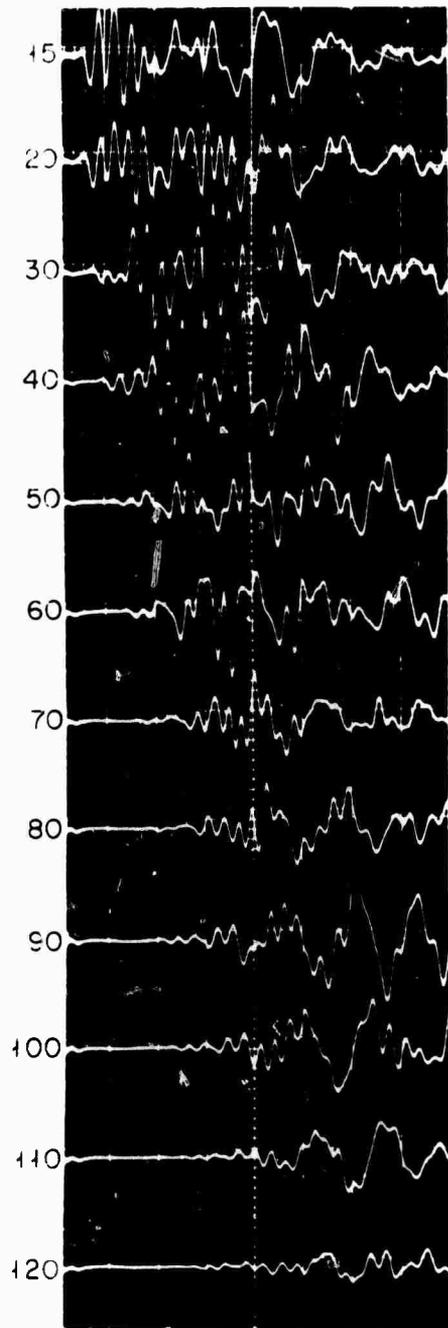
Figure 35. Seismograms for 3-inch Cut 10 cm from
Source (left) and 30 cm from Source (right)

Comparing the seismograms of Figure 27 with Figures 32 through 35, it can be seen that the arrivals in the later seismograms are not as clear as in Figure 27 (without cut). One interesting observation is that when the source is 30 cm from the cut, the amplitude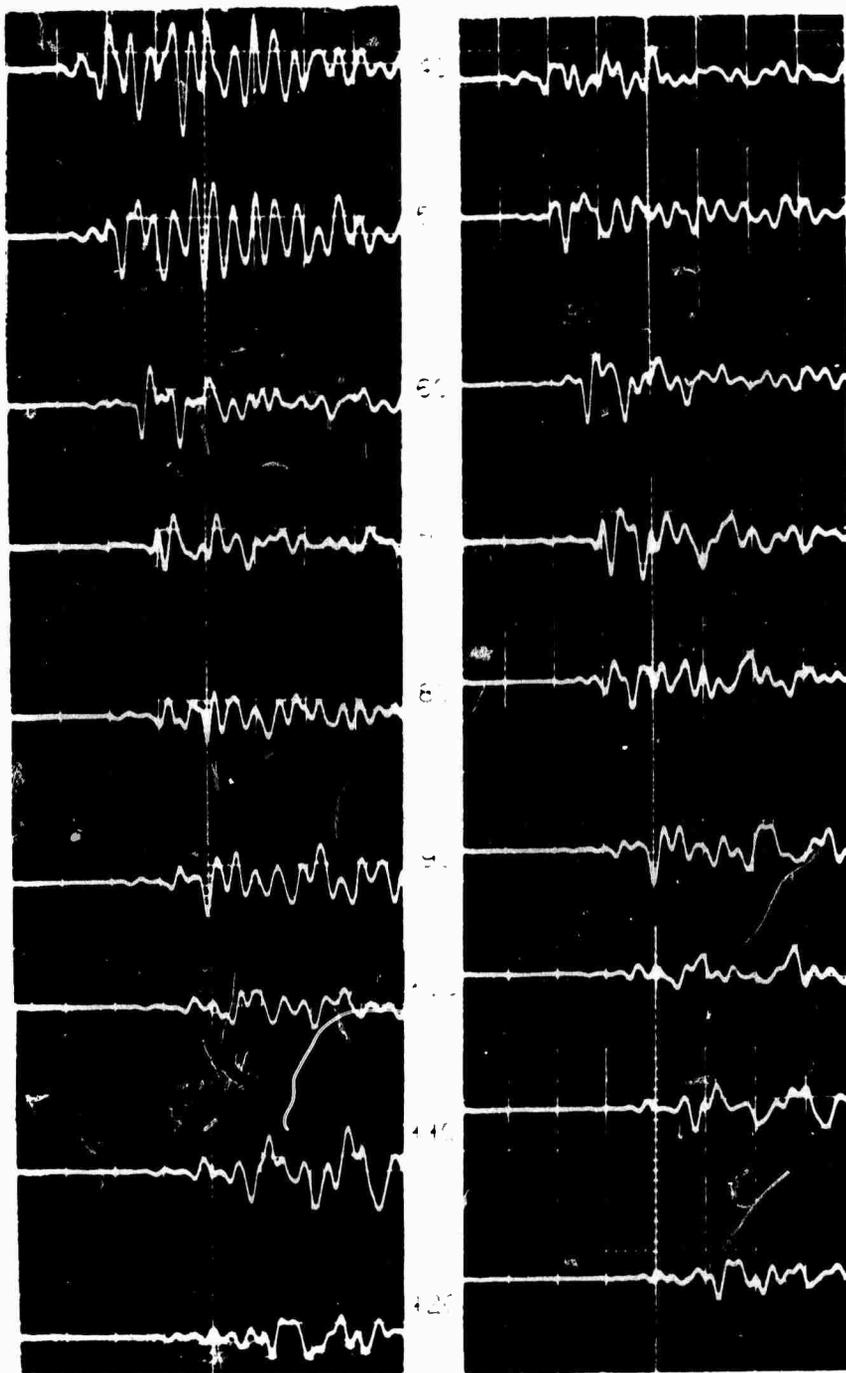 of the surface waves is much reduced from the situation when the source is only 10 cm from the cut. As the depth of the cut increases, the later arrivals show low-frequency signals.

Theoretical calculations of arrival times for reflection and diffraction paths are being made in an effort to more fully understand the effect of a cut on the waveform.

Further observations are also being made with the large model.

3.7.4 Source Sinking

The effect of surface waves should be greatly reduced by burying the source in the model. As a field procedure this approach would be simpler than blocking the surface waves by a cut.

Figures 36 through 38 show the results of sinking the source in the model up to 4 inches in steps of 1/2 inch. As the source is sunk deeper, the seismograms become more complicated. Furthermore, the train of surface waves does not seem to be shortened. An important observation is that there is no low-frequency effect as was observed with the cut. An immediate conclusion as to whether this technique will be useful in the field is not possible. Theoretical calculation of the arrivals and the travel time curves are being made. More data is being collected with the large model.

61
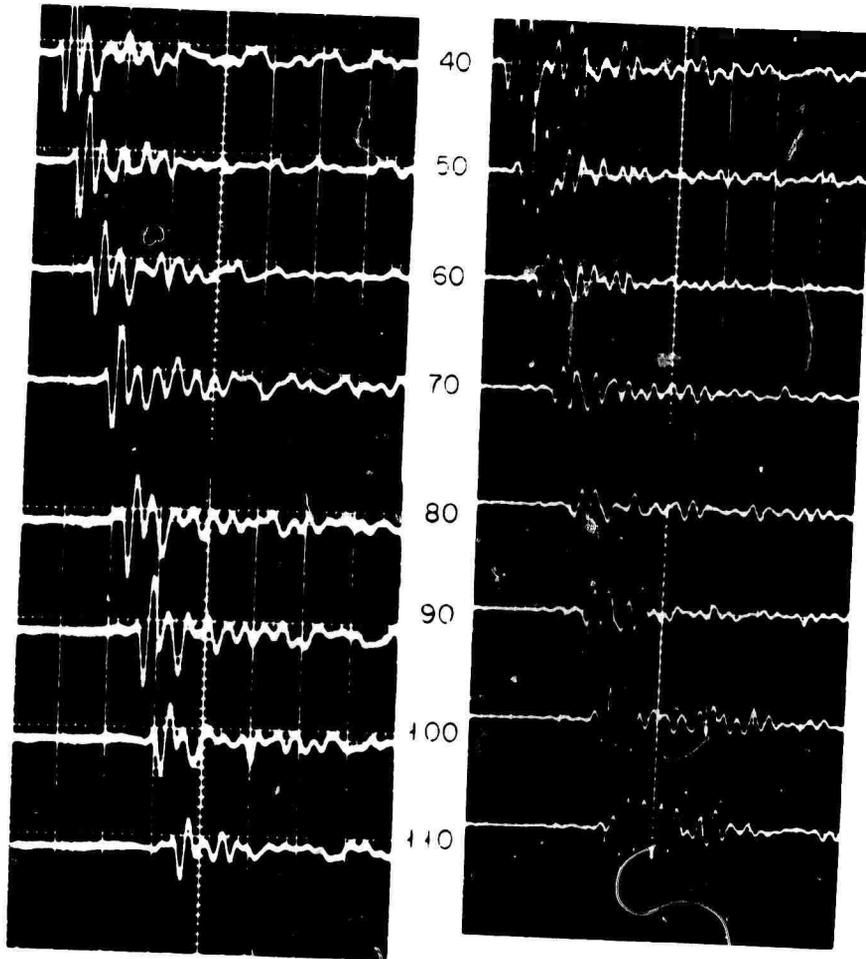
Figure 36. Seismograms for Source Depths of 1/2 inch (left) and 1 inch (right)
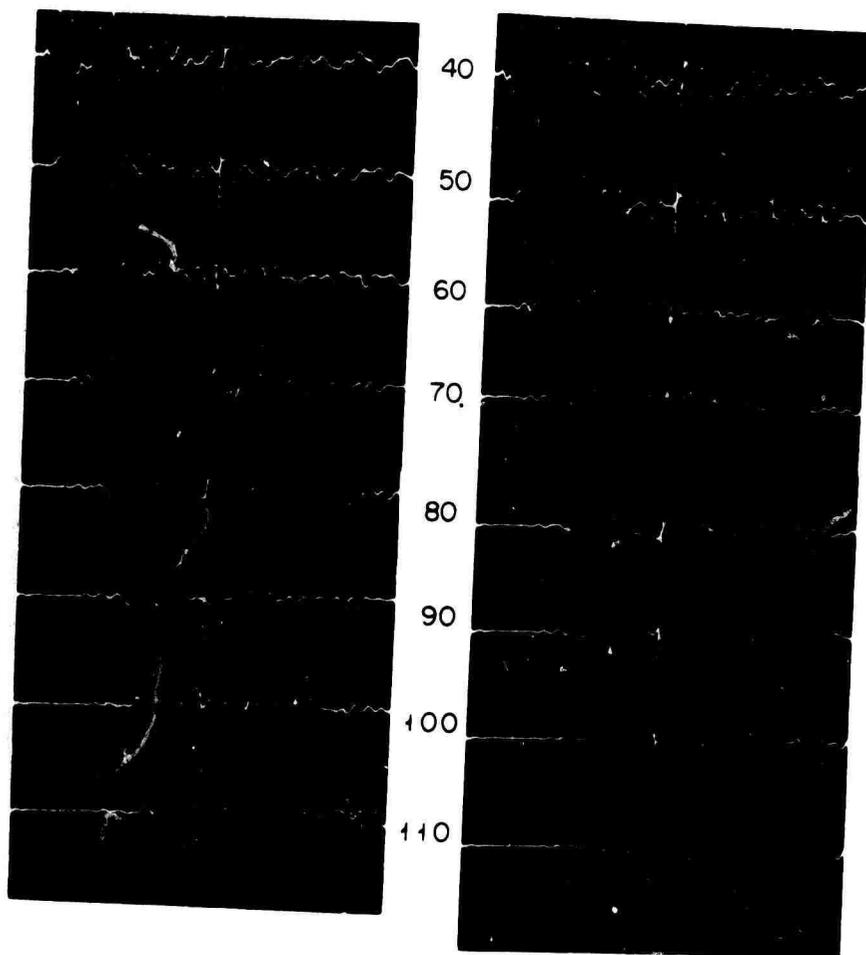
Figure 37. Seismograms for Source Depths of 1 1/2 inches (left) and 2 inches (right)
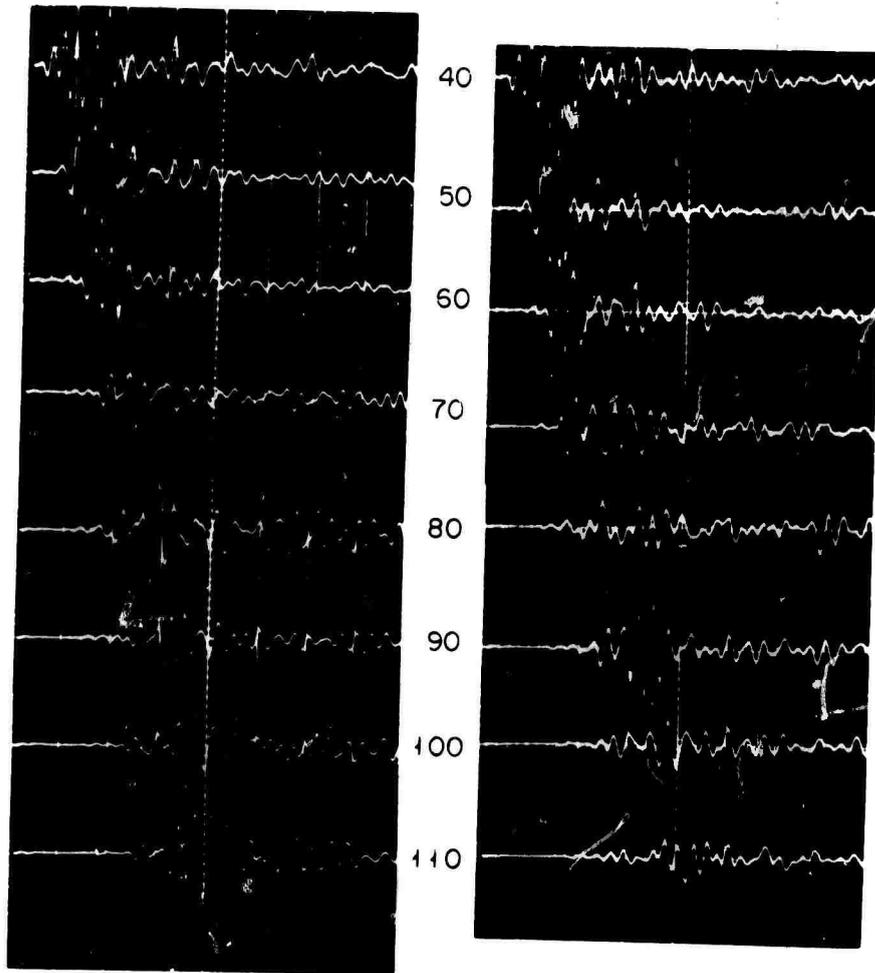
Figure 38. Seismograms for Source Depths of 3 inches (left) and 4 inches (right)

SECTION 4

SIGNAL PROCESSING STUDY

The goal of the excavation seismology program is to (a) identify, and (b) measure propagation time for seismic reflections. Toward this goal, several types of signal processing are under investigation. These various techniques for signal enhancement in the presence of interfering noise can be divided into three general classes:

- Correlation/convolution techniques

- Coherent time averaging

- Array filtering

The first two are temporal or single-channel methods and are reviewed in this section. The third, consisting of multichannel methods using spatial distributions of receiver locations, will be treated in depth in a later report.

4.1 CORRELATION/CONVOLUTION ANALYSIS

4.1.1 Possible Approaches

In terms of the linear model shown in Figure 39 (Figure 1 repeated here for convenience of reference), several possibilities for correlation-type analysis may be considered.

Each of the rectangular boxes shown on the diagram causes some kind of modification or distortion of the waveform. The simplest case is that of waveform delay which corresponds to passage through a linear filter with the transfer function

$$H(w) = e^{-iwt_o}$$

where t_o is the delay time. More generally, the waveform will be changed in shape and almost invariably prolonged in time duration.

Only two of the waveforms which appear at various points in the diagram are conveniently available for measurement. One of these is the input waveform, $f(t)$, from the waveform generator. This not only can be measured but can be manipulated almost at will by the operator. The other is the output waveform, $g(t)$.

65
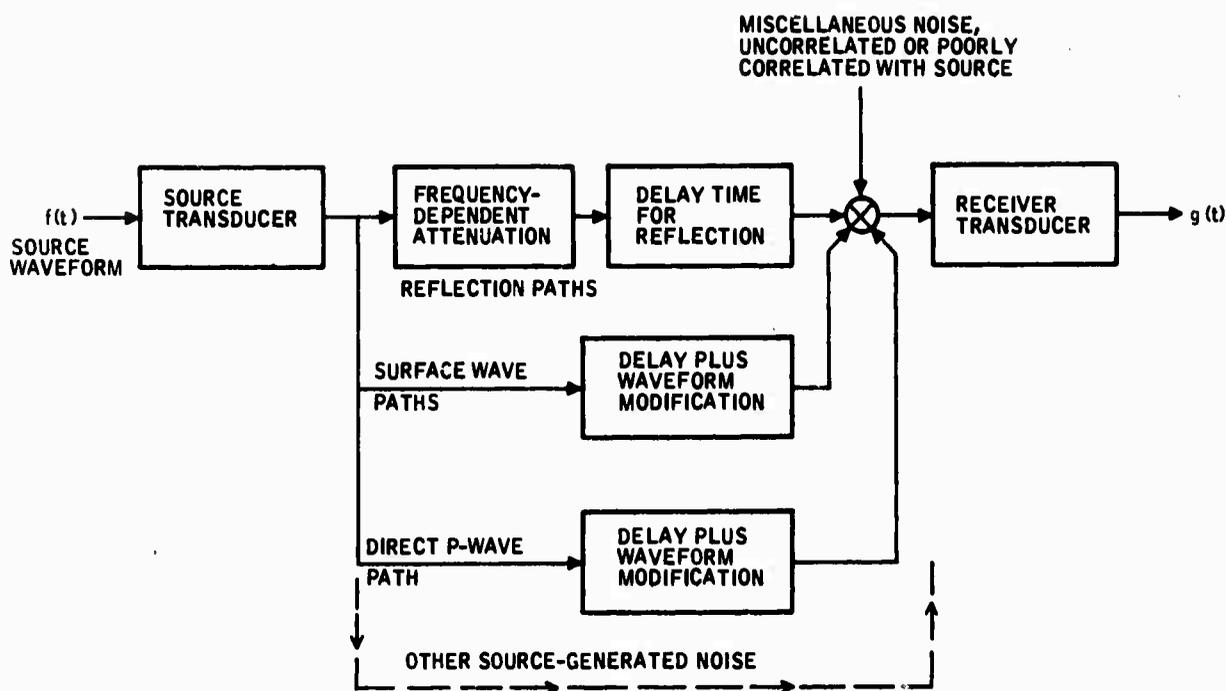
Figure 39. Linear Model for Excavation Seismology Program

Considerations of convenience suggest immediately that cross-correlation or matched filtering be carried out with these two waveforms, since they can be easily measured and easily modified. Cross-correlation is quite sensitive to waveform distortion, however, and is particularly sensitive to waveform elongation. So far as the noise paths (surface wave and P wave) are concerned, this represents an advantage rather than a disadvantage; poorly correlated signals will tend to become lost in the cross-correlation analysis The reflection path should not suffer greatly from waveform distortion, since the principal contributor -- attenuation -- will be small in a hard-rock environment.

Unfortunately for our purpose, the largest contributors to waveform distortion are the source and receiver transducers. Their effects appear for all of the possible wave paths, so that no benefit can be expected in terms of enhancement of the reflection signal. We conclude that any attempt to use cross-correlation analysis between the input, f(t), and the output, g(t), will require transducers which produce the lowest possible waveform distortion.

An attractive alternative would be to perform the cross-correlation analysis on the signals after the source transducer and before the receiver transducer. While these signals are not actually available for analysis, they can be simulated by observing the output, g(t), for a straight transmission path. The distortion produced by the transducers then becomes a known quantity which can be removed from the signal before cross-correlation. This possible technique is analysed in more detail elsewhere. A limitation arises from the requirement that transducer-rock coupling be kept closely the same from one location to the next.

66

A slight refinement of the analysis could be obtained by also removing the effect of frequency-dependent attenuation from the signal. This quantity can be computed to an approximation adequate for the purpose.

The preceding discussion has been concerned only with a single receiver. A later subsection will show how to extend this to multiple receivers and arrays.

4.1.2 Relationship of Cross-correlation to Other Signal Processing Techniques

We turn now to a more general discussion of the various analysis techniques and their interrelationships, drawing upon commentaries by Turin (1962), Schneider (1967), McMullen (1968), and others.

A general and widely used analysis process is the Wiener optimum filter. We specify some desired signal output, d(t). The Wiener filter has the property that it minimizes the mean-square error

$$\overline{(s(t) - d(t))}^2$$

between the actual and the desired outputs. The formal -- although not immediately useful -- solution is contained in the Wiener-Hopf equation (Lee, 1960, page 369)

$$\phi_{gd}(\tau) = \int_{\infty}^{\infty} h_{OPT}(t) \phi_{gg}(t-\tau) d\tau \tag{10}$$

where ϕ_{gg}, ϕ_{gd} are the input autocorrelation and the input-desired output cross-correlation.

The "desired output" may, as a special case, be the original input signal f(t). Alternatively it may be an impulse, in which case the filter is called a Wiener spiking filter.

A case which is well treated in the literature (but which does not well describe our situation) may be described as follows. The input signal f(t) is known only through its power spectral density $S_{ff}(w)$. The additive noise has a power spectral density $S_{nn}(w)$. The purpose of the filter is to provide the best estimate for the input signal. The desired filter has the transfer function

67

$$H_{OPT}(w) = \frac{S_{ff}(w) \, H^*(w)}{S_{ff}(w) \, H(w) \, H^*(w) + S_{nn}(w)} \tag{11}$$

(This formula with different symbols is given by Schneider. Equation 7-59 of McMullen can be shown to reduce to the same form if proper allowance is made for the difference in the models.)

Schneider considers two extreme cases. In the first, the signal to noise ratio is good: $S_{ff} \gg S_{nn}$. The filter reduces to

$$H_{opt}(w) = 1/H(w) \tag{12}$$

which is simply an inverse filter. In other words, if the noise is small, we can recover the input signal by straight deconvolution. This presumes, of course, that we know the transfer function of the distorting channel.

In the second case, the signal to noise ratio is poor: $S_{ff} \ll S_{nn}$. The filter reduces to

$$H_{opt}(w) = H^*(w) \, S_{ff}(w)/S_{nn}(w) \tag{13}$$

Since the signal will now have been passed through $H(w)H^*(w)$ (the first during distortion and the second as part of the filter), we will have removed all phase distortion but will have made the amplitude distortion worse. A special case arises for $H(w) = 1$; i.e., the distortion is negligible compared with the problem arising from the additive noise. Then

$$H_{opt}(w) = S_{ff}(w)/[S_{ff}(w) + S_{nn}(w)] \tag{14}$$

All that the filter can do in this situation is to pass those frequencies where the signal exists and not pass the others, with a kind of weighting effect where both signal and noise exist.

The preceding analysis does not seem to have direct application to the excavation seismology program because it assumes the properties of the distorting/delaying channel, $H(w)$, are fully known whereas those of the signal are not. The reverse is more nearly the situation.

The next kind of analysis we might consider is deconvolution. Let us suppose that the input $f(t)$ is an impulse or some other broadband signal, and that we have some method for determining or at least estimating $H(w)$, the transfer function of the distorting channel. The output signal has the transform

$$G(w) = F(w) \ H(w) \tag{15}$$

and to time-compress back into a high, narrow, impulse-like signal, we need simply pass through the inverse filter $1/H(w)$:

$$s(t) = \ \mathcal{F}^{-1} \left[\frac{G(w)}{H(w)} \right]$$

$$\cong \ f(t) \tag{16}$$

The problem with this approach lies in the existence of noise in the output signal, $g(t)$. For those w-values where $H(w)$ is small or zero, the noise components will be greatly amplified.

Several approaches have been suggested for overcoming this limitation. The most straightforward is that of George, et al (1962), who propose to multiply $G(w)/H(w)$ by a smoothing function which will eliminate the singularities arising from the zeros of $H(w)$. They suggest the hanning function

$$0.5 + 0.5 \cos Aw \text{ up to } w = B, \text{ and } 0 \text{ beyond.}$$

This process must inevitably degrade the deconvolution, but some degree of time-compression may still be attained.

A related approach (for example, Rice, 1962) uses approximations to $h(t)$ rather than $H(w)$.

A different kind of approximation to deconvolution leads directly to matched filtering. We note again that the signal has passed through the distorting filter,

$$H(w) = |H(w)| \ e^{-i\phi(w)} \tag{17}$$

and that true deconvolution would now pass it through

$$1/H(w) = e^{+i\phi(w)} \cdot \ 1/|H(w)| \tag{18}$$

Now if instead we passed it through the conjugate filter,

$$H^*(w) = |H(w)| \quad e^{+i\phi(w)} \tag{19}$$

we see that we have at least achieved the design criterion with respect to phase. The noise signals presumably have random phase anyhow, so we might as well use the optimum phase filter with respect to the signal.

69

The compromise filter has the further advantage that its characteristic is small at frequencies where the signal is small compared to the noise, and large where the signal is large compared to the noise. As noted in the section on matched filters, this filter is matched to h(t).

Another criterion of optimization is used by the matched or cross-correlation filter. The criterion is (Dwork, 1950) that the peak amplitude of the signal output shall be as large as possible compared to the rms of the noise output. It will be noted that the output waveform from this filter may - and in fact will - look substantially different from the original signal prior to the distorting process. The purpose of the matched filter lies, principally, in recognizing the existence of a signal and, secondarily, in determining its arrival time. Faithful reproduction of the signal does not enter into consideration.

A matched filter has the special characteristic that the passband is identically matched to the spectrum of the signal to be passed; the filter passes all frequencies within the spectrum of the signal and rejects all others. Thus in a certain sense it can be regarded as an optimum frequency domain filter for improving the signal-to-noise ratio.

Matched filtering does not preclude the use of other types of data processing. It would be perfectly feasible, for example, to use a matched filter to improve the S/N and then to operate on the resulting data with a Wiener shaping filter to increase resolution (Treitel and Robinson, 1969). Matched filtering is a linear process, so it may be shifted to various positions in the overall system without altering its effect. Capon (1970) suggests - for an entirely different application - a processor consisting of:

- Time shifter for various array elements
- Individual filters for the time-shifted signals
- Summation
- Noise-whitening filter
- Matched filter, matched to the whitened signal

His individual filters are maximum-likelihood to provide a minimum-variance unbiased estimate for the input signal. For the excavation seismology program, the input signal is known so that his filter criteria would not be relevant.

70

4.1.3 Master-signal Method of Data Analysis

As noted above, waveform distortion by the source and receiver transducers presents a major difficulty in the identification and timing of seismic reflections. The input signal will be altered in shape and prolonged in time duration, so that sharply defined pulses become diffuse and may overlap each other. Cross-correlation of the output signal against the source waveform will be severely degraded since this method is sensitive to even small changes in waveshape.

An obvious (but impractical) solution would be to measure the seismic waveform after it has left the source transducer and before it has reached the receiver transducer. A step in this direction would be to place a monitor transducer close to the source; the seismic wave leaving the source would actuate the monitor, and a bonus benefit would be that the distortion originating in the monitor would approximate that originating in the receiver transducer. This approach may deserve further investigation. One flaw in it is, however, that distortion by transducers is strongly dependent upon their loading by the rock surface, and the monitor-transducer method might not simulate this adequately.

An alternative solution may be available through a master-signal method. The approach would be to measure a seismic waveform which has already been distorted by the major contributors to distortion, and to use this for subsequent analysis. If the analysis consists of matched filtering or cross-correlation, for example, much better correlation should be found using this waveform than the original input waveform to the source transducer.

An example of the use of this method, in a different field and for a different purpose, is given by von Seggern (1972). He attempts to determine the travel time of a surface-wave train from a nuclear explosion by cross-correlating it against the wave train from a nearby reference explosion. Another example is given by Evernden (1969), whose goal is to determine station corrections for small earthquakes using a large earthquake in the same region. Helmberger and Wiggins (1971) use waveforms from nuclear explosions recorded at teleseismic distances for correlation against waveforms at shorter distances. The technique of cross-correlation against the actual input waveform is of course widely used, as in the Vibroseis method as well as radar and sonar applications, but the deficiency of this approach is explained above.

How can we obtain a suitable master waveform? First, a suitable input waveform must be selected. The criteria for this selection are presented in another section, but the principal two are: the waveform must be broadband, as for example an impulse, and it must be identical for the field conditions and the master-waveform conditions.

71

Second, the master waveform must include the distortion effects associated with transducer loading by the rock surface. Third, it would be desirable to include whatever distortion may arise from propagation through a rock path whose length is comparable to the reflection path, although the effect is probably small and could be corrected for if necessary. Fourth, to minimize uncertainties arising from the radiation pattern of the transducers, the wavepath for the master waveform should enter and leave the transducers perpendicular to the rock surface. Fifth, the master waveform must be an isolated pulse, free from interference with overlapping seismic arrivals.

All of these criteria can be satisfied if we are able to achieve the experimental arrangement shown in Figure 40.
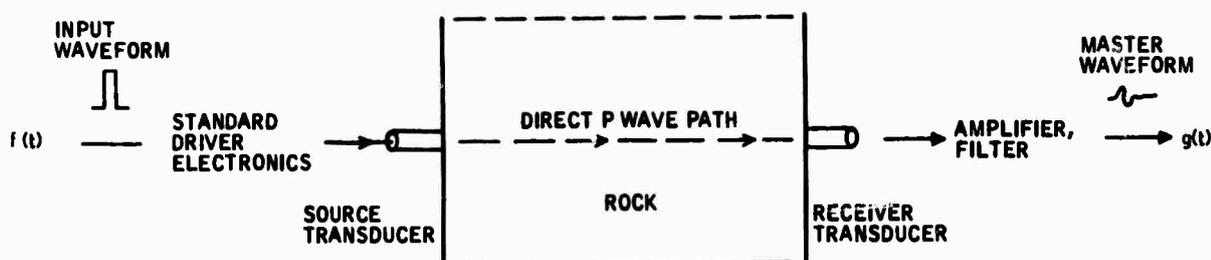

Figure 40. Ideal Experimental Arrangement

The arrangement requires access to opposite sides of a rock mass. Ideally, the path length would be comparable to that of the expected reflection path, but failure to achieve this will not cause serious difficulty. The rock type should be similar to that expected in field conditions, especially at the transducer contact points. The input waveform and the electronic circuitry must also be identical. If various filter settings are expected, it would be a simple matter to obtain one master waveform for each filter setting. The same could be done for various input waveforms if desired.

4.1.4 Cross Correlation: Definition, Normalization, and Equivalence to Matched Filter

For aperiodic (transient) functions of finite total energy, the cross-correlation function of $f_1(t)$ against $f_2(t)$ is defined (Lee, 1960, eq. 168) as

$$\phi_{12}(t) = \int_{-\infty}^{\infty} f_1(\tau)\, f_2(t + \tau)\, d\tau \tag{20}$$

The function may be normalized, if desired, to have values in the range ± 1 by dividing by the mean of the autocorrelation functions at zero lag (Bendat and Piersol, 1966, page 299):

$$\delta_{12}(t) = \frac{\phi_{12}(t)}{\sqrt{\phi_{11}(0)}\sqrt{\phi_{22}(0)}} \tag{21}$$

In a later subsection, we show that the cross-correlation of $f_1(t)$ against $f_2(t)$ yields a cross-correlation function of time, $\phi_{12}(t)$, which is identical to the output of a filter whose impulse response is $f_1(-t)$ when the input is $f_2(t)$. A filter with this characteristic is said to be matched to $f_1(t)$.

The Matched-Filter Theorem — If the purpose of the filter can be stated as maximizing the peak amplitude of the signal output compared to the rms of the noise output, then the matched filter which will accomplish this has the transfer function (Dwork, 1950; Tolstoy and Clay, 1966, page 249; Turin, 1960, page 312)

$$H(w) = \frac{F^*(w)}{|N(w)|^2} e^{-iwt_o} \tag{22}$$

where $F(w)$ is the transform of the signal to be matched, $N(w)$ is the power density spectrum of the noise, and t_o is the time at which the peak ratio occurs. The value of the peak S/N is (Dwork, 1950)

$$1/2\pi \int_{-\infty}^{\infty} \left|\frac{F(w)}{N(w)}\right|^2 dw$$

If the noise is white -- $N(w)$ = constant, of power density N_o (Turin, 1960, page 312) -- then the maximum S/N becomes

$$E/N_o$$

where E is the total energy in the signal. The transfer function of the matched filter reduces to

$$H(w) = C \, F^*(w) \, e^{-iwt_o} \tag{23}$$

73

where C is a constant.

For a matched filter to be physically realizable, Dwork (1950) points out that f(t) must have finite length. This is required so that h(t) can be 0 for negative t.

Equivalence of Cross-correlation and Matched Filtering — The matched-filter theorem states that a filter which is matched to a signal $f_1(t)$ has a transfer function

$$H(w) = F^*(w) \tag{24}$$

and an impulse response

$$h(t) = f_1(-t)$$

To establish that passage through such a filter is identical to cross-correlation against $f_1(t)$, suppose that a signal $f_2(t)$ is passed through the filter. By the convolution theorem, the output is

$$g(t) = \int_{-\infty}^{\infty} h(\tau) \, f_2(t-\tau) \, d\tau$$

$$= \int_{-\infty}^{\infty} f_1(-\tau) \, f_2(t-\tau) \, d\tau$$

$$= \int_{-\infty}^{\infty} f_1(\tau^1) \, f_2(t+\tau^1) \, d\tau^1$$

$$= \phi_{12}(t) \tag{25}$$

Thus the filter output is identical to the cross-correlation function.

If the input signal happens to be $f_1(t)$ itself, then the output reduces to the autocorrelation function of $f_1(t)$,

$$\phi_{11}(t)$$
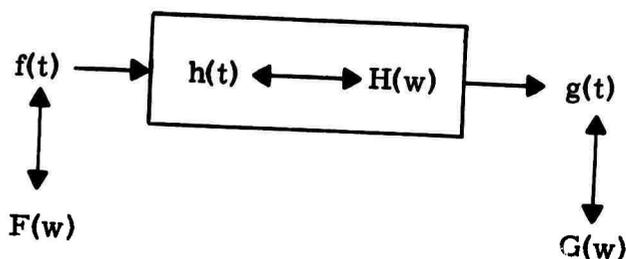
Equivalent results may be written in the frequency domain:

$$G(w) = F_1^*(w) \, F_2(w)$$

or if the input is $f_1(t)$, $G(w) = \left| F_1(w) \right|^2$.

4.1.5 Input/Output Relationships for a Linear System

The usual representation of input/output relationships for a linear system is

$$G(w) = H(w) \, F(w)$$

$$g(t) = \int_{-\infty}^{\infty} h(\tau) \, f(t-\tau) \, d\tau$$

$$= \int_{-\infty}^{\infty} h(t-\tau) \, f(\tau) \, d\tau$$

However, we may sometimes prefer to express equivalent relationships in terms of either the correlation functions or the spectra. For $f(t)$ a random function, we must do so because in that case $F(w)$ and $G(w)$ do not exist (Lee, 1960, p. 333).

We note first that the correlation and spectral density functions are defined slightly differently for aperiodic (transient) and random signals:

<center>Transient   <u>Random Time Series</u></center>

Correlation:

$$\phi_{12}(t) = \int_{-\infty}^{\infty} f_1(\tau) f_2(t+\tau) \, d\tau \left\| \phi_{12}(t) = \lim_{T \to \infty} \frac{1}{2T} \int_{-T}^{T} f_1(\tau) f_2(t+\tau) \, d\tau \right.$$

$$= \frac{1}{2\pi} \int_{-\infty}^{\infty} \Phi_{12}(w) \, e^{iwt} \, dw$$

Spectrum:

$$\Phi_{12}(w) = \int_{-\infty}^{\infty} \phi_{12}(t) \, e^{-iwt} dt \tag{28}$$

energy density spectrum   <u>power</u> density spectrum

(These formulas follow the usual convention in placement of 2π for definition of Fourier transform, as for example in Bendat and Piersol, 1966. Lee, 1960, uses a different convention whereby $1/2\pi$ appears in the third line above rather than the second.)

Following the nomenclature of Lee (1960, Chapter 13) with subscripts i and o for input and output, with

$$\phi_{hh}(t) = \int_{-\infty}^{\infty} h(\tau) h(t+\tau) \, d\tau = \frac{1}{2\pi} \int_{-\infty}^{\infty} |H(w)|^2 \, e^{iwt} dw \tag{29}$$

the following input/output relationships may be written:

$$\phi_{oo}(t) = \lim_{T \to \infty} \frac{1}{2T} \int_{-T}^{T} f_o(\tau) f_o(t+\tau) \, d\tau$$

$$= \int_{-\infty}^{\infty} h(\upsilon) d\upsilon \int_{-\infty}^{\infty} h(\tau) \phi_{ii}(t+\upsilon-\tau) \, d\tau$$

$$= \int_{-\infty}^{\infty} \phi_{hh}(\tau) \phi_{ii}(t+\tau) \, d\tau \tag{30}$$

$$\phi_{io}(t) = \int_{-\infty}^{\infty} h(\tau) \phi_{ii}(t-\tau) \, d\tau \tag{31}$$

$$\Phi_{oo}(w) = |H(w)|^2 \Phi_{ii}(w) \tag{32}$$

$$\tag{33}$$

<center>76</center>

$$\Phi_{io}(w) = H(w)\,\Phi_{ii}(w) \qquad (33)$$

Application to determining the impulse response of a linear system:
Consider a system into which is fed white-noise input. In this context,
white noise is defined as having a power density spectrum which is flat
over a band of frequencies considerably wider than the band of the
system under investigation. Such a signal has

$$\Phi_{ii}(w) = K, \text{ a constant}$$

which yields an autocorrelation function

$$\Phi_{ii}(t) = \frac{1}{2\pi}\int_{-\infty}^{\infty} \Phi_{ii}(w)\,\epsilon^{iwt}\,dw$$

$$= \frac{K}{2\pi}\int_{-\infty}^{\infty} \epsilon^{iwt}\,dw \qquad (34)$$

$$= K\,\delta(t)$$

Substituting into the expression above

$$\phi_{io}(t) = \int_{-\infty}^{\infty} h(\tau)\,\phi_{ii}(t-\tau)\,d\tau$$

$$= \int_{-\infty}^{\infty} h(\tau)\,\delta(t-\tau)\,d\tau$$
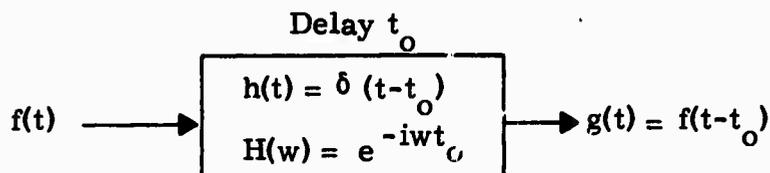
$$= K h(t) \qquad (35)$$

Thus, aside from a multiplying constant, the impulse response of the
system equals the cross-correlation of the input and the output when the
input is white noise.

In the frequency domain, the transfer function is

$$H(w) = \frac{1}{K}\,\Phi_{io}(w) \qquad (36)$$

4.2 CROSS-CORRELATION ANALYSIS APPLIED TO A DELAYED REFLECTION

Consider the results of a cross-correlation analysis where the second signal is simply a delayed version of the first, as, for example, an undistorted seismic reflection:

$$
f(t) \longrightarrow \boxed{\begin{array}{c} \text{Delay } t_o \\ h(t) = \delta(t-t_o) \\ H(w) = e^{-iwt_o} \end{array}} \longrightarrow g(t) = f(t-t_o)
$$

Thus

$$
\phi_{fg}(t) = \int_{-\infty}^{\infty} f(\tau)\, g(t+\tau)\, d\tau
$$

$$
= \int_{-\infty}^{\infty} f(\tau)\, f(t+\tau-t_o)\, d\tau
$$

$$
= \phi_{ff}(t-t_o) \tag{37}
$$

In words: the cross-correlation function between input and output is identical to a delayed version of the auto-correlation function of the input signal.

We now consider the implications of this type of analysis for the excavation seismology program. The program includes two principal goals with respect to the seismic reflections: to recognize them and to measure their arrival times. We proceed to analyse these goals in the context of two alternative methods of presenting the data: either directly as the output waveform, $g(t)$, or by study of the cross-correlation function, $\phi_{fg}(t)$.

The known properties of the auto-correlation function permit us to draw the following conclusions under the assumptions of the present section (undistorted and noise-free transmission):

- The output of the cross-correlation analyser will be elongated in time by exactly a factor of two, compared with the seismic reflection itself. Thus the resolution between adjacent seismic arrivals may be inferior on the correlation.

- Since elongation in time corresponds to compression in frequency we conclude that $\phi_{fg}(t)$ is a narrower-band signal than $g(t)$.

  Specifically, aside from a phase shift of magnitude e^{-iwt_o} the transforms are

  $$G(w) = F(w)$$
  $$\Phi_{fg}(w) = |F(w)|^2$$

  For any $f(t)$ of finite bandwidth, the second expression will be compressed in frequency compared to the first.

- The output of the cross-correlation analyser will have a peak value at $t = t_o$, the delay time, and will decrease symmetrically in both directions from this peak. The location of the peak is completely independent of the input waveform $f(t)$, although the sharpness of the peak will increase as the bandwidth of $f(t)$ increases. Thus the cross-correlation output provides an immediate display of the reflection time. These points are illustrated in Figure 41.
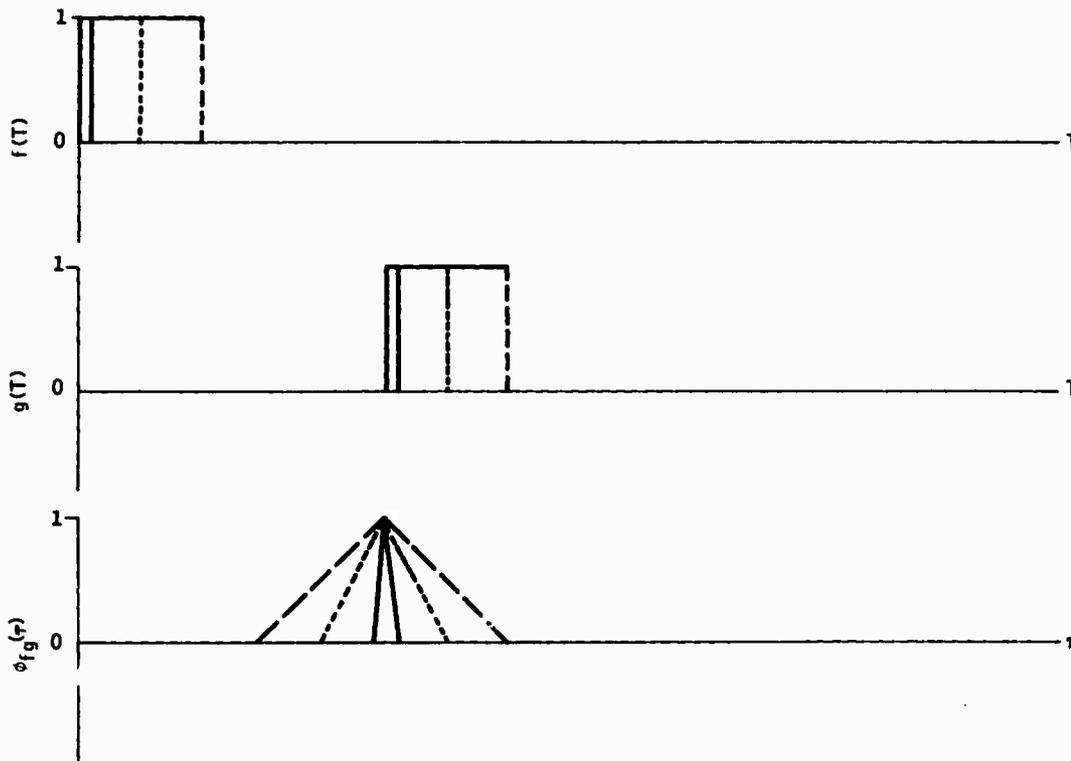

Figure 41. Cross-Correlation of Identical Pulses of Different Lengths

From the preceding, we conclude that <u>for a noise-free and
undistorted reflection,</u> direct display of the seismic waveform provides
increased resolution and may provide easier recognition of the reflection
if the waveform character happens to be distinctive. On the other hand,
the cross-correlation output gives a peak signal at exactly the reflection
time, independent of the choice of input waveform.

In practice, the effect of noise and interfering seismic arrivals
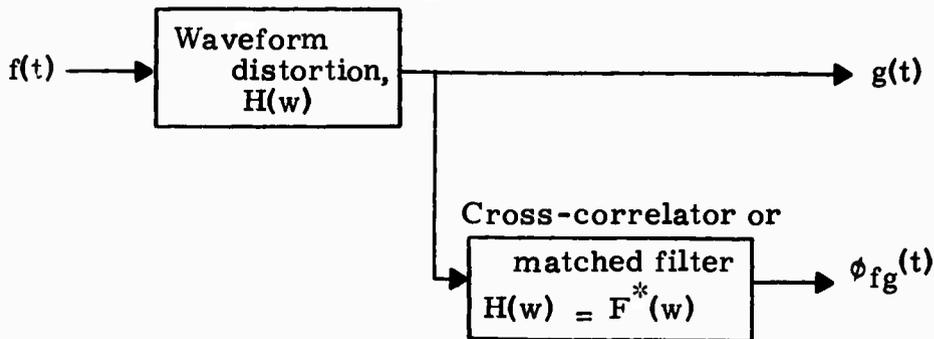has great importance in choosing between these two methods of data
analysis.

4.2.1 The Effect of Waveform Distort' i on Cross-Correlation Analysis

In the preceding subsection, we considered the output from a cross-
correlation analyser when the output waveform differs from the input
waveform due only to a time delay. Two complicating effects may be
anticipated: the signal may be distorted during transmission, and
additive noise may be superposed. In this subsection, we consider the
effects of signal distortion.

Distortion may arise from source and receiver transducer effects,
frequency-dependent attenuation, or other causes. The transducer
contribution is likely to be the most serious for the excavation seismology
program. A method is proposed elsewhere by which to eliminate this
effect, namely by using as input to the correlator a waveform which has
already been modified by the transducers. Here, however, we consider
distortion in general terms.

Two situations are considered. In one case, the nature of the
distortion is not known a priori, as, for example, distortion produced
by the transducers. In the other case, some information is available
on the expected distortion, as for example frequency-dependent attenuation.
In the latter situation, the possibility exists for removing the distortion
prior to cross-correlation.

The system under consideration may be shown as follows:

$f(t) \longrightarrow$ | Waveform distortion, $H(w)$ | $\longrightarrow g(t)$

Cross-correlator or
| matched filter $H(w) = F^{*}(w)$ | $\longrightarrow \phi_{fg}(t)$

80

We wish to compare the two possible observational quantities, $g(t)$ and $\phi_{fg}(t)$, with respect to (1) how easily can the seismic arrival be recognized, and (2) how reliably can the seismic arrival time be measured? We consider these questions for various types of waveform distortion.

General solutions may be written immediately:

$$G(w) = H(w) \, F(w)$$

$$g(t) = \mathcal{F}^{-1}\left\{G(w)\right\}$$

$$\Phi_{fg}(w) = F(w) \, F^*(w) \, H(w)$$

$$= F(w)^2 \, H(w)$$

$$\phi_{fg}(t) = \mathcal{F}^{-1}\left\{\Phi_{fg}(w)\right\}$$

Before considering examples, some general comments may be made:

- The case of simple delay without distortion, considered earlier, appears as a special case with

$$H(w) = e^{-iwt_o}$$

- Comparing the transforms, $G(w)$ with $\Phi_{fg}(w)$, we see that - no matter what type or degree of distortion, $H(w)$ - the cross-correlation function is a narrower-band signal than $g(t)$ hence has greater time duration. The elongation in time by a factor of two for delay-without-distortion now appears, however, as an upper limit. The presence of distortion will cause elongation in time for both $g(t)$ and $\phi_{fg}(t)$, but the ratio of pulse lengths will fall below the factor of two.

- One limiting condition is the case of no distortion (although possibly delay), corresponding to

$$|H(w)| = \text{constant}$$

The analysis for this case was given in the previous subsection.

- The opposite limiting condition occurs when $H(w)$ is much narrower in bandwidth than $F(w)$. This will occur for moderate distortion with a broadband input signal, $f(t)$, or for severe distortion with almost any input signal.

Under this condition, the transforms $G(w)$ and $\Phi_{fg}(w)$ both reduce to essentially $H(w)$. The output signals $g(t)$ and $\phi_{fg}(t)$ become nearly identical, and equal to the impulse response $h(t)$ of the distorting channel.

81

In practical terms, this limiting condition is approached in the presence of severe transducer distortion. The technique of cross-correlation analysis will yield negligible improvement.

- A constraint exists on types of distortion which are physically possible. The constraint requires that

$$H(w) = H_R(w) + i H_I(w)$$

have an even real part and an odd imaginary part

$$H_R(-w) = H_R(w)$$

$$H_I(-w) = -H_I(w)$$

The requirement emerges because the impulse response, $h(t)$, must be real:

$$h(t) = \frac{1}{2\pi} \int_{-\infty}^{\infty} H(w) \ e^{iwt} dw$$

which leads to the conclusion that $h(t)$ may also be written,

$$h(t) = \frac{1}{\pi} \int_{0}^{\infty} (H_R \cos wt - H_I \sin wt) \ dw$$

Similar requirements apply also to $f(t)$, $g(t)$, and $\phi_{fg}(t)$, but they will be satisfied automatically.

- If the distortion includes a delay, as, for example, with a seismic reflection, we can write

$$H(w) = H_o(w) \ e^{-iwt_o}$$

where $H_o(w)$ describes all distortion other than delay. If the input signal $f(t)$ is broadband with respect to the distortion, the output of the cross-correlation analyser becomes

$$\phi_{fg}(t) = \frac{1}{2\pi} \int_{-\infty}^{\infty} H_o(w) \ e^{-iwt_o} \ e^{iwt} \ dw$$

or

$$\phi_{fg}(t') = \frac{1}{2\pi} \int_{-\infty}^{\infty} H_o(w) \ e^{iwt'} \ dw$$

$$\text{with } t' = t - t_o$$

Thus the shape of the cross-correlation function remains unchanged, but it is shifted along the time axis by an amount t_o.

We consider now some specific examples of waveform distortion. We ask first, which types of distortion are likely to have greatest significance for the excavation seismology program? Three categories may be considered:

- Distortion through the transducers - This will affect all seismic wave types and wave paths identically. Typically, we might expect a ringing effect for an impulse input, perhaps a decaying sinusoid

  $$e^{-At} \sin Bt$$

- Distortion of the reflected wave during transmission - Two factors may enter: frequency-dependent attenuation, and near-field versus far-field effects. The former produces

  $$e^{-kwx}$$

  amplitude attenuation, where k is some constant and w is angular frequency. The second factor is characteristic of curved wavefronts and will produce a different waveform far from the source than that which exists close to the source.

  Both of these factors can be represented mathematically and corrected for if necessary. For the excavation seismology program, we expect that their effect will be small in comparison with distortion from other sources.

- Distortion of direct P, surface, and other waves during transmission - For reflection seismic work, these other wave types and wavepaths constitute noise. They are source-generated noise, however, so that they will contribute to the cross-correlation function. We wish to keep their contribution as small as possible; distortion of the waveforms is desirable in the sense that it will degrade the cross-correlation output, although undesirable in the sense that the waveform will thereby be elongated in time, with possible overlap onto the reflection.

  The surface wave will create the most difficulty as a noise problem, due to large amplitude and a pulse duration which is often quite long. On the other hand, the waveform can be expected to differ substantially from those of direct and reflected P. For the excavation seismology program, we do not expect the dispersed wave train associated with a dispersive medium but rather a pulse of the type described by Lamb (1904):

83

Source: Distant vertical impulse

Vertical
surface
displacement

P

S

Rayleigh
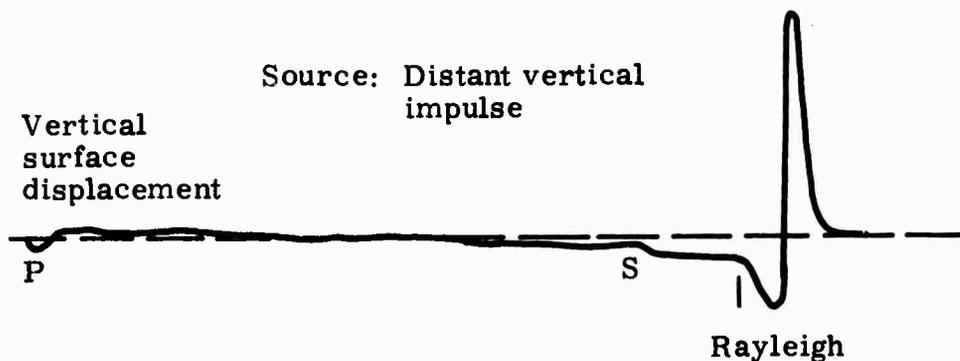
convolved with the impulse response of the source and receiver
transducers. Thus, we expect that the cross-correlation process
will discriminate against the surface wave to some extent; the
effectiveness of discrimination will depend on the ratio of surface
waveform distortion to transducer distortion, and will be improved
if the latter can be kept small or else eliminated from the analysis.

The shear waveform will also differ from the compressional
waveform, tending toward a longer pulse and lower frequencies.
We would expect that this factor, together with the small
amplitude and the arrival time close to the surface wave, should
result in relatively little noise problem from this cause.

The direct P wave should have much the same waveform as the
reflected P. The arrival time should be much earlier however,
and since the wave should be a relatively short pulse, we would
expect the cross-correlation analysis to keep the two well
separated.

To summarize the preceding discussion, two possible situations may
arise. In the first, we cross-correlate output after the transducers against
input before the transducers. Transducer distortion then becomes the
dominant contributor and affects the various seismic waves in the same way.
The second possible situation arises if we can somehow eliminate the
transducer distortion from the system; this goal may be attainable by the
master-signal method described above in section 4.3. The various seismic
waves will now undergo different kinds of distortion; the cross-correlation
analysis may attenuate those which we regard as noise.

In the following, we consider the first situation above, where trans-
ducer distortion is dominant. The second situation is treated in the next
section.

The remainder of this subsection is devoted to some numerical examples (Figures 42 through 52) of cross-correlation or matched-filter analysis for specific waveforms. The purpose is to show the cross-correlation function and its dependence on:

- Pulse length
- Waveform character
- Differences in waveform character between input and output
- Differences in dominant frequency.

The basic waveform in all cases is an exponentially-attenuated sinusoid. Each graph contains results for three cases: waveforms consisting of 1 2, or 4 cycles of the sinusoid.

The cases shown in Figures 42 through 52 are organized as follows:

- Case I: Identical pulses for input and output

    IA: Unattenuated
    IB: Slightly attenuated
    IC: Strongly attenuated

- Case II: Pulses differ in attenuation characteristics

    IIA: Input unattenuated, output slightly attenuated
    IIB: Input unattenuated, output strongly attenuated
    IIC: Input slightly, output strongly attenuated
    IID: Input strongly, output slightly attenuated

- Case III: Pulses differ in frequency

    IIIA: Unattenuated, 4% frequency difference
    IIIB: Unattenuated, 20% frequency difference
    IIIC: Slightly attenuated, 20% frequency difference
    IIID: Strongly attenuated, 20% frequency difference

Note that all of the cross-correlation functions have been normalized as defined in section 4.4.

The results for Case I represent simply the autocorrelation function of the waveform since the cross-correlation of a function against itself yields the autocorrelation. The graphs illustrate several well-known results however. The cross-correlation function is exactly twice as long in time as the original function; the shorter pulses yield shorter results. The identity of the input and output waveforms yields a peak value of 1.0 at a time precisely equal to the delay between output and input. The longer pulse lengths yield higher side lobes in the cross-correlation function; the side lobes decrease in amplitude, however, for the more attenuated pulses. The cross-correlation function is completely symmetrical on both sides of the peak.

85

The results for Case II show the effect of attenuating one of the signals more than the other. As before, shorter pulses yield shorter cross-correlations, but the symmetry about the peak no longer exists. The peak itself does not reach a value of 1.0; it decreases as the similarity between the waveforms decreases (Case IIB). The side lobes become larger as the pulse length increases.

The results for Case III show the effect of a frequency change in the pulse. Even for a 4% change (Case IIIA), the position of the peak has shifted, the peak value has decreased, and the lack of symmetry can be detected. For a 20% frequency difference, the effect has become marked, especially for the greater pulse lengths. Interestingly, the effect of attenuation is to partially cancel the effect of the frequency difference; this happens because the strongly attenuated signal looks more like a single cycle as the later cycles decay.

These numerical examples are not intended as realistic models for the excavating seismology program but they do illustrate the character and magnitude of the cross-correlation effect for simple well-defined waveforms.
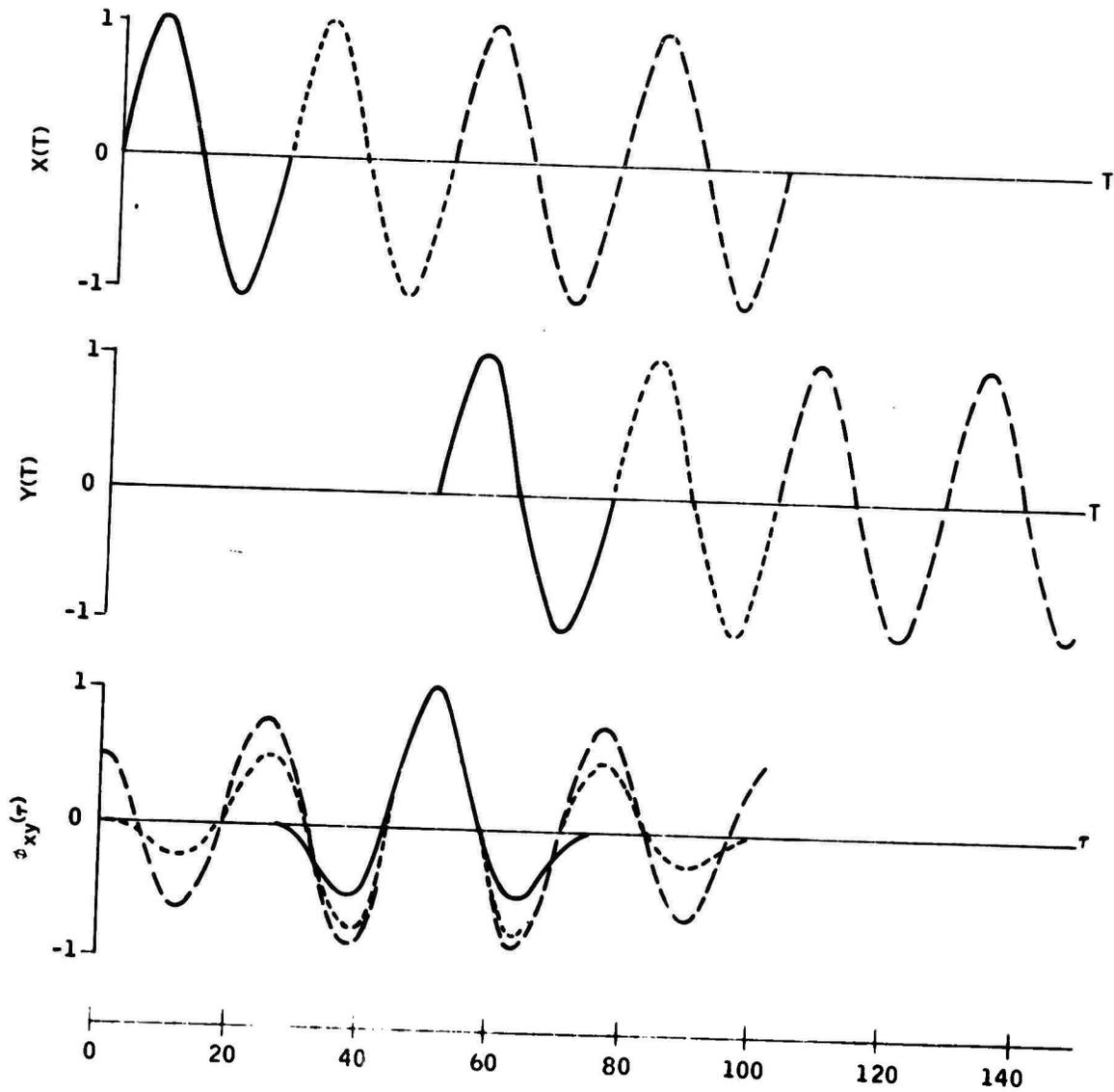
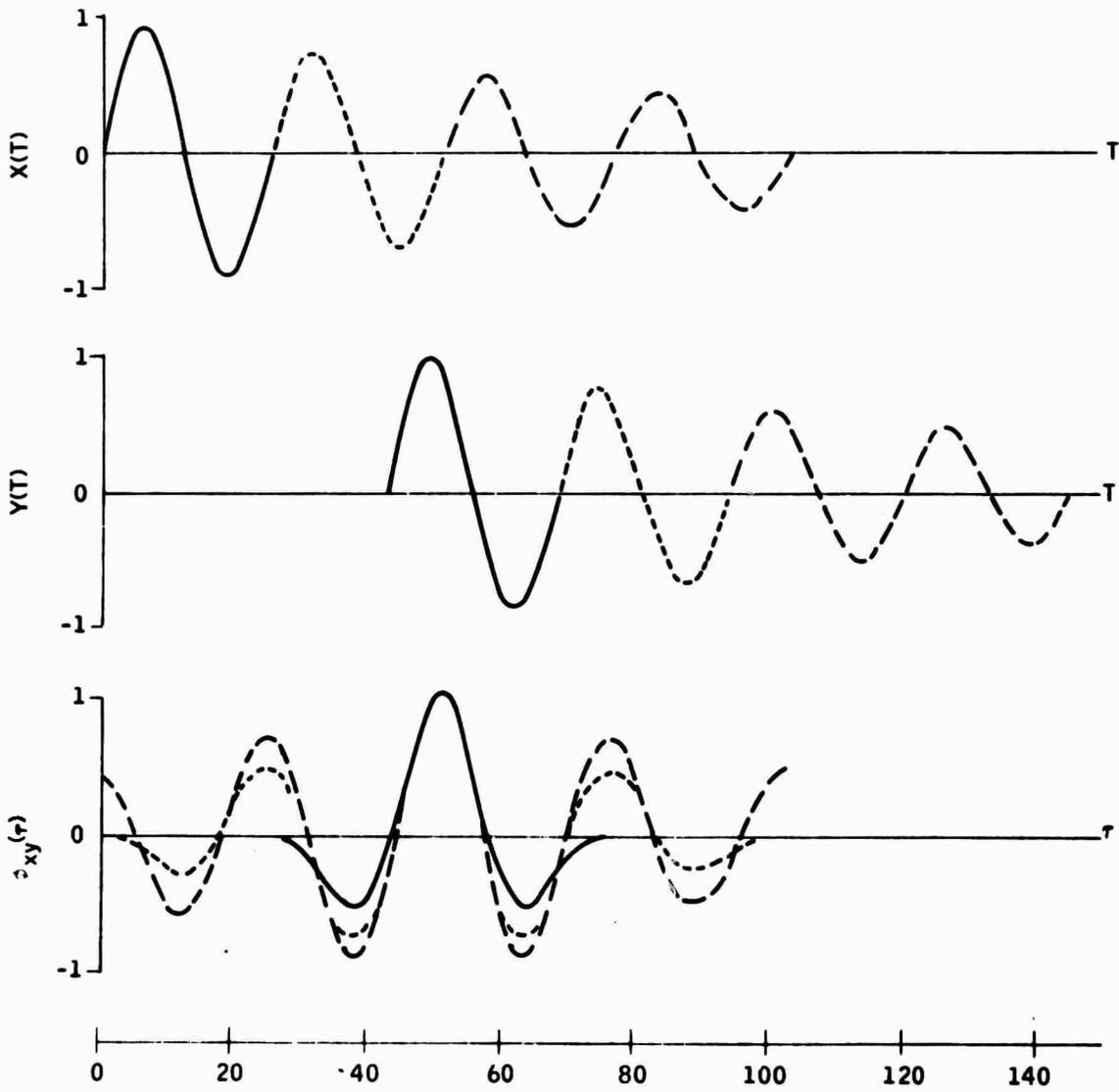Figure 42. Case IA: Identical, Unattenuated Sinusoidal Pulses

87

Figure 43. Case IB: Identical, Slightly Attenuated Sinusoidal Pulses
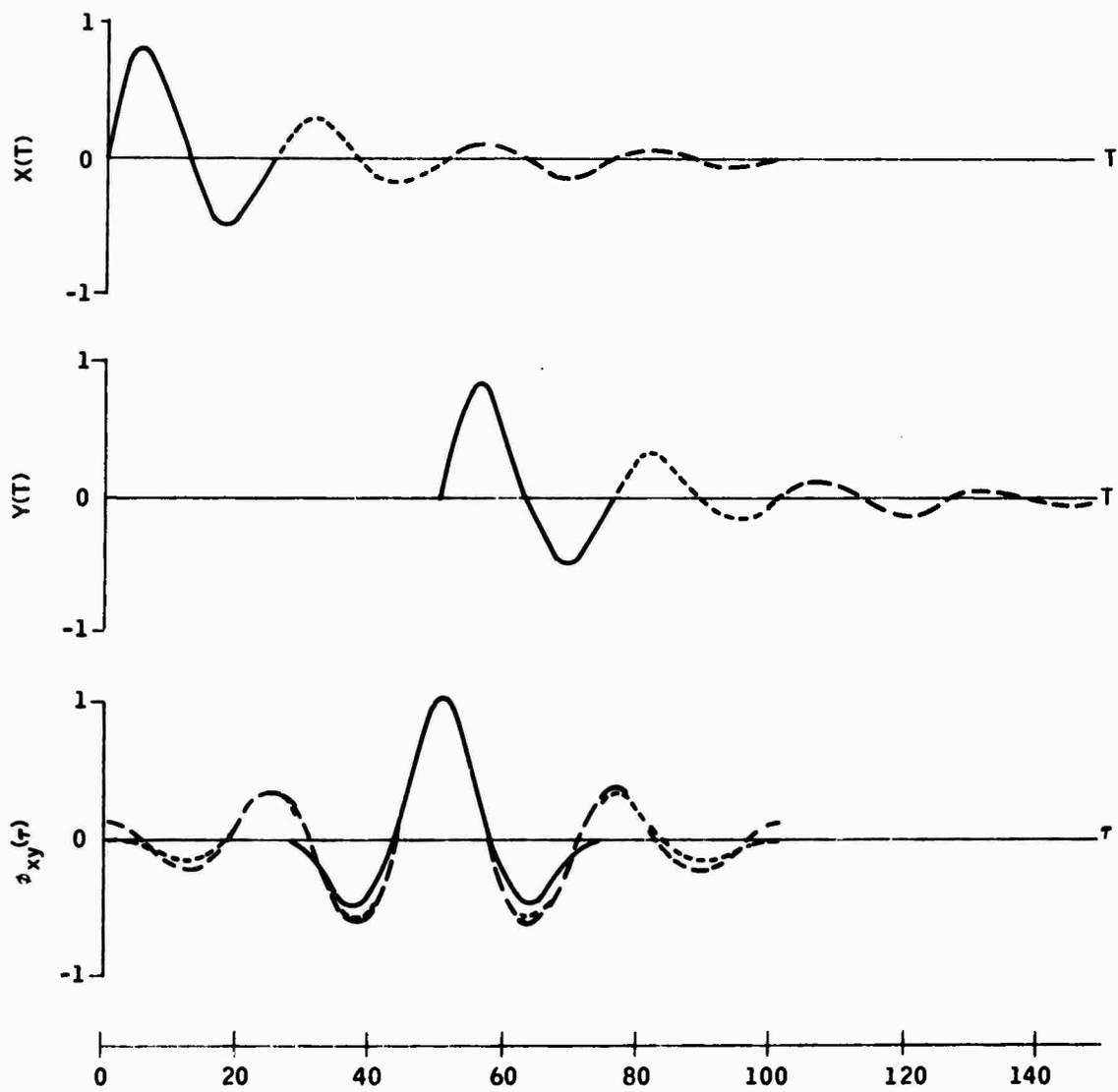
88

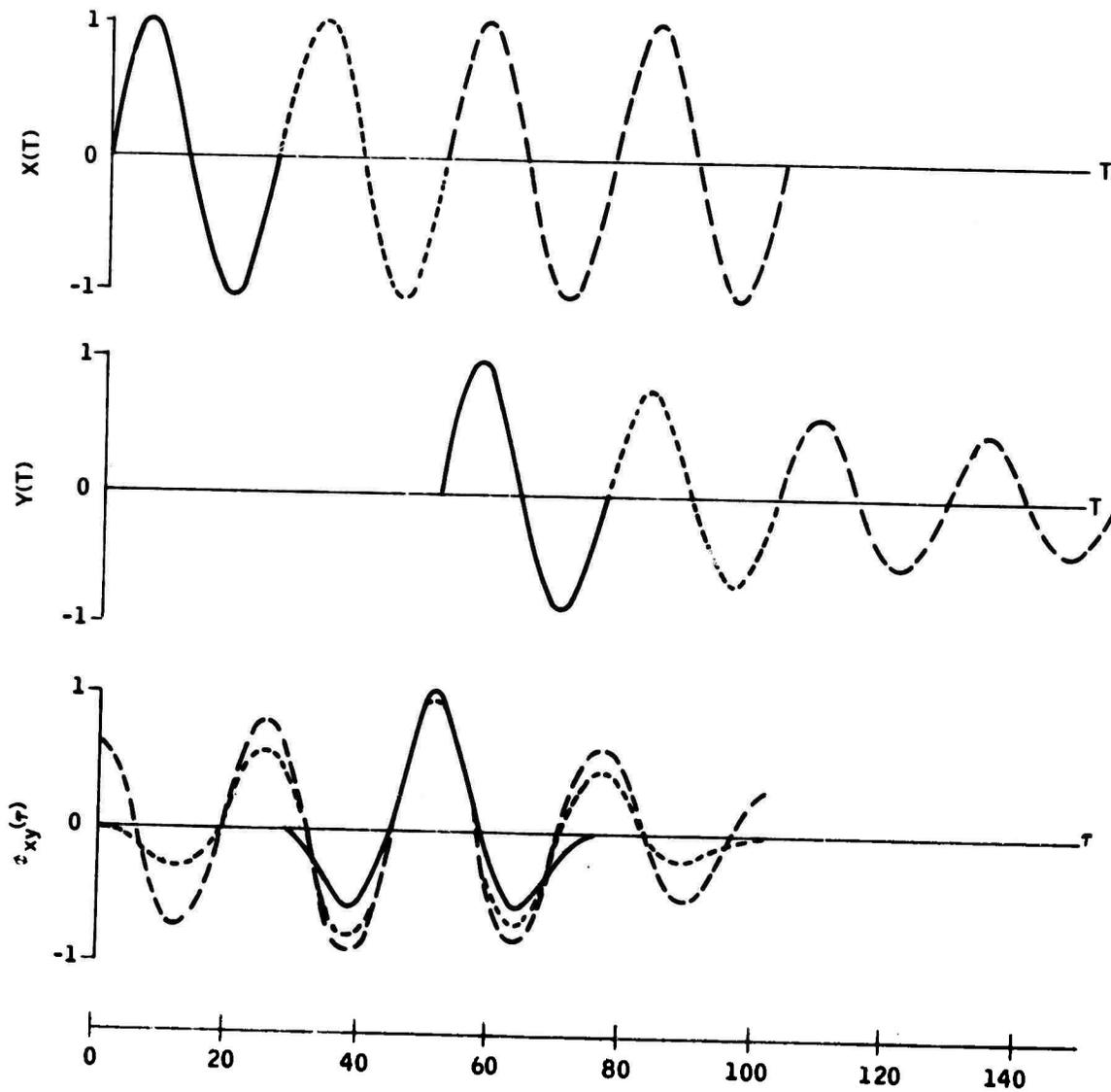Figure 44.   Case IC: Identical, Strongly Attenuated
Sinusoidal Pulses

89

Figure 45. Case IIA: Sinusoidal Pulses, Same Frequency, Different Damping (no damping X, light damping Y)
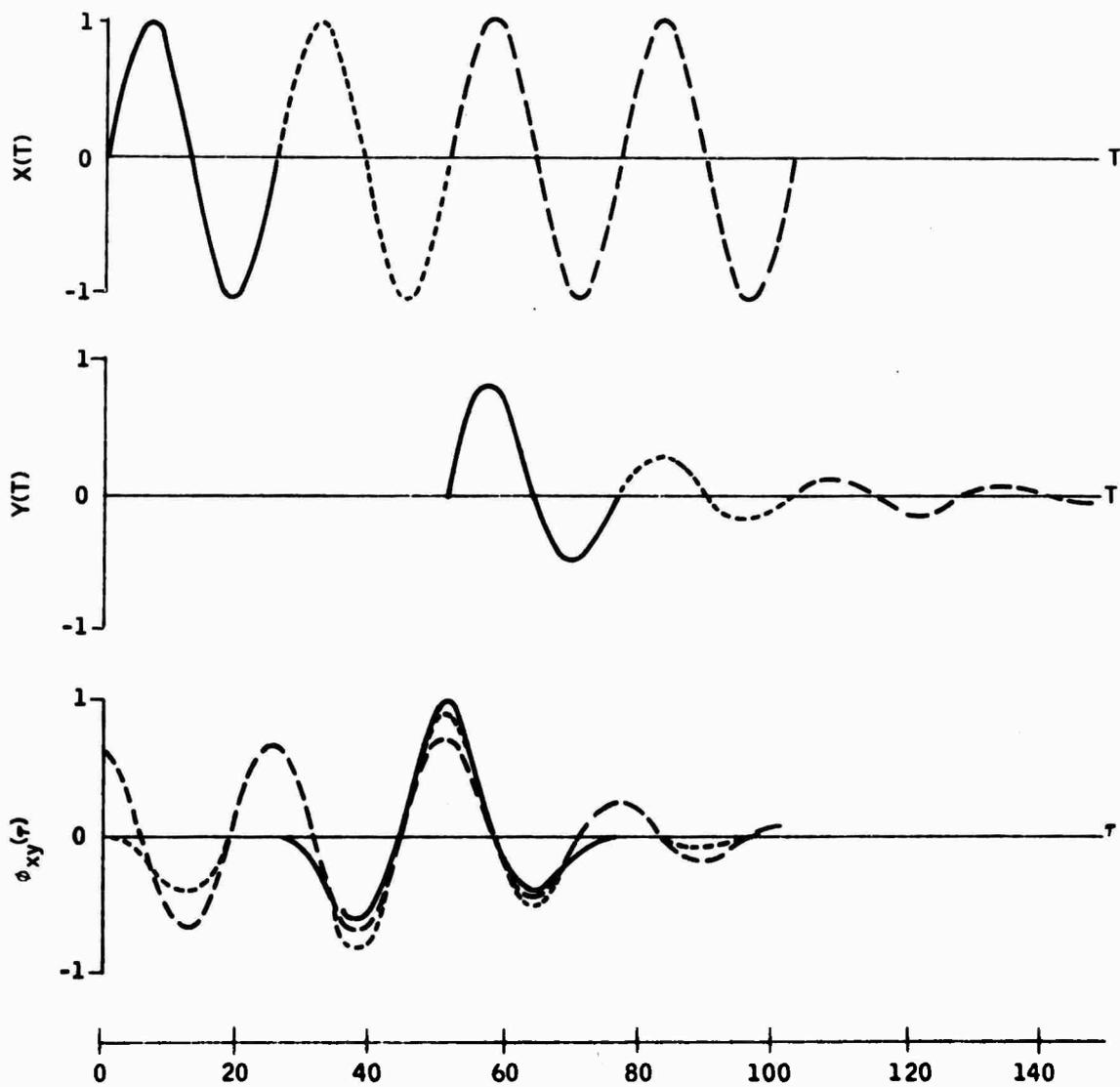
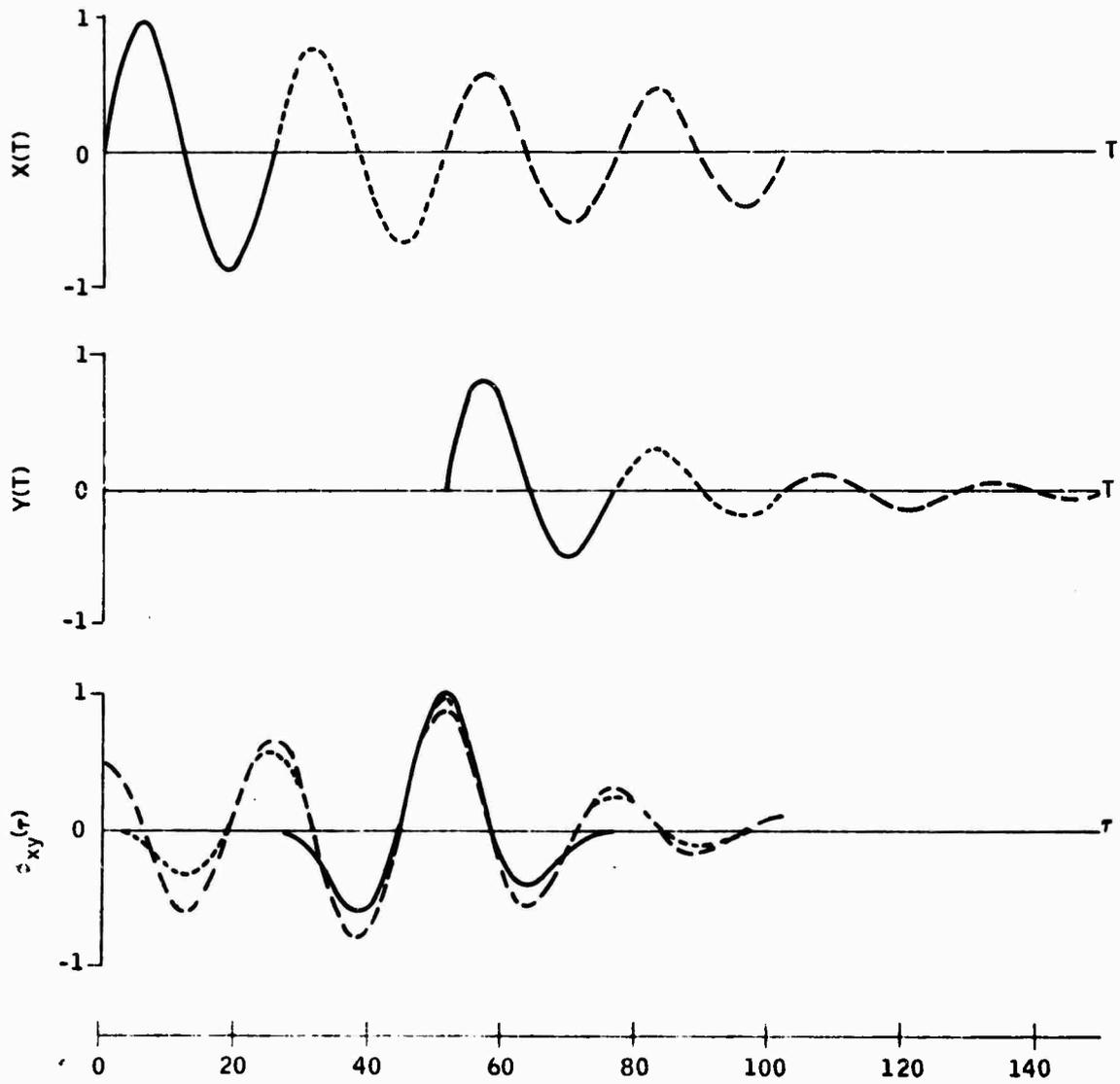Figure 46. Case IIB: Sinusoidal Pulses, Same Frequency, Different Damping (no damping X, heavy damping Y)

91

Figure 47. Case IIC: Sinusoidal Pulses, Same Frequency, Different Damping (light damping X, heavy damping Y)
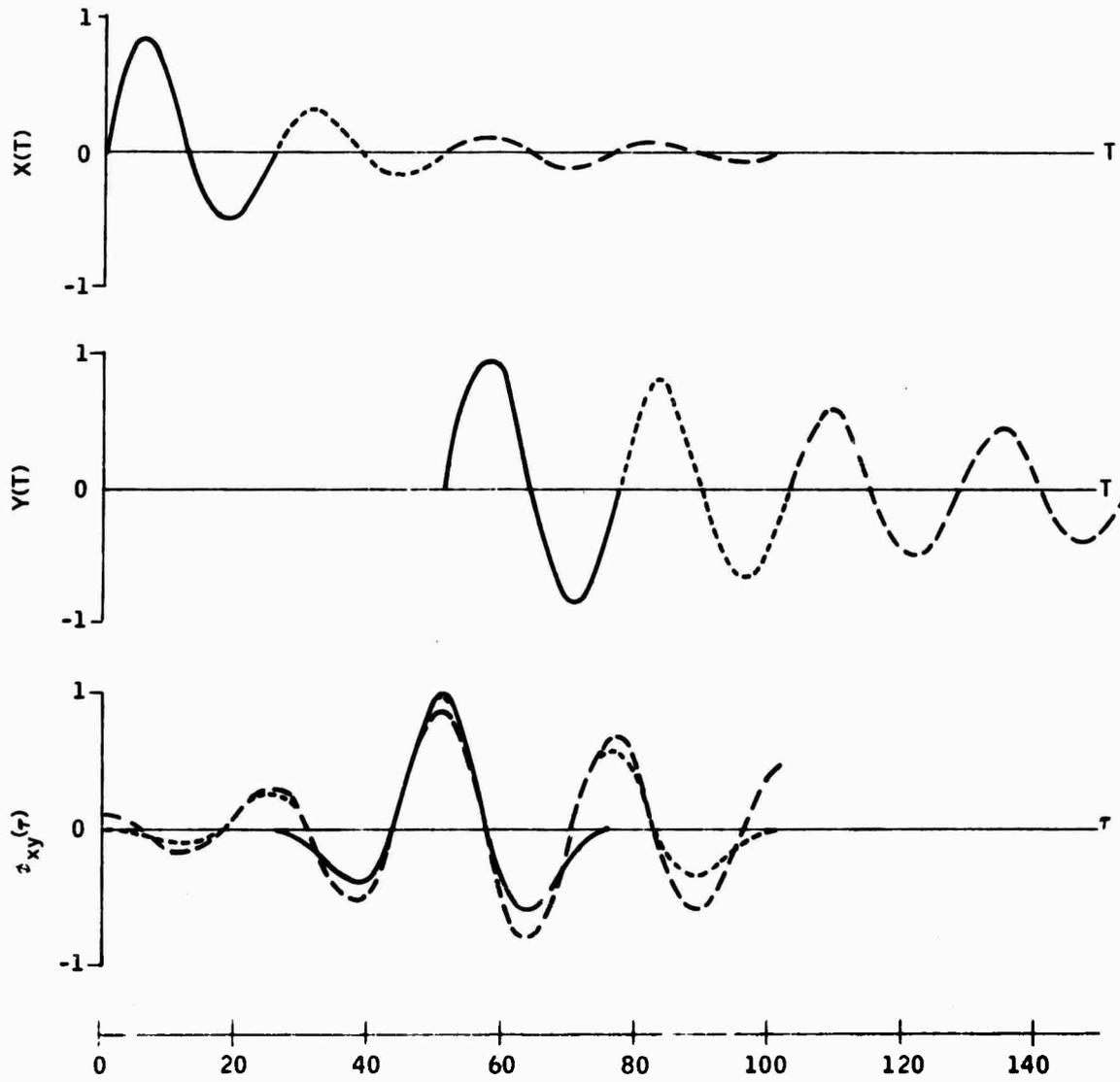
92

Figure 48. Case IID: Sinusoidal Pulses, Same Frequency, Different Damping (heavy damping X, light damping Y)
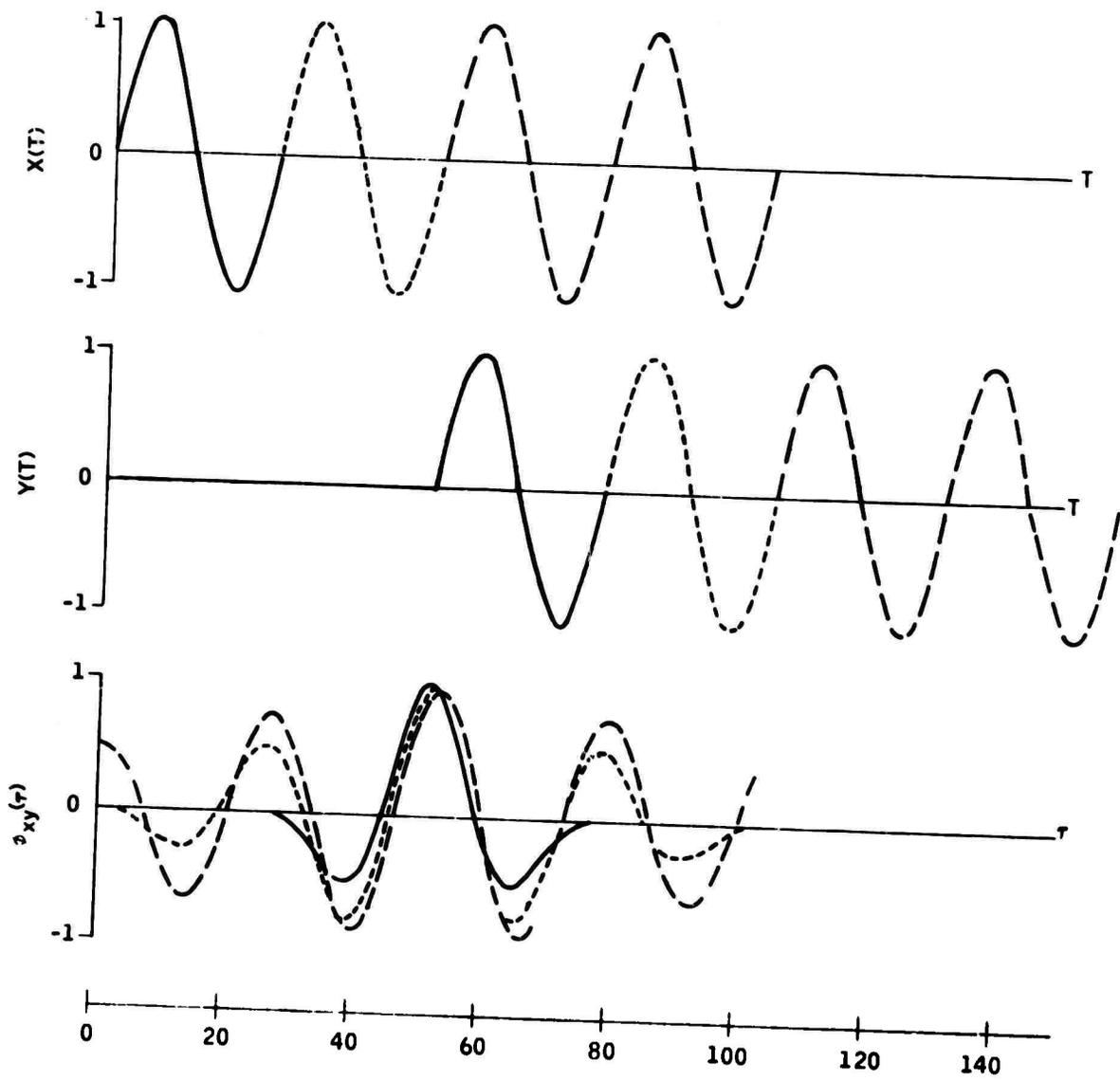
93

Figure 49. Case IIIA: Sinusoidal Pulses, Unattenuated,
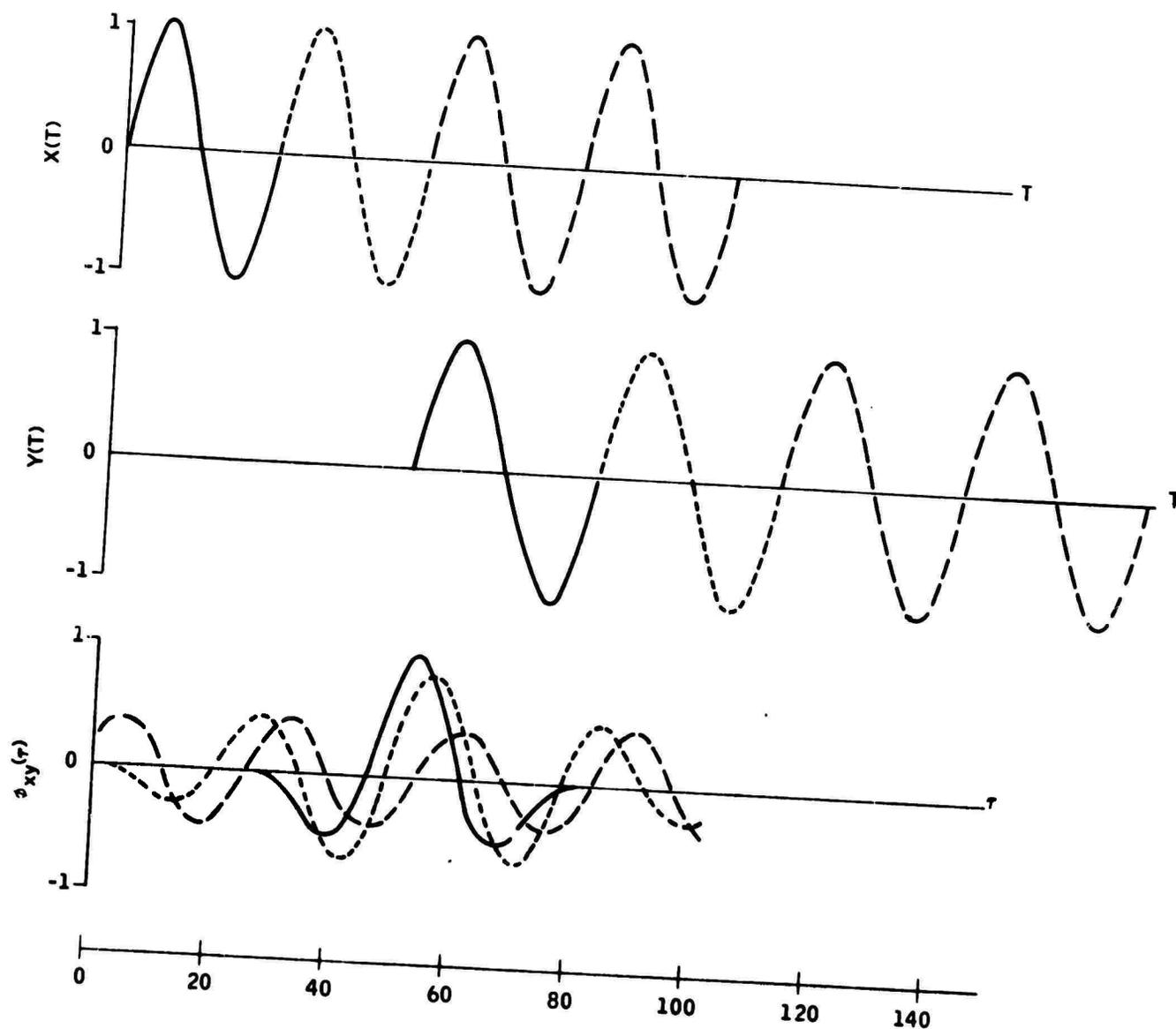4 Percent Frequency Difference

Figure 50.   Case IIIB: Sinusoidal Pulses, Unattenuated, 20 Percent Frequency Difference
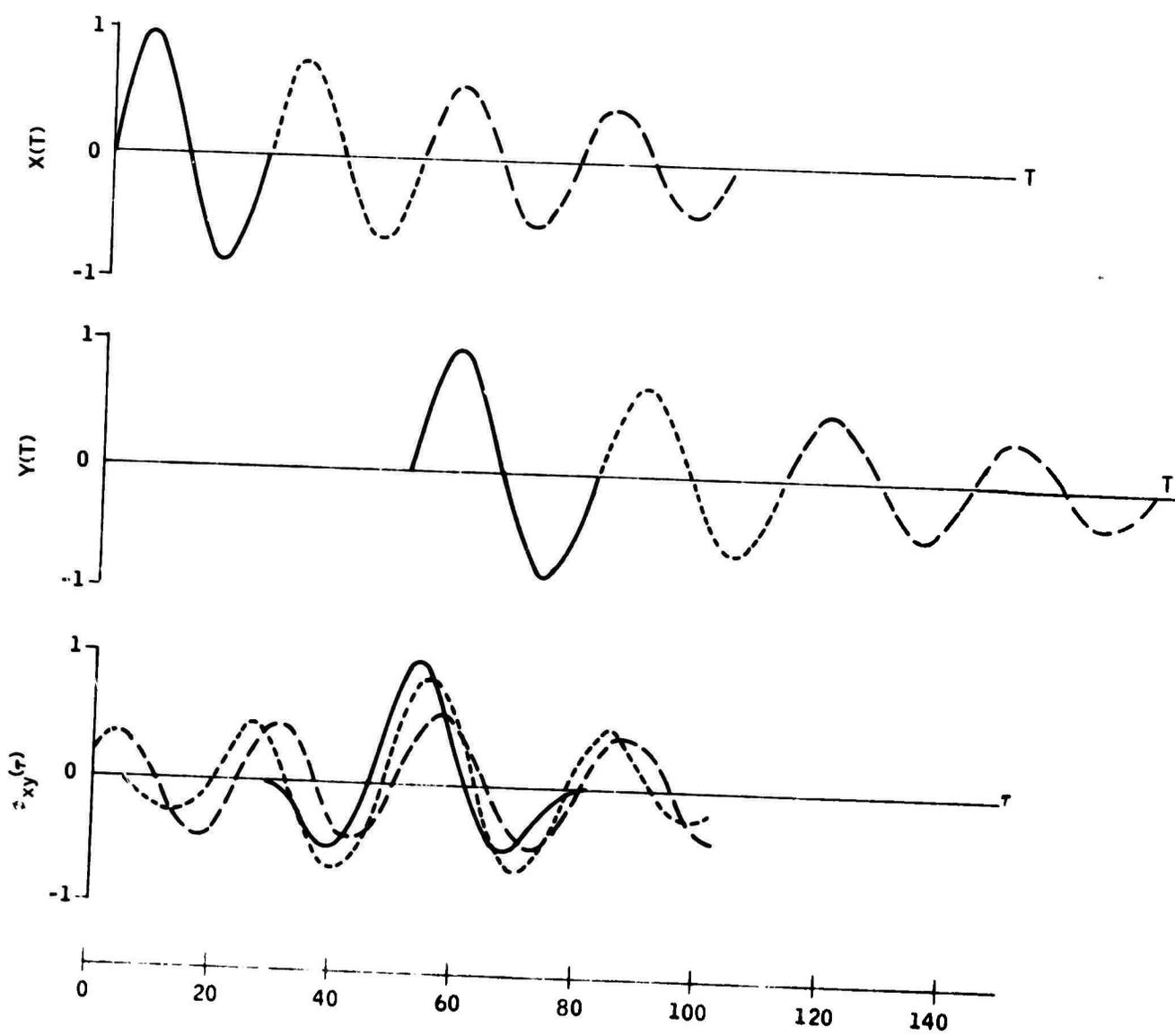
95

Figure 51. Case IIIC: Sinusoidal Pulses, Lightly Damped,
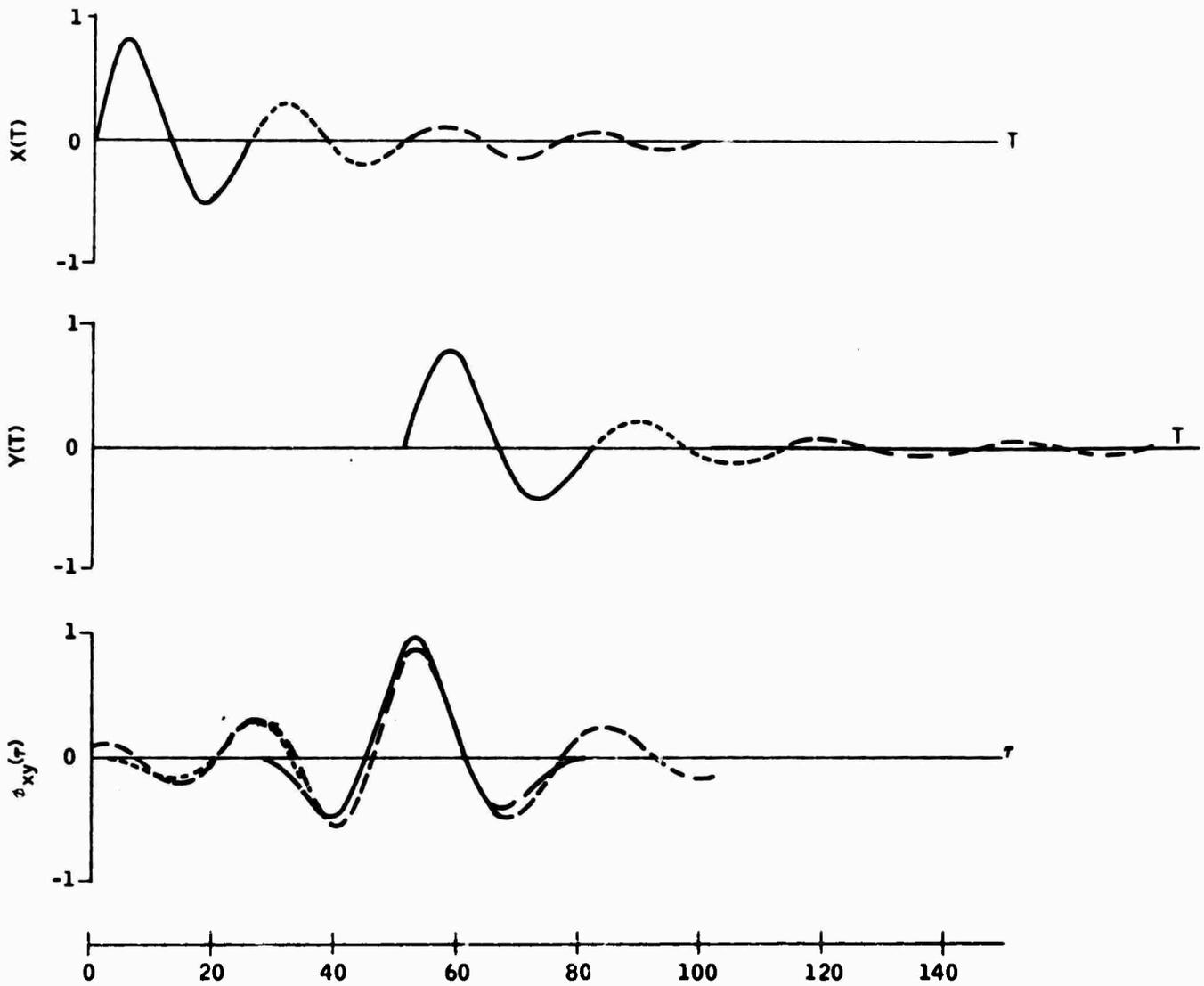20 Percent Frequency Difference

Figure 52.   Case IIID: Sinusoidal Pulses, Heavily Damped,
20 Percent Frequency Difference

97

4.2.2 Cross-Correlation in the Presence of Random Noise

In the preceding subsection we considered cross-correlation analysis where the waveform had been distorted by passage through the system (principally the transducers). We now consider the alternative situation, where the waveform has not been greatly distorted but appears superposed on background noise.

For the excavation seismology program, the background noise will consist principally of residual vibrations remaining from seismic arrivals preceding the desired reflection. The surface wave train will be the most important contributor. These earlier seismic arrivals will not be random with respect to the source, since they are source-generated. They will have some random characteristics, however, for the following reasons: (1) their arrival time is uncorrelated with the reflection arrival time; (2) the character of the wave train will depend strongly upon the transducer coupling, which may be expected to be quite variable; and (3) the waveforms for different seismic paths (and especially for the surface wave) will differ somewhat.

We conclude therefore that the reflection arrival will appear super-posed on a noise background, and that a crude approximation to this noise might be a random signal with power density $N(w)$. A special case would be white noise with $N(w) = $ constant.

Once we have accepted a model in which the noise is additive, the only remaining decision lies in whether to add it at the input or the output. The decision is not of great consequence, since we can always convert from one to the other. The two, or even three, possibilities may be shown as:
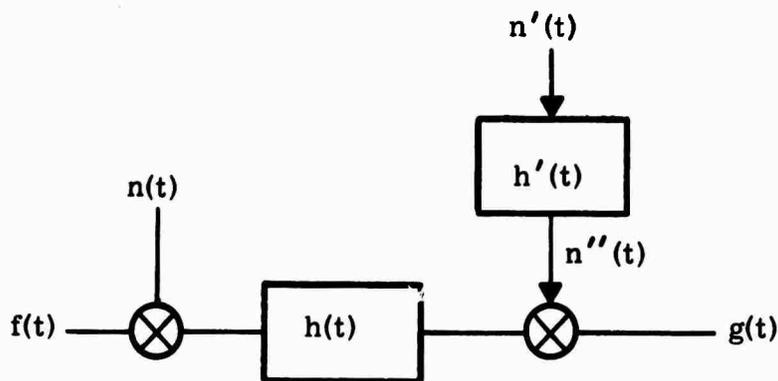
We will take the first of these three possibilities n(t) added to the input, as most realistic for the excavation seismology program, although the analysis for the other two is very similar.

The output can be written formally as

$$g(t) = \int_{-\infty}^{\infty} h(t') \,[\, f(t-t') + n\,(t-t') \,]\, dt' \tag{38}$$

and the cross-correlation between input and output becomes

$$\phi_{fg}\,(\tau) = \lim_{T \to \infty} \frac{1}{2T} \int_{-T}^{T} f(t)\, g(t + \tau)\, dt$$

$$= \lim_{T \to \infty} \frac{1}{2T} \int_{-T}^{T} f(t)\, dt \int_{-\infty}^{\infty} h(t')\, [\, f(t + \tau - t') + n(t+\tau-\tau') \,]\, d$$

$$= \int_{-\infty}^{\infty} h(t')\, \phi_{ff}(\tau - t')\, dt' + \int_{-\infty}^{\infty} h(t')\, dt' \lim_{T \to \infty} \frac{1}{2T} \int_{-T}^{T} f(t)\, n(t+\tau-t')\, d$$

$$= \int_{-\infty}^{\infty} h(t')\, [\, \phi_{ff}(\tau - t') + \phi_{fn}\,(\tau - t') \,]\, dt'$$

$$= \int_{-\infty}^{\infty} h(t')\, \phi_{ff}\,(\tau - t')\, dt' + \int_{-\infty}^{\infty} h(t')\, \phi_{fn}\,(\tau - t')\, dt' \tag{39}$$

If it happens that the input f(t) and the noise n(t) are uncorrelated, the last integral reduces to

$$\overline{f(t)} \;\; \overline{n(t)} \int_{-\infty}^{\infty} h(t')\, dt'$$

The first integral in the preceding is identical with the input-output cross-correlation relationship of section 4.5, as it should be. The second integral shows that the contamination produced by additive noise appears as an additive term in the cross-correlation function. If the input and the noise are uncorrelated, the additive term reduces to a constant; if either the input or the noise has zero mean, the constant is identically zero.

99

4.2.3 Cross-Correlation Analysis in Conjunction with Array Processor:

Since both array processing and cross-correlation/matched filtering are linear processes   we conclude that they may be carried out sequentially in either order. The results will equal the sum of the effects from each of the two methods of analysis.
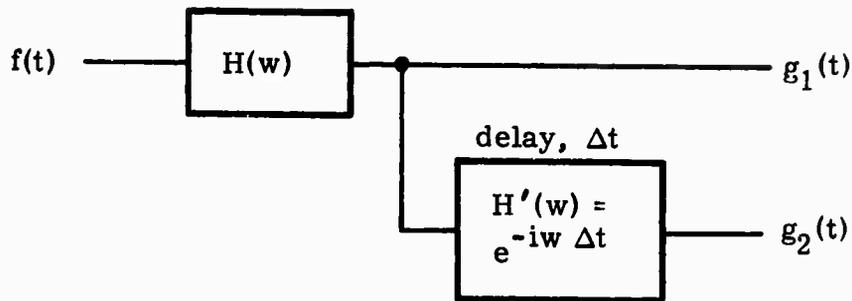
A simple example will serve to show the total effect from these two methods. In the nomenclature of the generalized signal processor of Figure 2, Section 2, we are considering first a spatial and then a temporal processor.

The physical model under consideration may be illustrated using only two receivers:
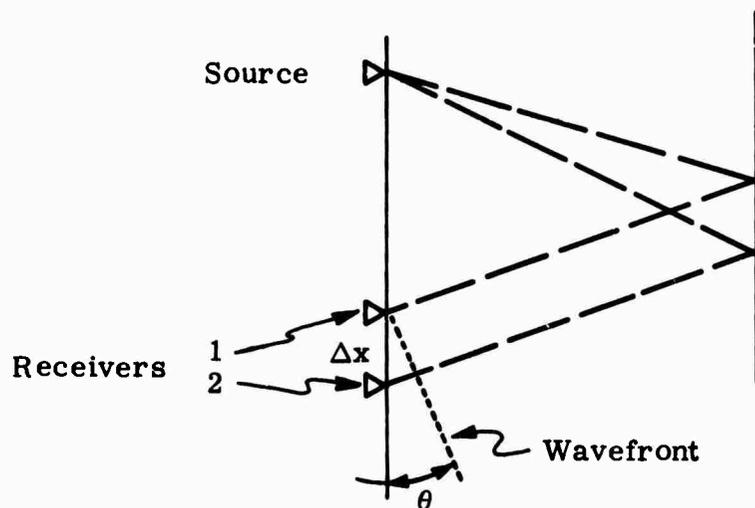
We assume that the source input waveform f t), differs from the receiver waveforms, $g_1(t)$ and $g_2(t)$, but that the latter are identical except for different arrival times. From geometry, the difference in arrival time will be a delay at receiver 2 of magnitude
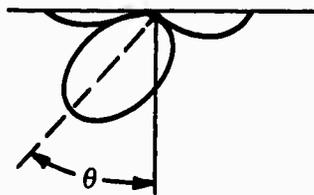
$$\Delta t = \Delta x(\sin \theta)/V$$

100

$$f(t) \longrightarrow \boxed{H(w)} \bullet \longrightarrow g_1(t)$$

delay, Δt

$$\boxed{\begin{array}{c} H'(w) = \\ e^{-iw\,\Delta t} \end{array}} \longrightarrow g_2(t)$$

If the array processor is a delay-and-sum, then the output signal becomes

$$g(t) = g_1 (t - \Delta t) + g_2(t)$$

$$= 2g_2(t) \tag{40}$$

if the delay is correctly set equal to Δt. For other delays - which would arise from other angles of incidence - we get the characteri;tic lobes associated with beam-steering:

With respect to the present discussion, the essential point to be noted is that a cross-correlation analysis applied to $g(t)$ will simply reduce to a sum of terms with the following result:

$$\phi_{fg}(\tau)$$

$\Delta t' \neq \Delta t:$

$$\phi_{fg}(\tau)$$

$\Delta t' = \Delta t:$
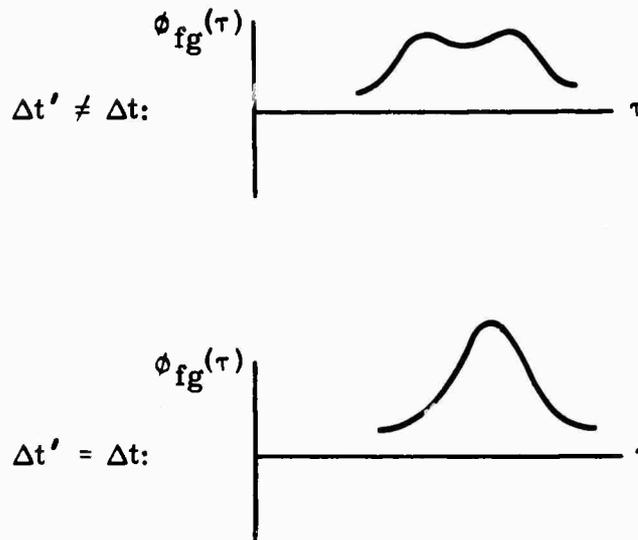
4.3 COHERENT TIME AVERAGING

A possible disadvantage to the use of cross-correlation techniques for signal enhancement is the need to know the transmitted waveform. Coherent time averaging techniques can be used to enhance repetitive signals in noise in cases where the characteristics of the signal are not known.

This technique recovers the wave shape of a repetitive signal from noise by averaging each point of the waveform many times, utilizing the property of random noise that the time average approaches zero.

A disadvantage of coherent time averaging is the time required for the large number of repetitions necessary when the signal-to-noise ration is very small. In excavation seismology, the maximum repetition rate is determined by the delay time of a reflection at the maximum depth of interest. For example, if the compressional-wave velocity of the rock is 5 km/sec and reflections from depths up to 25 meters are of interest, the minimum repetition interval is 10 milliseconds, or 100 repetitions/sec. The signal-to-noise ratio increases as the square root of the number of repetitions, so if an increase of a factor of 100 (40 db) is needed, 10,000 repetitions are necessary, which would take 100 seconds.

4.3.1 Averaging Algorithms

Three principal averaging algorithms are (Rhyne, 1969):

- Equally weighted, nonrunning average

102

- "Sliding window" average

- Exponentially weighted average

The second and third are primarily useful for recovering signals in noise when the signal characteristics vary slowly with time. For the seismic problem, the signal will be invariant, however, so that only the first algorithm is of interest.

For the first algorithm, the average consists of simple summation, with the signal present in the summation building up linearly with the number of repetitions. The random noise adds up in a root-mean-square sense, so that, after N repetitions, the signal-to-noise ratio has been improved by $\sqrt{N}$.

Let the input to the averager be $f(t)$, consisting of a repetitive signal $s(t)$ and noise $n(t)$. Let the ith repetition begin at t_i and assume the waveform is sampled every τ seconds. Then

$$f(t) = s(t) + n(t) \tag{41}$$

$$f(t_i + k\tau) = s(t_i + k\tau) + n(t_i + k\tau) = s(k\tau) + (n(t_i + k\tau) \tag{42}$$

After N repetitions, the value stored at the kth memory location is

$$S_N(k) = \sum_{k=1}^{N} f(t_i + k\tau) = Ns(k\tau) + \sum_{k=1}^{N} n(t_i + k\tau) \tag{43}$$

The noise summation term on the right tends to zero (ignoring source-produced noise) as N becomes large, leaving $N s(kT)$ stored in the kth memory location.

4.3.2 Stable Averaging

An alternative to equation (43) which leaves the value $S(k\tau)$ stored in the kth memory location is known as stable averaging. Instead of computing a simple summation of N terms, the mean value of N terms is computed. This can be accomplished recursively as follows:

Let $M_n(k)$ be the mean value of N terms, stored in the kth memory location. Then

103

$$M_N(k) = \frac{1}{N} S_N(k)$$

$$= \frac{1}{N} \sum_{k=1}^{N} f(t_i + k\tau)$$

$$= \frac{N-1}{N} M_{N-1}(k) + \frac{1}{N} f(t_i + N\tau)$$

$$= M_{N-1}(k) + \frac{f(t_i + N\tau) - M_{N-1}(k)}{N} \tag{44}$$

From equation (44), we see that

$$\lim_{N \to \infty} M_N(k) = s(k\tau) + \lim_{N \to \infty} \frac{1}{N} \sum_{k=1}^{N} n(t_i + k\tau) = s(k\tau) \tag{45}$$

4.3.3 Coherent Averaging and Array Processing

The compatibility between coherent averaging and array processing can be illustrated by simple delay-and-sum beamforming. Let $f_\ell(t)$ be the output of the ℓth element of the array, and assume that the proper delays have been applied to line up the signal in each of the L elements of the array. Then,

$$f_\ell(t) = s(t) + n_\ell(t) \tag{46}$$

$$f_\ell(t_i + k\tau) = s(t_i + k\tau) + n_\ell(t_i + k\tau) = s(k\tau) + n_\ell(t_i + k\tau) \tag{47}$$

The output of the delay-and-sum processor is

$$g(t_i + k\tau) = \frac{1}{L} \sum_{\ell=1}^{L} f_\ell(t_i + k\tau) = s(k\tau) + \frac{1}{L} \sum_{\ell=1}^{L} n_\ell(t_i + k\tau) \tag{48}$$

Applying coherent averaging to the output of the delay-and-sum processor,

$$M_N(k) = s(k\tau) + \frac{1}{NL} \sum_{k=1}^{N} \sum_{\ell=1}^{L} n_\ell(t_i + k\tau) \tag{49}$$

104

Again, the noise term on the right tends to zero as N becomes large, assuming no source-produced noise. For source-produced interference, including reflections from directions other than that for which the proper delays have been applied, the summation across the L elements of the array will attenuate the interference relative to the signal component. A study of more general array processors is currently in progress.

REFERENCES

Anstey, N., 1964, Correlation techniques - a review: Geophysical Prospecting, v. 12, p. 355.

Anzai, T., 1959, Generation and detection of ultrasonic waves in solids by small barium titanate transducers: Tohoku Univ. Res. Inst. Sci. Repts. v. 11, p. 152.

Bendat, J., and A. Piersol, 1966, Measurement and analysis of random data: John Wiley Co., 390 pp.

Brown, B.M., 1970, Sonar signal processing: in, Underwater Acoustics, Chapter 10, by L.W. Camp, John Wiley Co., 308 pp.

Brown, G.L., 1956, Theory and design of pressure pulse transducers and transient detectors for solid media, Ph. D. Thesis, UCLA.

Cannaday, F.X., and G.M. Leo, 1966, Development of controlled impulse technique for in site testing of rock, Bureau of Mines, Denver, Colo. AFWL-TR-65-156.

Capon, J., 1970, Applications of detection and estimation theory to large array seismology: Proc. IEEE, v. 58, p. 760.

Dwork, B., 1950, Detection of a pulse superimposed on fluctuation noise: Proc. Inst. Radio Eng. v. 38, p. 771.

Ergin, K., 1952, Energy ratio of the seismic waves reflected and refracted at a rock-water boundary: Bull. Seis. Soc. Amer. v. 42, p. 349.

Evernden, J., 1969, Identification of earthquakes and explosions by teleseismic data: Jour. Geoph. Res. v. 74, p. 3828.

Ewing, W.M., et al, 1957, Elastic waves in layered media: McGraw Hill Company, New York, 380 pp.

George, C., et al, 1962, Applications of inverse convolution techniques to geophysical data: Proc. IRE, Nov., P. 2313.

Gutenberg, B, 1944, Energy ratio of reflected and refracted seismic waves: Bull. Seis. Soc. Amer. v. 34, p. 85.

Hales, A., and J. Roberts, 1970, The travel times of S and SKS: Bul. Seis. Soc. Amer. v. 60, p. 461.

Helmberger, D., and R. Wiggins, 1971, Upper mantle structure of Midwestern U.S.: Jour. Geoph. Res. v. 76, p. 3229.

Jones, H., and J. Morrison, 1954, Cross correlation filtering: Geophysics, v. 19, p. 660.

Preceding page blank

Lee, Y., 1960, Statistical theory of communication: John Wiley Co.,
509 pp.

Loren, J.D., 1961, Amplitude studies by model seismology of reflections
from a free surface: M.S. Thesis, Univ. Minnesota, 150 pp.

McMullen, C., 1968, Communication theory principles: MacMillan Co.,
New York, 416 pp.

Oliver, J., Press, F., and Ewing, M. 1954, Two-dimensional model
seismology, Geophysics, V. 19, p. 202-219.

Press, F., Oliver, J., and Ewing, M. 1954, Seismic model studies of
refractions. Geophysics, v. 19, p. 388-401.

Rhyne, V.T., 1969, A comparison of coherent averaging techniques for
repetitive biological signals, Med. Res. Engrg., Aug-Sept. 1969,
pp. 22-26.

Rice, R., 1962, Inverse convolution filters: Geophysics, v. 27, p. 4.

Schneider, W., 1967, Single and multichannel filtering of seismic data:
World Oil, November.

Tolstoy, I., and C. Clay, 1966, Ocean acoustics: McGraw Hill, 293 pp,
Chapter 7.

Treitel, S., and E. Robinson, 1969, Optimum digital filters for signal to
noise ratio enhancement: Geophysical Prospecting v. 17, p. 248.

Turin, G., 1960, An introduction to matched filter: IRE Trans, Information
Theory, v. IT-6, p. 311. (Entire issue is devoted to matched filters).

Von Seggern, D., 1972, Relative location of seismic events using surface
waves: Geophysical Journal (in press).

Zadeh, L., and J. Ragazzini, 1952, Optimum filters for the detection of
signals in noise: Proc. Inst. Radio Eng. v. 40, p. 1223.

APPENDIX A

SEISMIC REFLECTION COEFFICIENT MEASUREMENTS

Figures A1, A2 and A3 are taken from Loren (1961). Figure A1 shows the variation of free-surface reflection coefficients for incident S and reflected P, calculated for a two-dimensional seismic model constructed from plexiglass (the ordinate is displacement amplitude ratio). Figure A2 shows the effect for incident P and reflected S, and Figure A3 for incident P-reflected P or incident S-reflected S.

The model work was carried out in such a way as to completely eliminate variations due to the other factors noted in section 2.4, leaving only variations due to reflection coefficients (the other factors were the free surface effect at the receiver and the radiation pattern of the source and receiver transducers). This was achieved by use of a model shaped as shown below.
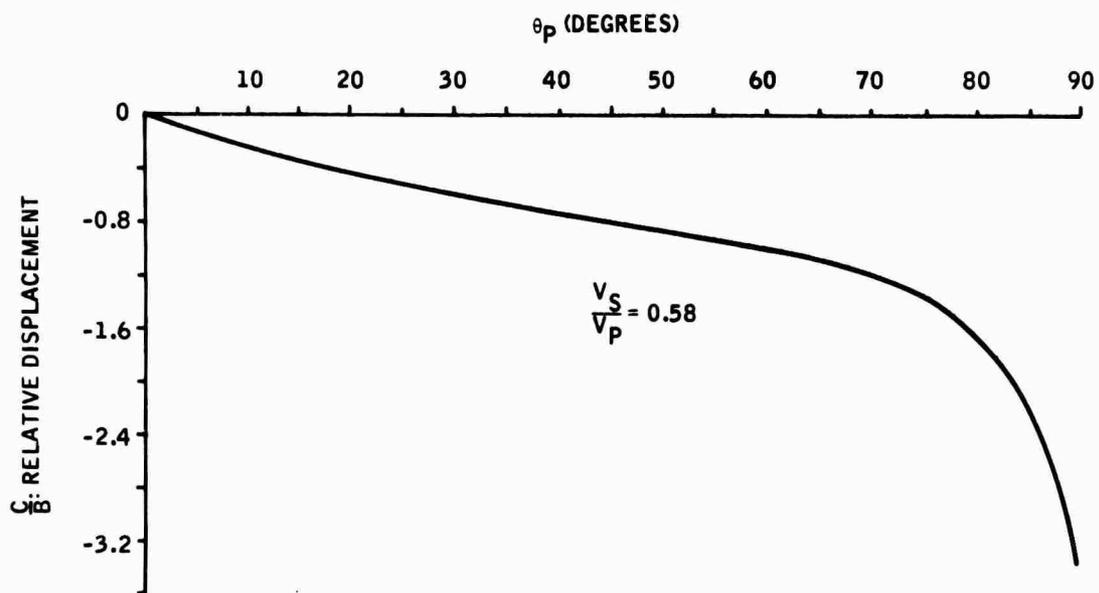

A1
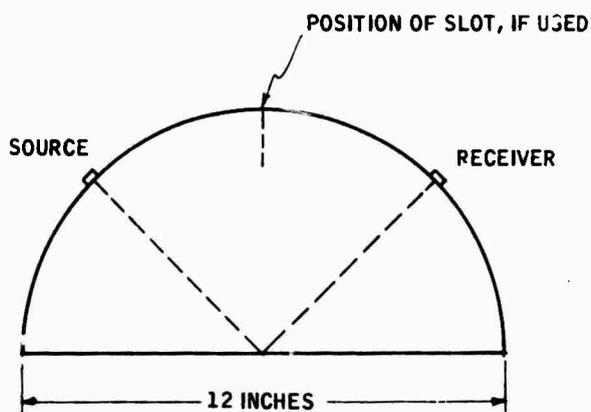
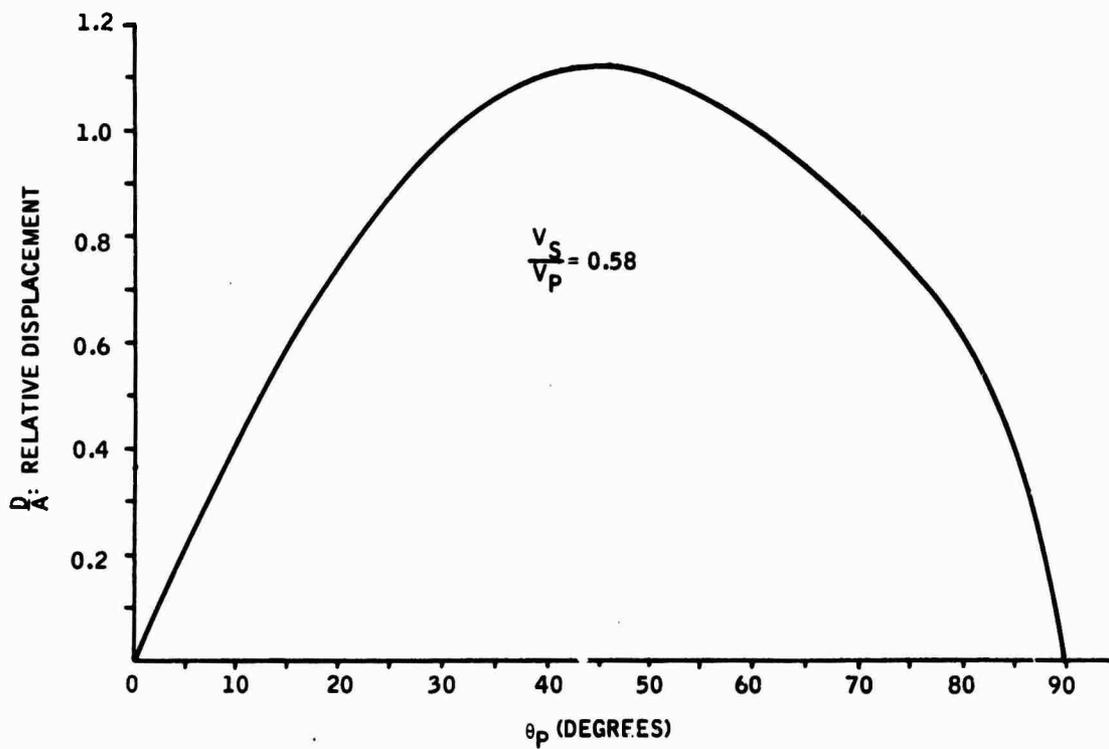Figure A1. Free-Surface Reflection Coefficients for SP

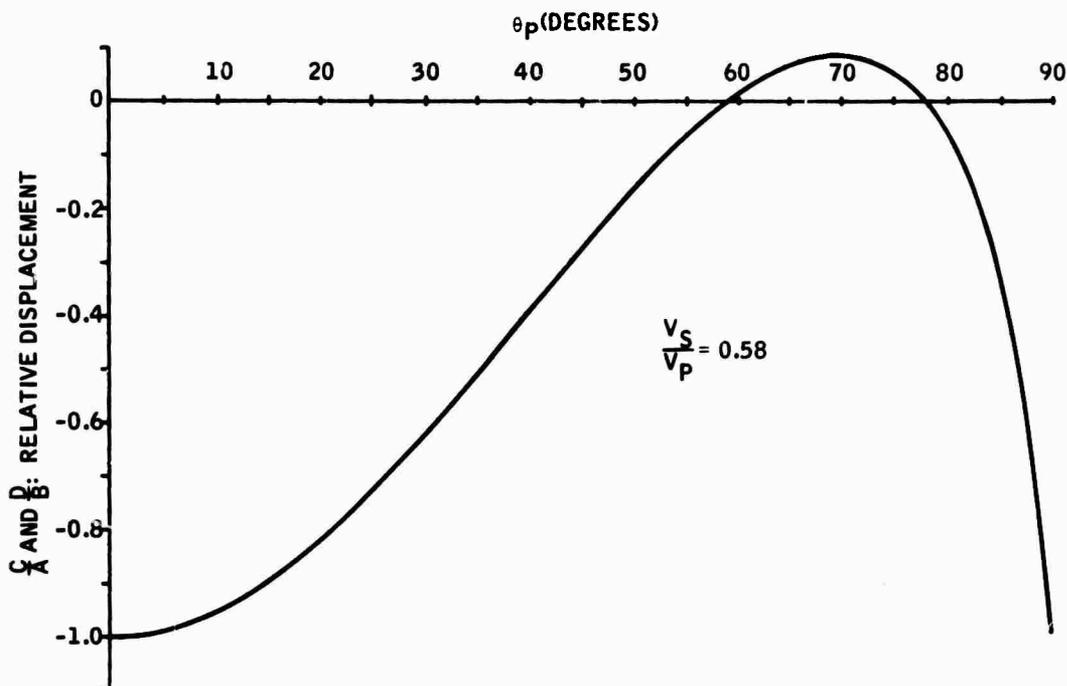Figure A2. Free-Surface Reflection Coefficients for PS

A2

Figure A3.   Free-Surface Reflection Coefficients for PP and SS

The transducers are always perpendicular to the surface, hence we operate on a fixed position with respect to their radiation pattern.

Furthermore, the geometry was carefully arranged so that the seismic ray paths always lay along a radius of the disc. For PP or SS, this simply required keeping source and receiver symmetrical. For PS or SP, corrections were made in the source and receiver positions to achieve the same goal.

A further extension of the work involved cutting a slot to various depths at the positions shown. The purpose of the slot was to reduce interference from seismic waves which have travelled other paths, in particular the Rayleigh wave. Section 3.7 contains the results of a related investigation, using a rectangular seismic model, on the effect upon Rayleigh waves of cutting a slot in the model. Some of the results for the disc model are given here.

The experimental data presented were taken on a sheet of 1/16-inch plexiglass. Source and receiver transducers were piezoelectric ceramics of rectangular shape with a thickness of 1/16 inch. The electrical signal supplied to the source transducer was designed to approximate to a step function; it had a rise time of 8 μsec and an exponential decay to 1/e of about

A3

2 msec. Two positions were used for the mechanical mounting bracket for the transducers; the first, which we will call position A, places the bracket toward the diameter from the transducer, and the second, which we will call position B, places the bracket away from the diameter. Due to the necessity to shift from position A to position B during each individual traverse, two sets of waveforms with considerable overlap are presented.

The basic waveform results from the seismic model study are presented as Figures A4 through A9. Successive waveforms are taken at angle increments of 2 degrees around the periphery of the disc model, using the same angle for source and receiver as measured from the vertical line of symmetry. The horizontal scale is 50 μsec per large division, or 10 μsec per small division, or 500 μsec sweep length. The vertical scale is arbitrary but is kept the same for all waveforms to permit amplitude analysis.

Two prominent arrivals may be seen on the waveform of Figure A4 (1-inch cut). The direct wave comes in first; the time moveout is large for small angles but becomes smaller at large angles as should be the case for this geometry of the model. The reflected P wave appears as a large downward signal at approximately 260 μsec, but it is obscured and difficult to measure because of interfering waves.

The theoretical arrival time for the PP reflection is (2) (12 in.)/ (7760/ft/sec) = 258 μsec, which agrees closely with the observed arrival time and serves to confirm the identification. Strong additional confirmation is provided by the fact that arrival time is almost completely independent of azimuthal angle.

Figures A5 through A9 demonstrate the improvement which can be obtained by inserting a cut of increasing depth into the seismic model. The purpose of the cut is to block the passage of interfering seismic waves, although it must be recognized that the edge of the cut itself will give rise to diffracted waves. A brief study has been made of these diffracted waves, and also of PS and SP arrivals, but they are not reported here.

Figure A9 shows the dramatic improvement which can be achieved in isolating the PP arrival by means of a deep cut in the seismic model for the larger angles of incidence. This is accomplished, however, at the expense of some loss of reflected signal at smaller angles of incidence, where the effect of the cut interferes with propagation. Thus, our study of amplitude effects must use a judicious selection of data from Figures A4 through A9, by which to minimize the effects of interferring waves without introducing extraneous factors from the cut itself.

Tables A1 and A2 provide numerical data for the amplitude of the PP arrivals as measured from the waveforms of Figures A4 through A9. The numbers are in arbitrary units.
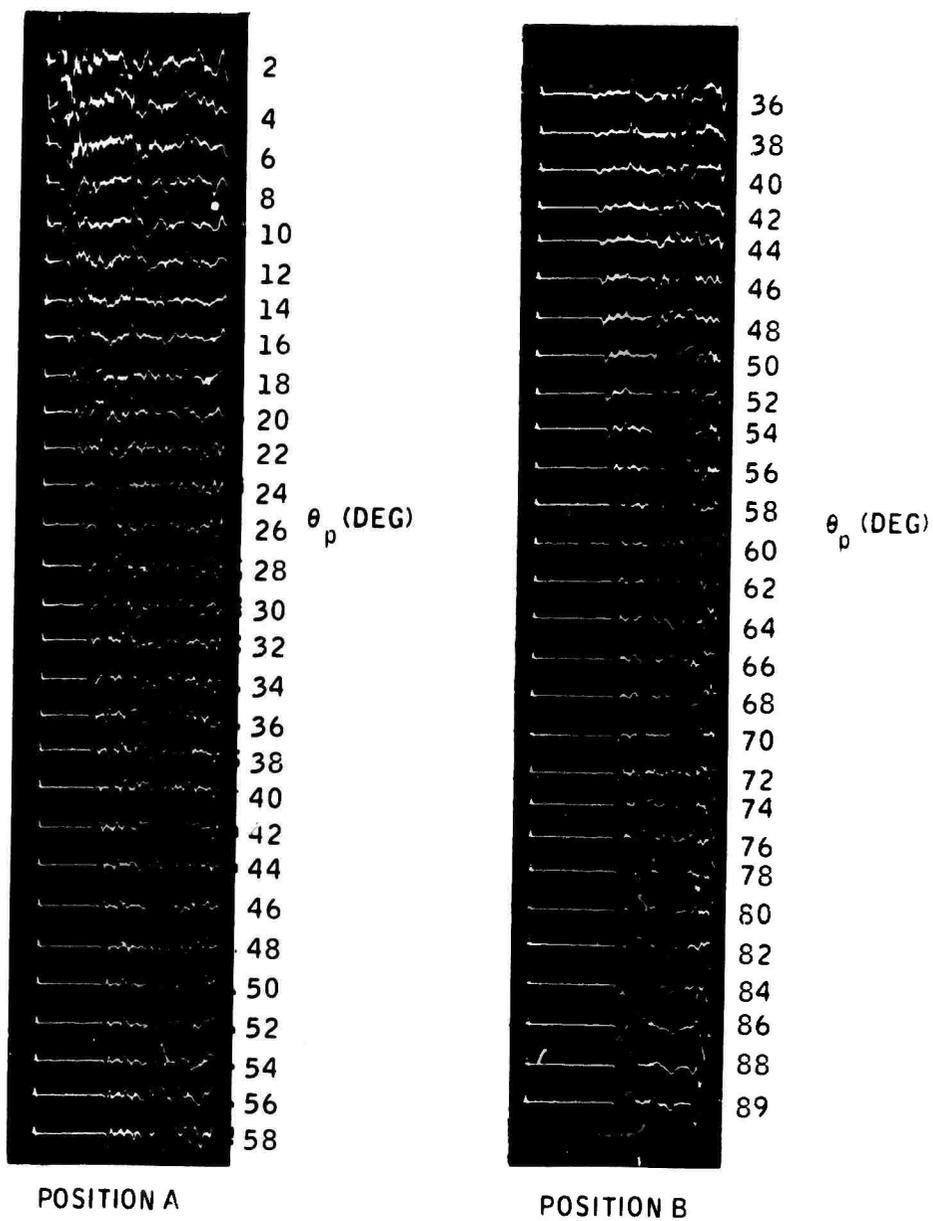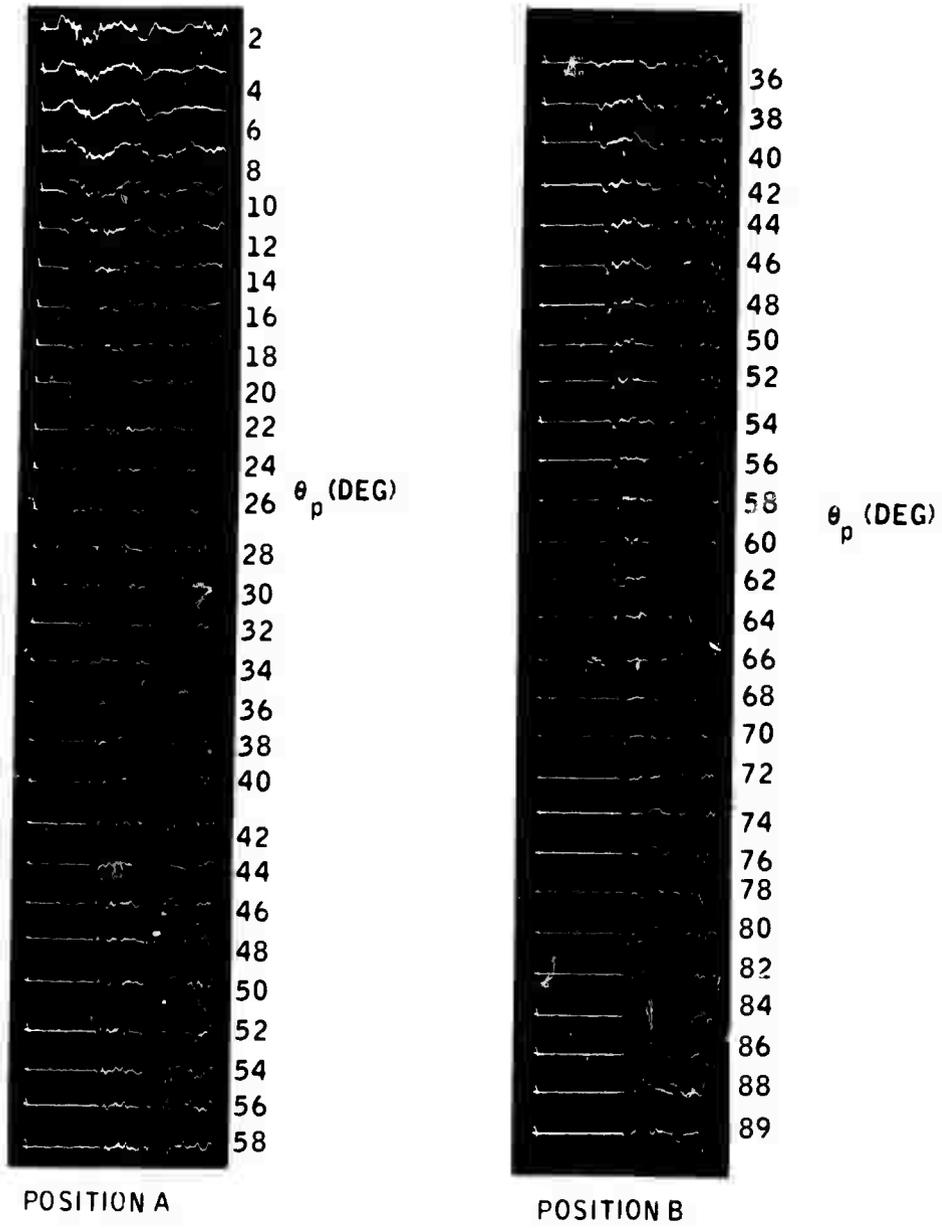
A4

Figure A4. Waveform Results, 1-inch Cut

A5

POSITION A   POSITION B

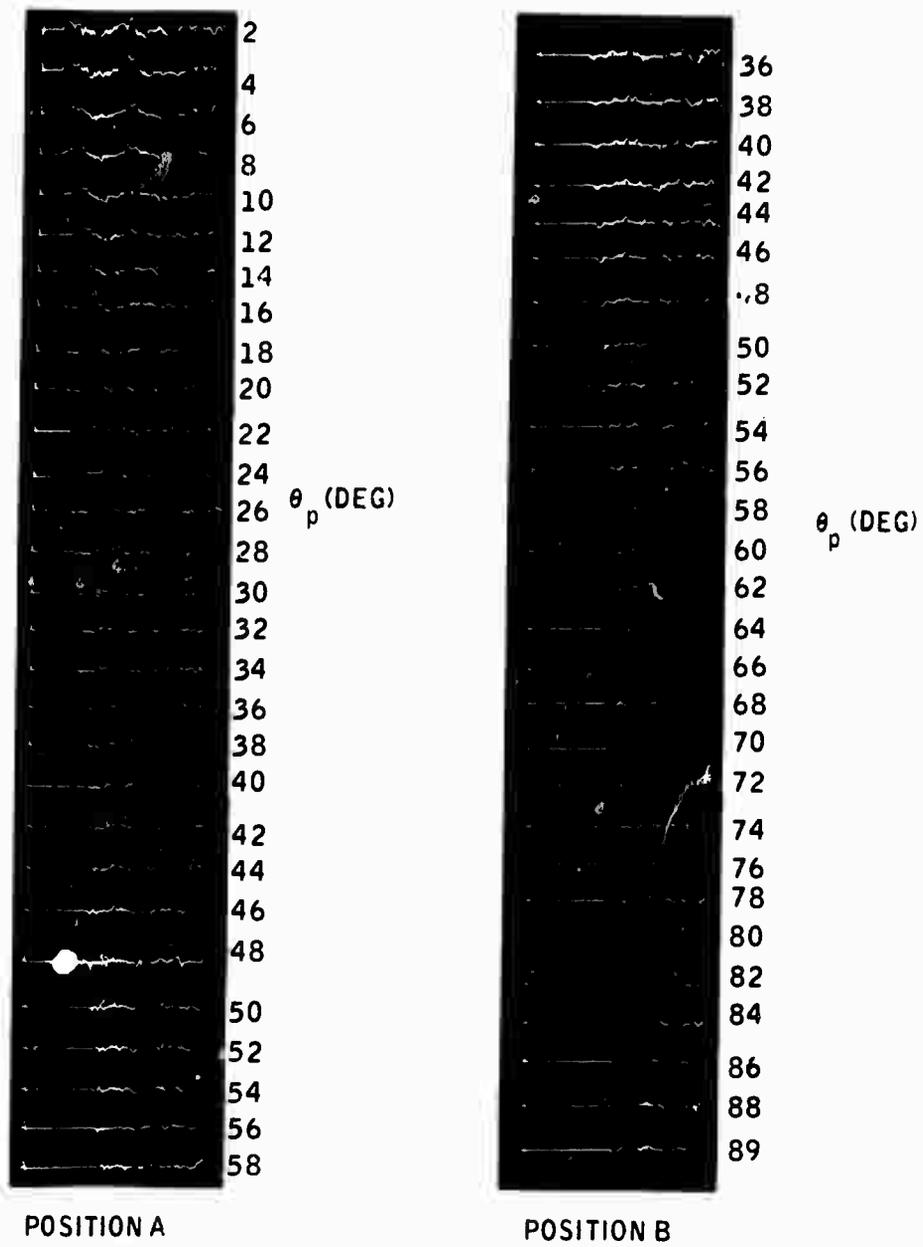Figure A5.   Waveform Results, 2-inch Cut

A 6

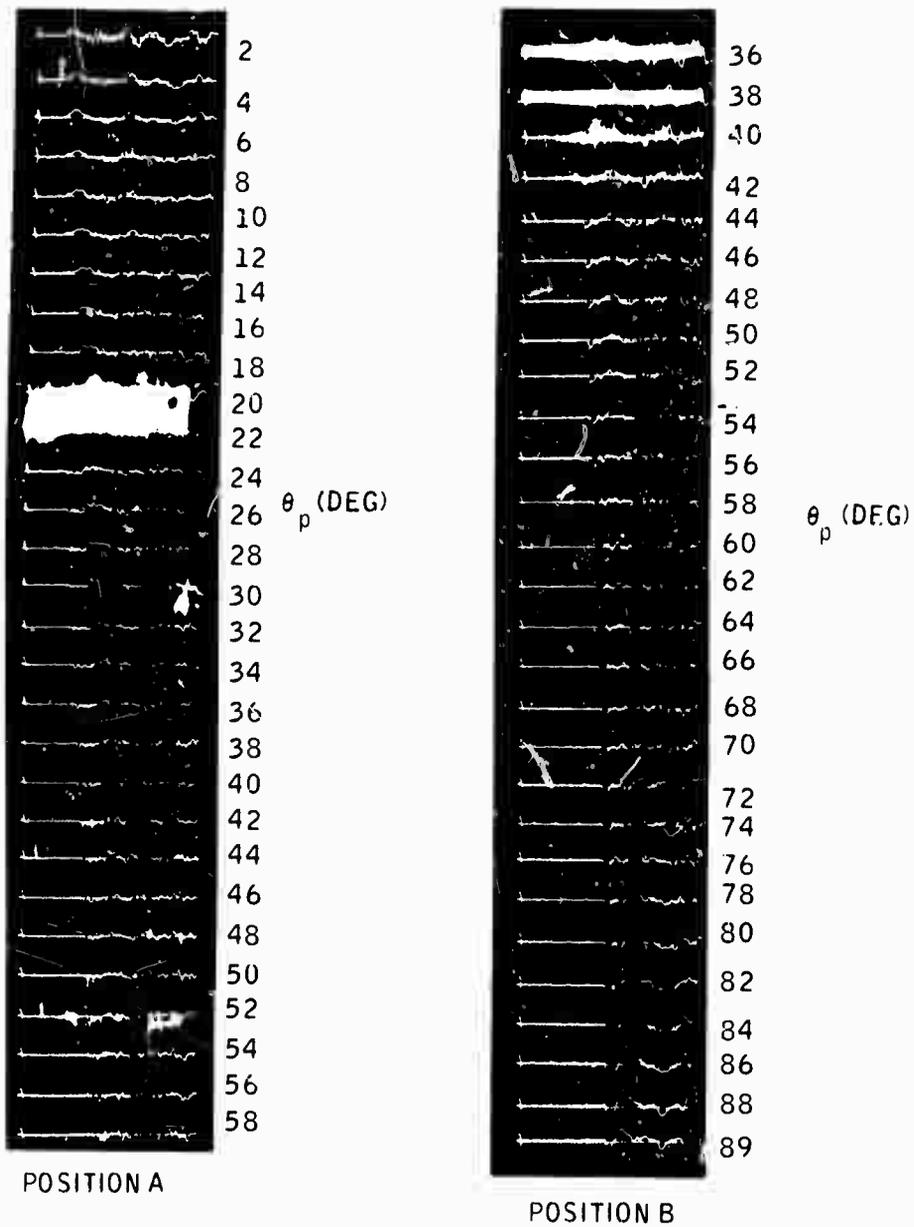Figure A6. Waveform Results, 3-inch Cut

A7

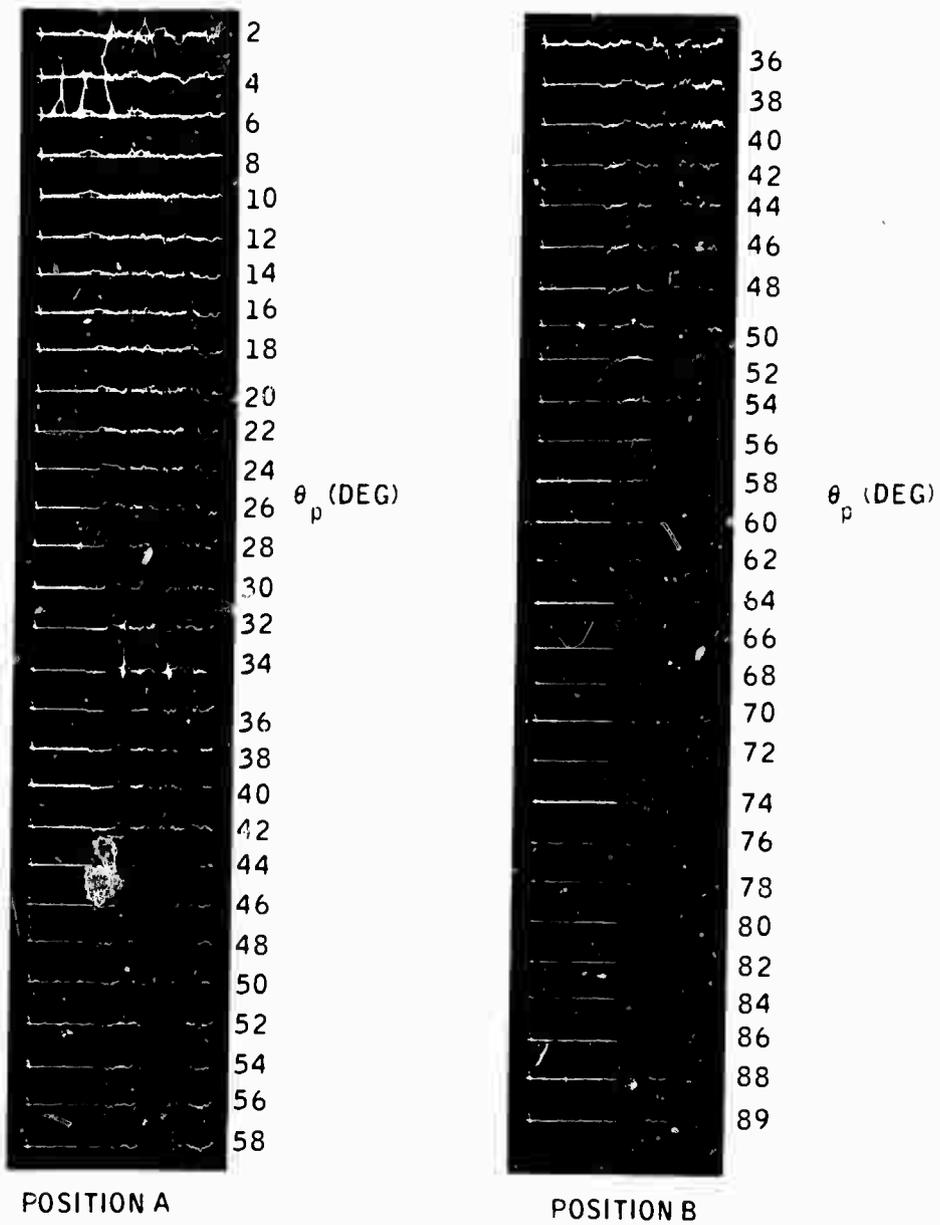Figure A7.   Waveform Results, 4-inch Cut

A 8

Figure A 8. Waveform Results, 5-inch Cut
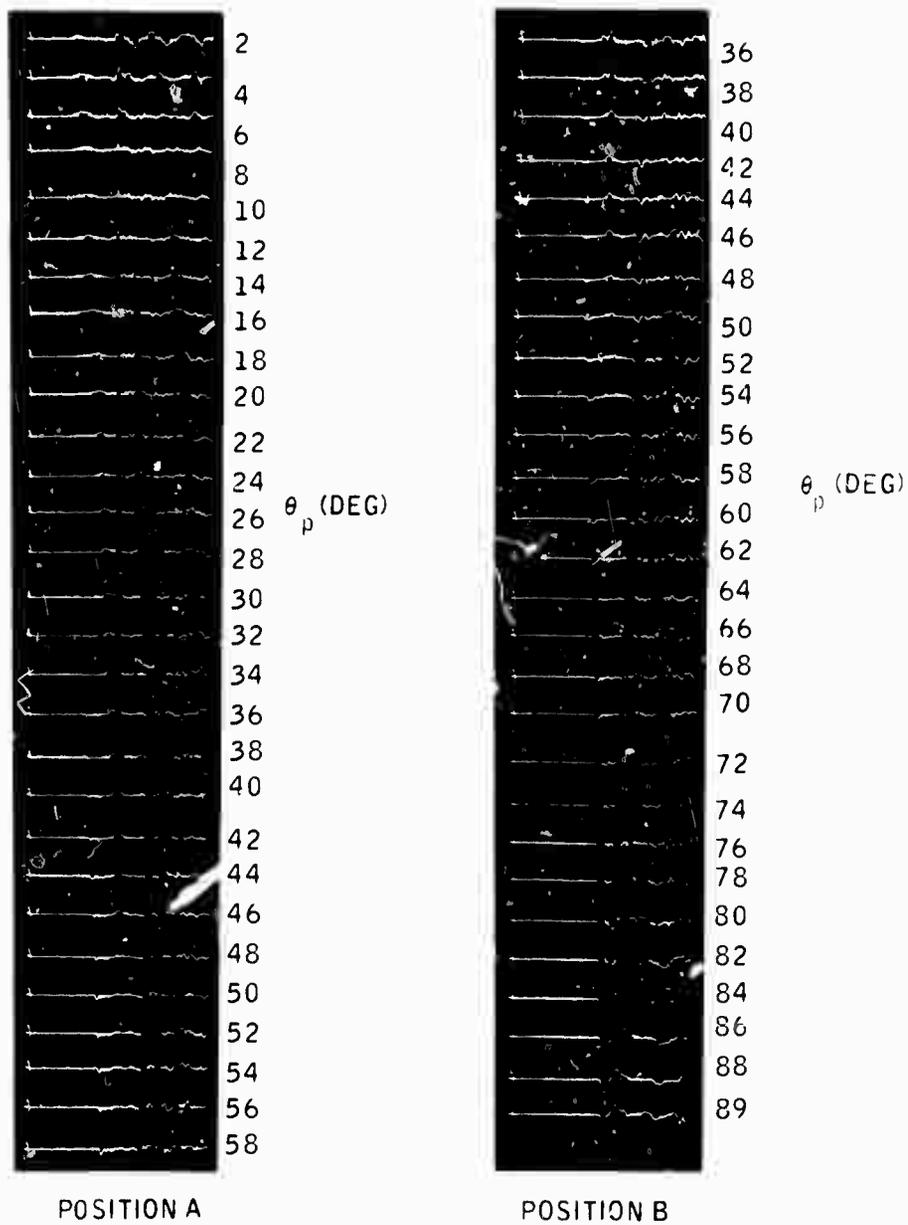
Figure A9.   Waveform Results, 6-inch Cut

Table A1. Amplitude of PP for Transducers at Position A

θ_p	Cut Depth (inches)					
	1	2	3	4	5	6
2	0.68*	0.49*	0.69		0.23	0.40
4	0.68*	0.36*	0.52*	0.66	0.38	0.84
6	0.68*	0.39*	0.59*	0.66	0.52	0.64
8	0.96*	0.52*	0.49*	0.69	0.55	0.50
10	0.93	0.52*	1.02	0.85	0.66	0.60
12	0.89	0.65	0.95	0.97	0.66	0.64
14	0.82	0.55	0.69	0.79	0.60	0.80
16	0.68	0.36	0.79	0.84	0.68	0.92
18	0.88	0.47	0.66	0.59	0.60	0.80
20	0.82	0.39	0.52	0.62	0.57	0.76
22				0.66	0.68	0.84
24				0.66	0.57	0.68
26				0.82	0.57	0.72
28				0.74	0.62	0.66
30				0.66	0.62	0.72
32				0.69	0.55	0.60
34				0.69	0.57	0.74
36				0.69	0.57	0.64
38				0.59	0.64	0.76
40				0.66	0.57	0.64
42				0.66	0.55	0.72
44					0.52	0.40
46					0.27	0.30
48					0.21	0.22
50					0.14	0.18

Table A2. Amplitude of PP for Transducers at Position B

θ_p	Cut Depth (inches)					
	1	2	3	4	5	6
36	0.85	0.73	0.66	1.02	0.63	0.76
38	0.59	0.73	0.46	0.98	0.52	0.60
40	0.41	0.56	0.49	0.93	0.52	0.56
42	0.30	0.52	0.46	0.82	0.55	0.48
44	0.34	0.47	0.46	0.82	0.49	0.44
46	0.27	0.49	0.46	0.77	0.66	0.40
48	0.51	0.40	0.16	0.57	0.27	0.20
50	0.33	0.40	0.33	0.33	0.37	0.20
52	0.34	0.39	0.44	0.46		
54			0.25			
56			0.16			

A11

Figures A10 through A15 show the amplitude measurements in graphical form, as well as a theoretical curve against which to compare them. The measured quantity is the amplitude of the negative part of the PP arrival, referenced to a zero base line. All of the values have been normalized to unity at $\theta = 90$ degrees.

Several conclusions can immediately be drawn from these figures:

- The data show considerable scatter, part of which arises from the limited precision with which amplitudes can be measured on on a laboratory model.

- In accordance with theoretical predictions, the agreement between theory and observation is best for:

    (a)   small angles with the models using s nall cuts, and
    (b)   large angles with the models using large cuts

- The theoretical prediction of decreasing amplitude with increasing incidence angle is clearly displayed.

A further modification of the experimental procedure was attempted aimed at reducing interference from the diffracted signal at the bottom of the cut. This modification consisted of a clamp at the bottom of the 6-inch split; the clamp was constructed of two 1-1/4-inch washers bolted through a small hole in the model. The clamp proved very effective.

The resulting waveforms are shown in Figure A16. This should be compared with Figure A9, without the clamp. The reflection signal is now beautifully displayed, so that good amplitude measurements can be taken. Tabulated values are given as Table A3 and a graphical presentation in Figure A17. The conclusion is clear. For angles up to 25 degrees, the clamp itself creates serious interference with the reflected wave, but beyond 25 degrees the agreement with theoretical results becomes very good indeed.

Further experimental work to validate the theory, particularly for P-S conversions, would be valuable. We feel that the results to date, however, provide confidence in the relevance of theoretical reflection coefficients to the excavation seismoloty program.
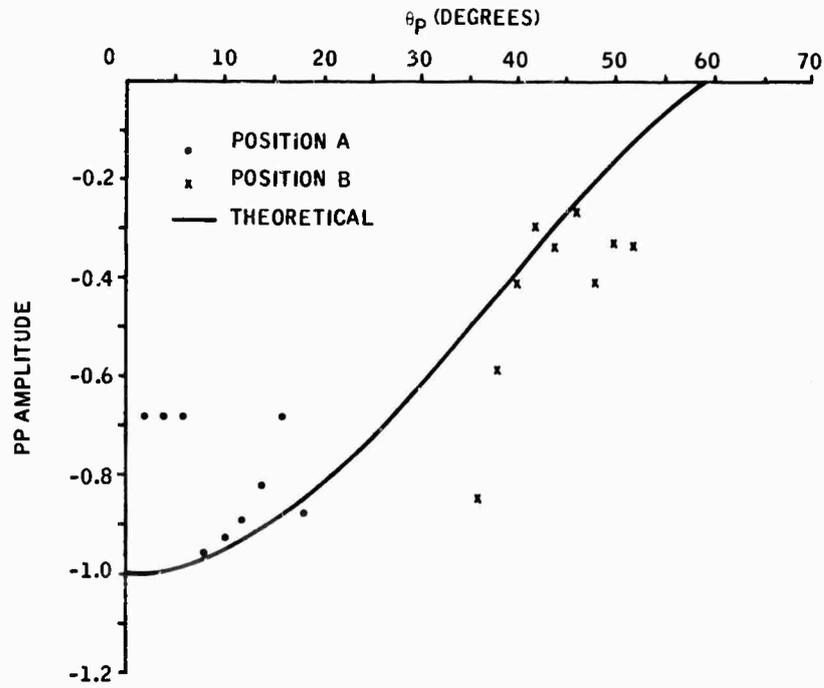
A12

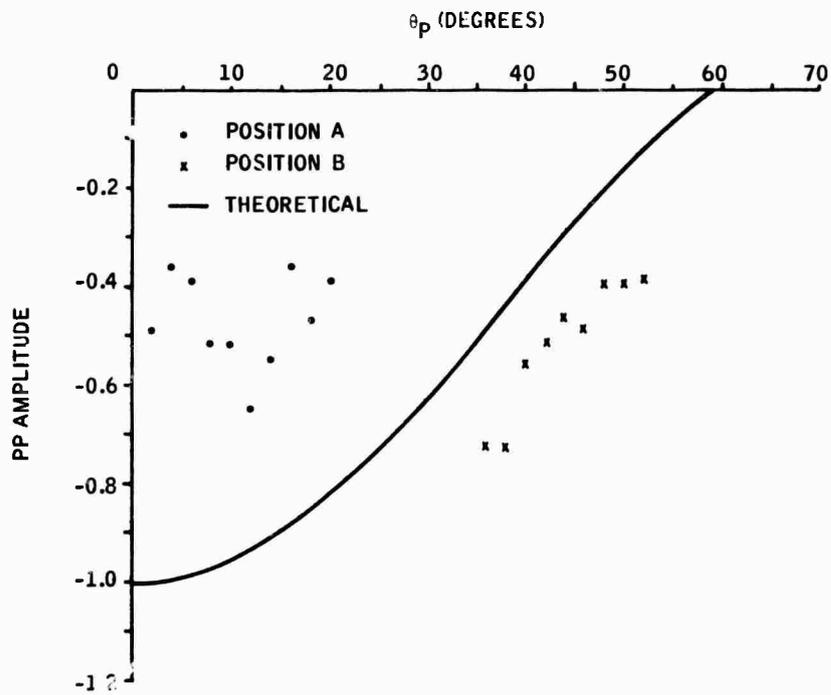Figure A10. PP Amplitude with 1-inch Cut

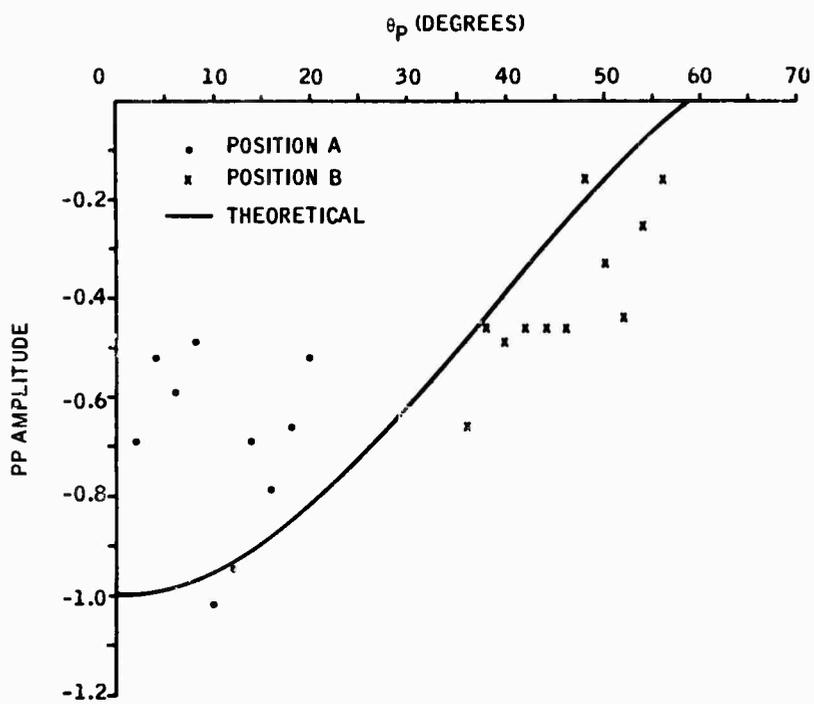Figure A11. PP Amplitude with 2-inch Cut

A13

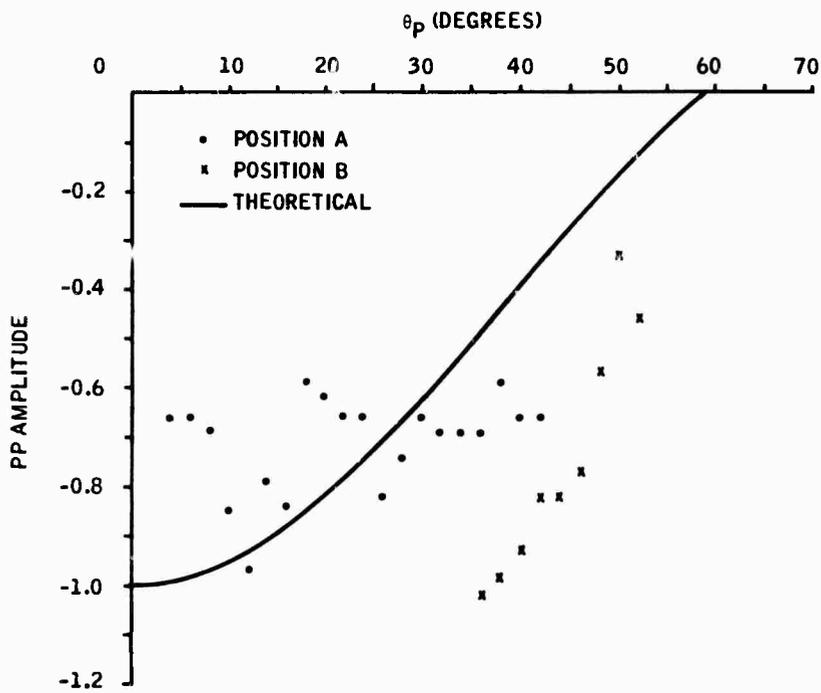Figure A12. PP Amplitude with 3-inch Cut

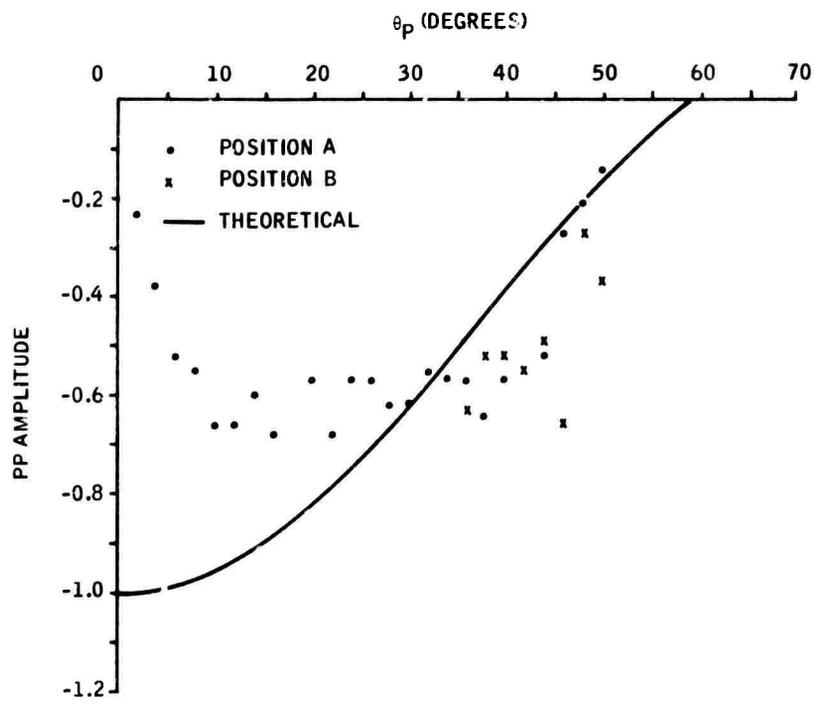Figure A13. PP Amplitude with 4-inch Cut

A14

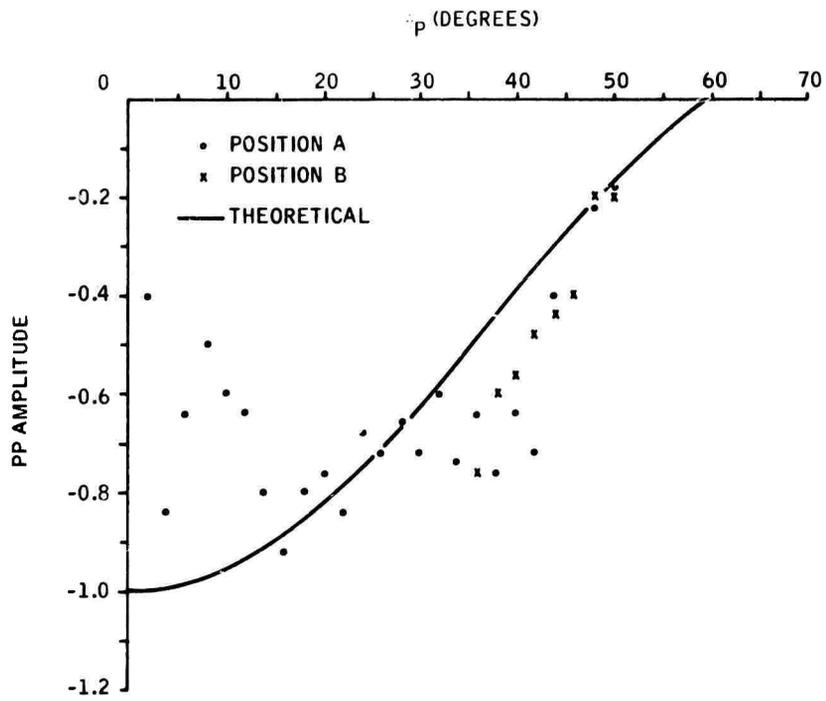Figure A14. PP Amplitude with 5-inch Cut

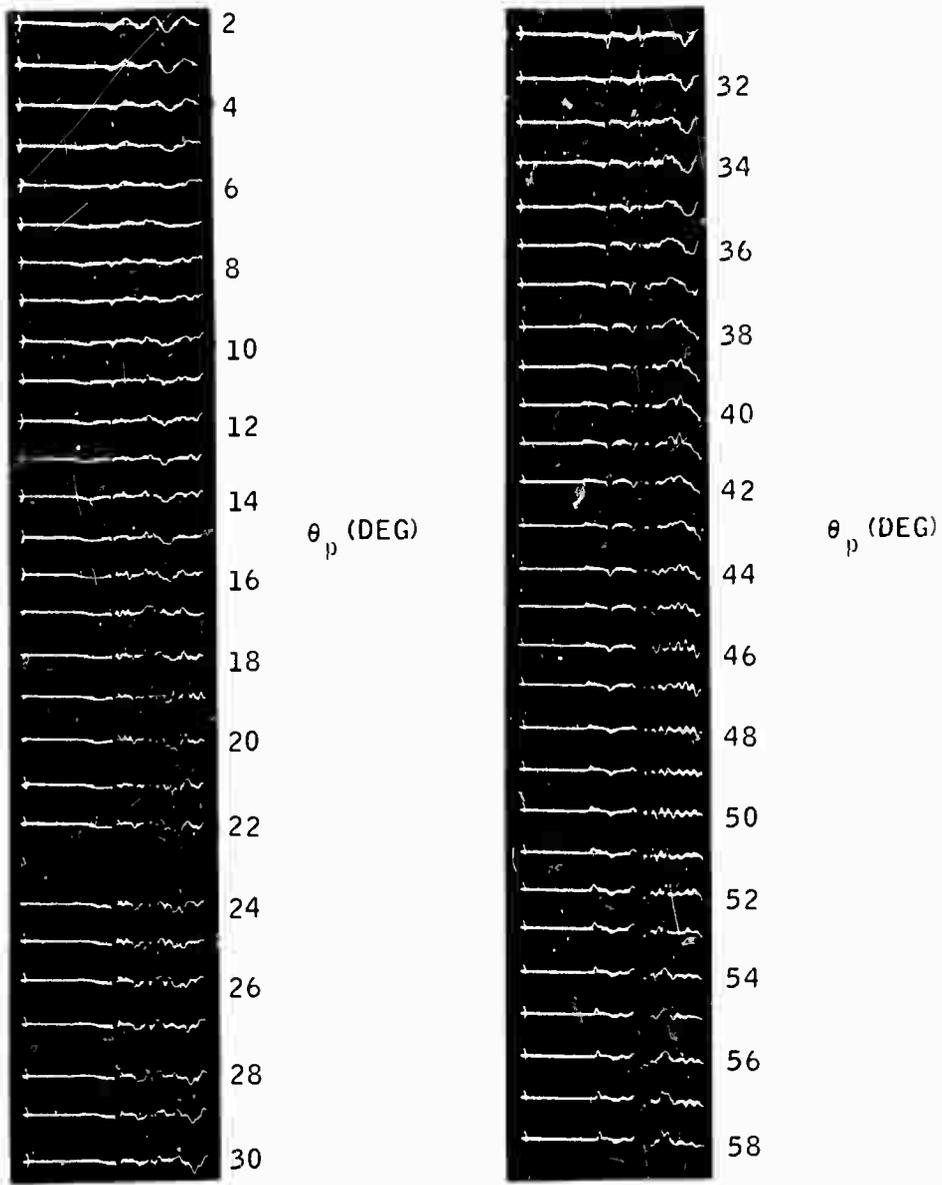Figure A15. PP Amplitude with 6-inch Cut

A15

Figure A16. Waveform Results, Clamp at Bottom of 6-inch Cut

Table A3. PP Amplitude with Clamp at Bottom of 6-inch Cut

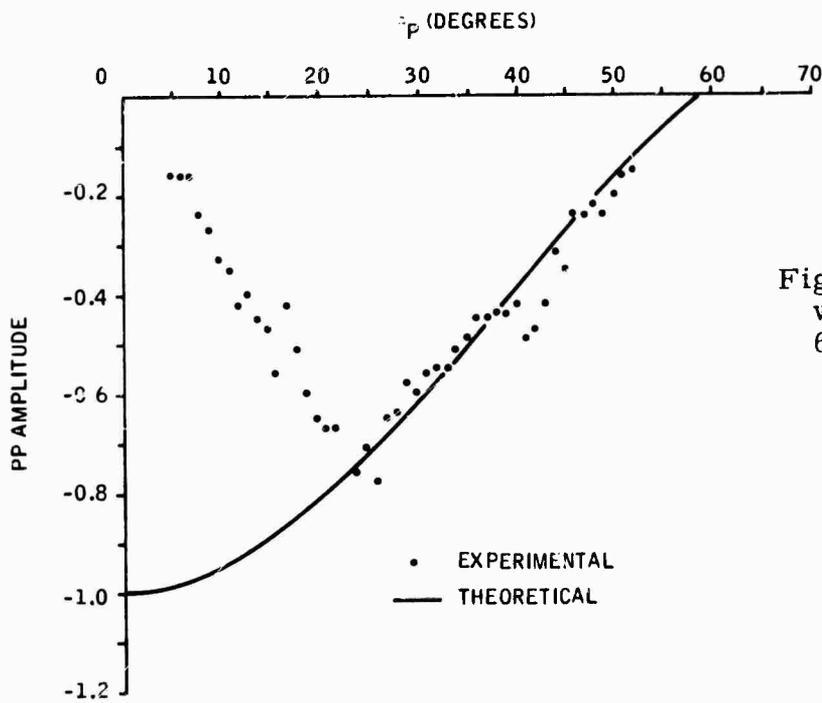| θ_p	Amplitude	θ_p	Amplitude
5	0.16	29	0.58
6	0.16	30	0.60
7	0.16	31	0.56
8	0.24	32	0.55
9	0.27	33	0.55
10	0.33	34	0.51
11	0.35	35	0.49
12	0.42	36	0.45
13	0.40	37	0.45
14	0.45	38	0.44
15	0.47	39	0.44
16	0.56	40	0.42
17	0.42	41	0.49
18	0.51	42	0.47
19	0.60	43	0.42
20	0.65	44	0.31
21	0.67	45	0.35
22	0.67	46	0.24
23		47	0.24
24	0.76	48	0.22
25	0.71	49	0.24
26	0.78	50	0.20
27	0.65	51	0.16
28	0.64	52	0.15

Figure A17. PP Amplitudes with Clamp at Bottom of 6-inch Cut

A17